

Learning Dynamics of Deep Matrix Factorization Beyond the Edge of Stability

Anonymous CPAL submission

1 Deep neural networks trained using gradient descent with a fixed learning rate η
2 often operate in the regime of “edge of stability” (EOS), where the largest eigen-
3 value of the Hessian equilibrates about the stability threshold $2/\eta$. In this work,
4 we present a fine-grained analysis of the learning dynamics of (deep) linear net-
5 works (DLN) within the deep matrix factorization loss beyond EOS. For DLNs,
6 loss oscillations within EOS follow a period-doubling route to chaos. We theo-
7 retically analyze the regime of the 2-period orbit and show that the loss oscilla-
8 tions occur within a small subspace, with the dimension of the subspace precisely
9 characterized by the learning rate. Our analysis contributes to explaining two key
10 phenomena in deep networks: (i) shallow models and simple tasks do not always
11 exhibit EOS [1]; and (ii) oscillations occur within low-dimensional subspaces [2].
12 We present experiments to support our theory, along with examples demonstrating
13 how these phenomena occur in nonlinear networks and how they differ from those
14 in DLNs.

15 1. Introduction

16 Understanding generalization in deep neural networks requires an understanding of the optimiza-
17 tion process in gradient descent (GD). In the literature, it has been empirically observed that the
18 learning rate η plays a key role in driving generalization [3, 4]. The “descent lemma” from classical
19 optimization theory says that for a β -smooth loss $\mathcal{L}(\Theta)$ parameterized by Θ , GD iterates satisfy

$$\mathcal{L}(\Theta(t+1)) \leq \mathcal{L}(\Theta(t)) - \frac{\eta(2-\eta\beta)}{2} \|\nabla \mathcal{L}(\Theta(t))\|_2^2,$$

20 and so the learning rate should be chosen as $\eta < 2/\beta$ to monotonically decrease the loss. How-
21 ever, many recent works have shown that the training loss decreases even for $\eta > 2/\beta$, albeit non-
22 monotonically. Surprisingly, it has been observed that choosing such a learning rate often provides
23 better generalization over smaller ones that lie within the stability threshold. This observation has
24 led to a series of works analyzing the behavior of GD within a regime dubbed “the edge of stability”
25 (EOS). By letting Θ parameterize a deep network, we formally define EOS as follows:

26 **Definition 1** (Edge of Stability [1]). *During training, the sharpness of the loss, defined as $S(\Theta) :=$
27 $\|\nabla^2 \mathcal{L}(\Theta)\|_2$, continues to grow until it reaches $2/\eta$ (progressive sharpening), after which it stabilizes around
28 $2/\eta$. During this process, the training loss behaves non-monotonically over short timescales but consistently
29 decreases over long timescales.*

30 Using a large learning rate to operate within the EOS regime is hypothesized to give better gen-
31 eralization performance by inducing “catapults” in the training loss [2]. Intuitively, whenever the
32 sharpness $S(\Theta)$ exceeds the local stability limit $2/\eta$, the GD iterates momentarily diverge (or cata-
33 pults) out of a sharp region and self-stabilizes [5] to settle for a flatter region where the sharpness is
34 below $2/\eta$, which has shown to correlate with better generalization [6–10]. Of course, the dynamics
35 within EOS differ based on the loss landscape. When the loss landscape is highly non-convex with
36 many local valleys, catapults may occur, whereas sustained oscillations may exist for other land-
37 scapes. It is of great interest to understand these behaviors within different network architectures
38 to further our understanding of EOS.

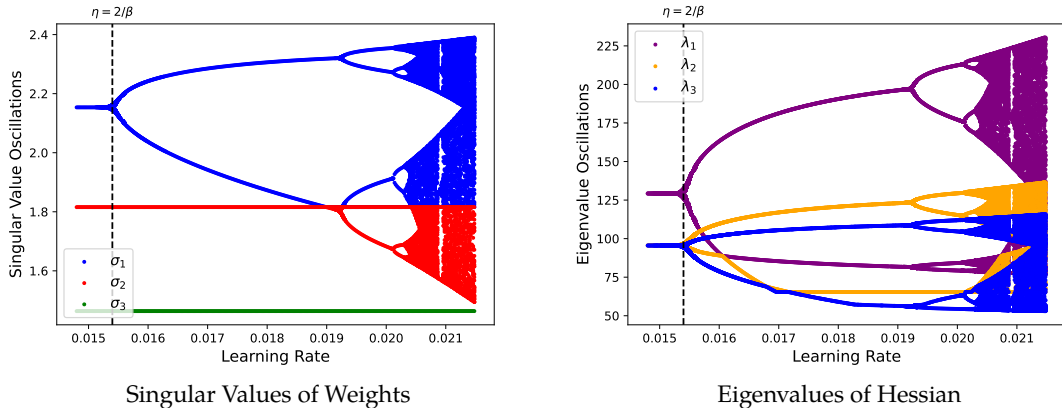


Figure 1: Bifurcation plot of the oscillations in the singular values (left) and the eigenvalues of the Hessian (right) of a 3-layer end-to-end DLN. The bifurcation plots indicate the existence of a period-doubling route to chaos in DLNs, which we analyze by examining the two-period orbit. Here, $\eta > 2/\beta$ corresponds to the EOS regime, where $\beta = L\sigma_{*,1}^{2-2/L}$ is the sharpness at the minima, L is the depth of the network and $\sigma_{*,1}$ is the first singular value of the target matrix \mathbf{M}_* .

39 From a theoretical perspective, there have been many recent efforts to understand EOS. These
 40 works generally focus on analyzing “simple” functions, examples including scalar losses [11–13],
 41 quadratic regression models [14], diagonal linear networks [15] and two-layer matrix factorization
 42 [16]. However, the simplicity of these functions cannot fully capture the behaviors of deep neural
 43 networks within the EOS regime. Specifically, the following observations remain unexplained by
 44 existing analyses: (i) mild (or no) sharpening occurs when either networks are shallow or “simple”
 45 datasets are used for training (Caveat 2 from [1]); and (ii) the oscillations and catapults in the
 46 training loss occur in the span of the top eigenvectors of the NTK [2].

47 In this work, we present a fine-grained analysis of the learning dynamics of deep linear networks
 48 (DLNs) within the EOS regime, demonstrating that these phenomena can be replicated and effec-
 49 tively explained using DLNs. Generally, there are two lines of work for DLNs: (i) those that analyze
 50 the effects of depth and initialization scale, and how they implicitly bias the trajectory of gradient
 51 flow towards low-rank solutions when the learning rate is chosen to be stable [17–24], and (ii) those
 52 that analyze the similarities in behavior between linear and nonlinear networks [25–27]. Our anal-
 53 ysis builds upon these works to show that DLNs exhibit intricate and interesting behaviors outside
 54 the stability regime and to demonstrate how factors such as depth and initialization scale contribute
 55 to the EOS regime. Our main results can be summarized as follows:

- 56 • **Oscillations in Low-Dimensional Subspaces.** We show that there exist periodic oscillations
 57 within r -dimensional subspaces in DLNs, where r is precisely characterized by the learning
 58 rate. For DLNs, a period-doubling route to chaos [28] exists in both the singular values of the
 59 DLN and the eigenvalues of the Hessian, as shown in Figure 1. We rigorously characterize the
 60 case of the two-period orbit, aiming to contribute to explaining the empirical observations by [2]
 61 and [1]. We also prove that the learning rate needed to enter EOS is a function of the network
 62 depth, further revealing its role in deep networks.
- 63 • **EOS Dynamics for DLNs and Diagonal Linear Networks.** We prove that while DLNs and di-
 64 agonal linear networks have different curvatures about the global minimum, they exhibit similar
 65 behaviors within the EOS regime. We show that the additional eigendirections present in DLNs
 66 are not explored during training, making the behavior of the two networks synonymous.

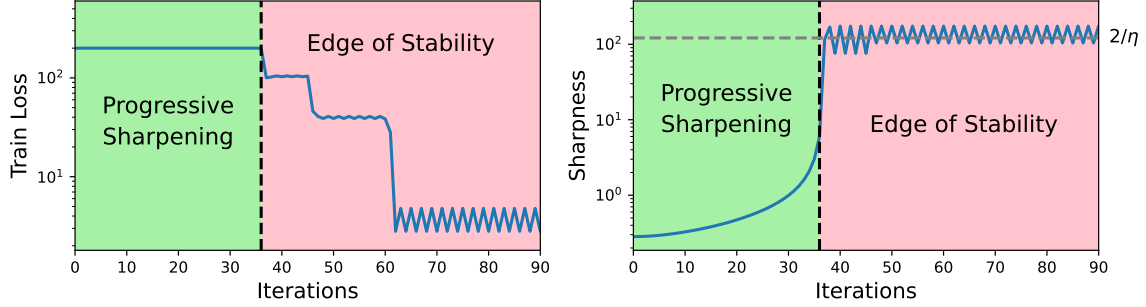


Figure 2: Depiction of the two phases of learning in the deep matrix factorization problem for a network of depth 3. It appears that upon escaping the first saddle point, the GD iterates enter the EOS regime, where the sharpness hovers just above $2/\eta$. Figure (left) shows the training loss undergoing saddle to saddle jump followed by periodic oscillation. Figure (right) plots the corresponding sharpness.

2. Notation and Problem Setup

Notation. We denote vectors with bold lower-case letters (e.g., \mathbf{x}) and matrices with bold upper-case letters (e.g., \mathbf{X}). We use \mathbf{I}_n to denote an identity matrix of size $n \in \mathbb{N}$. We use $[L]$ to denote the set $\{1, 2, \dots, L\}$. We use the notation $\sigma_i(\mathbf{A})$ to denote the i -th singular value of the matrix \mathbf{A} . We also use the notation $\sigma_{\ell,i}$ to denote the i -th singular value of the matrix \mathbf{W}_ℓ .

Deep Matrix Factorization Loss. The objective in deep matrix factorization is to model a low-rank matrix $\mathbf{M}_\star \in \mathbb{R}^{d \times d}$ with $\text{rank}(\mathbf{M}_\star) = r$ via a DLN parameterized by a set of parameters $\Theta = (\mathbf{W}_1, \mathbf{W}_2, \dots, \mathbf{W}_L)$, which can be estimated by solving

$$\underset{\Theta}{\text{argmin}} f(\Theta) := \frac{1}{2} \|\underbrace{\mathbf{W}_L \cdots \mathbf{W}_1}_{=: \mathbf{W}_{L:1}} - \mathbf{M}_\star\|_F^2, \quad (1)$$

where we adopt the abbreviation $\mathbf{W}_{j:i} = \mathbf{W}_j \cdots \mathbf{W}_i$ to denote the end-to-end DLN and is identity when $j < i$. We assume that each weight matrix has dimensions $\mathbf{W}_\ell \in \mathbb{R}^{d \times d}$ to observe the effects of overparameterization. We also assume that the singular values of \mathbf{M}_\star are distinct.

Optimization. We update each weight matrix $\mathbf{W}_\ell \in \mathbb{R}^{d \times d}$ using GD with iterations given by

$$\mathbf{W}_\ell(t) = \mathbf{W}_\ell(t-1) - \eta \cdot \nabla_{\mathbf{W}_\ell} f(\Theta(t-1)), \quad \forall \ell \in [L], \quad (2)$$

where $\eta > 0$ is the learning rate and $\nabla_{\mathbf{W}_\ell} f(\Theta(t))$ is the gradient of $f(\Theta)$ with respect to the ℓ -th weight matrix at the t -th GD iterate.

Initialization. In this work, we consider both balanced and unbalanced initializations, respectively:

$$\begin{aligned} \mathbf{W}_\ell(0) &= \alpha \mathbf{I}_d, \quad \forall \ell \in [L], && \text{(Balanced Initialization)} \\ \mathbf{W}_L(0) &= \mathbf{0}, \quad \mathbf{W}_\ell(0) = \alpha \mathbf{I}_d, \quad \forall \ell \in [L-1], && \text{(Unbalanced Initialization)} \end{aligned}$$

where $\alpha > 0$ is a small constant. We assume α is chosen small enough such that $\alpha \in (0, \sigma_{\star,r})$, where $\sigma_{\star,r}$ is the r -th singular value of \mathbf{M}_\star . Generally, many existing works on both shallow and deep linear networks assume a zero-balanced initialization (i.e., $\mathbf{W}_i^\top(0)\mathbf{W}_i(0) = \mathbf{W}_j(0)\mathbf{W}_j^\top(0)$ for $i \neq j$). This introduces the invariant $\mathbf{W}_i^\top(t)\mathbf{W}_i(t) = \mathbf{W}_j(t)\mathbf{W}_j^\top(t)$ for all $t > 0$, ensuring two (degenerate) conditions throughout the training trajectory: (i) the singular vectors of each of the layers remain aligned and (ii) the singular values stay balanced. For the unbalanced initialization, the zero weight layer can be viewed as the limiting case of initializing the weights with a (very) small constant $\alpha' \ll \alpha$, and has been similarly explored by [29, 30], albeit for two-layer networks. The zero weight layer relieves the balancing condition of the singular values. Rather than staying balanced, we show that the singular values become increasingly balanced (see Lemma 2). This allows us to jointly analyze the singular values of the weights for either case.

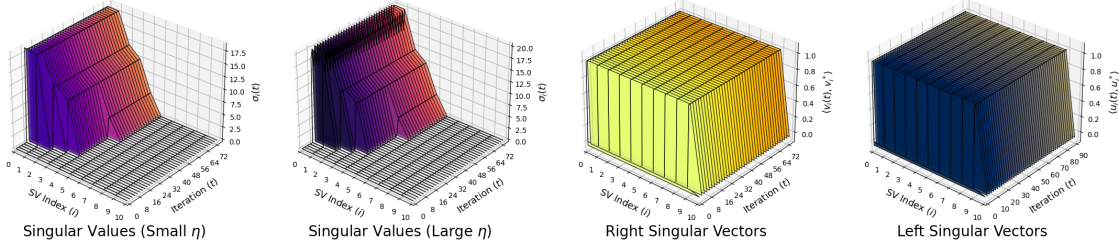


Figure 3: Illustrations of the singular vector and value evolution of the end-to-end DLN. The singular vectors of the network remain static across all iterations, as suggested by the singular vector stationary set, regardless of the learning rate. The angle between the true singular vectors and those of the network remains aligned throughout. The first singular values undergo oscillations in the large η regime, whereas they remain constant in the small η regime.

93 Nevertheless, we also show that our analysis is not limited to either initialization but applies to *any*
 94 *initialization* that converges to a set we call the singular vector stationary set (see Proposition 1).
 95 To the best of our knowledge, it is common to assume that the singular vectors remain aligned, as
 96 many existing works make the same assumption [17, 19, 29, 31–33].

97 3. Deep Matrix Factorization Beyond the Edge of Stability

98 When using a large learning rate, the learning dynamics can typically be separated into two distinct
 99 stages: (i) progressive sharpening and (ii) the edge of stability. Within the progressive sharpening
 100 stage, the sharpness lies below $2/\eta$ and tends to continually rise. Our goal is to analyze the EOS stage
 101 under the deep matrix factorization formulation. Here, we observe that the training loss fluctuates
 102 due to layerwise singular value oscillations, as illustrated in Figure 2.

103 3.1. Main Results

104 Before we present our main results, we provide a definition of what we refer to as a strict balanced
 105 state of the singular values of the weight matrices. The parameters are said to be in a strict balanced
 106 state if the singular values of each weight matrix take the same values across all layers.

107 **Definition 2** (Strict Balanced State). *The parameters Θ of the DLN from Equation (1) are said to be in a*
 108 *strict balanced state if for some $t \geq 0$*

$$\sigma_i(\mathbf{W}_\ell(t)) = \sigma_i(\mathbf{W}_k(t)), \quad \forall i \in [r], \quad \forall \ell, k \in [L],$$

109 where $\sigma_i(\mathbf{W}_\ell)$ denotes the i -th singular value of the ℓ -th layer and r is the rank of the matrix \mathbf{M}_* .

110 It is straightforward to show that the parameters are in a strictly balanced state for all $t \geq 0$ if we ini-
 111 tialize the singular values to be the same across all weight matrices \mathbf{W}_ℓ . Hence, it immediately holds
 112 that the balanced initialization is in a strictly balanced state. However, the one-zero initialization
 113 (i.e., the unbalanced initialization) sets the singular values of \mathbf{W}_L to zero, meaning the parameters
 114 are not initially in a strictly balanced state. However, in Lemma 2 of Section 3.2, we prove that the
 115 balancing increasingly occurs throughout GD iterations within the EOS regime. Consequently, we
 116 assume a strictly balanced state for the remainder of this paper and analyze the EOS regime in rela-
 117 tion to the balanced minimum. Next, we derive the eigenvalues of the Hessian at convergence, such
 118 that we can identify the learning rate needed to enter the EOS regime for DLNs.

119 **Lemma 1** (Eigenvalues of Hessian at the Balanced Minimum). *Consider running GD on the deep*
 120 *matrix factorization loss $f(\Theta)$ defined in Equation (1). The set of all non-zero eigenvalues of the training*

121 loss Hessian at the balanced minimum is given by

$$\lambda_{\Theta} = \underbrace{\left\{ L\sigma_{*,i}^{2-\frac{2}{L}}, \sigma_{*,i}^{2-\frac{2}{L}} \right\}_{i=1}^r}_{\text{self-interaction}} \cup \underbrace{\left\{ \sum_{\ell=0}^{L-1} \left(\sigma_{*,i}^{1-\frac{1}{L}-\frac{1}{L}\ell} \cdot \sigma_{*,j}^{\frac{1}{L}\ell} \right)^2 \right\}_{i \neq j}}_{\text{interaction with other singular values}} \cup \underbrace{\left\{ \sum_{\ell=0}^{L-1} \left(\sigma_{*,k}^{1-\frac{1}{L}-\frac{1}{L}\ell} \cdot \alpha^{\ell} \right)^2 \right\}_{k=1}}_{\text{interaction with initialization}}$$

122 where $\sigma_{*,i}$ is the i -th singular value of the target matrix $\mathbf{M}_* \in \mathbb{R}^{d \times d}$, $\alpha \in \mathbb{R}$ is the initialization scale, L is
 123 the depth of the network, and the second element of the set under ‘‘self-interaction’’ has a multiplicity of $d - r$.

124 We defer all of the proofs to Appendix C. Let λ_i denote the i -th largest eigenvalue of the Hessian.
 125 By Lemma 1, we observe that the sharpness is equal to $\lambda_1 = \|\nabla^2 f(\Theta)\|_2 = L\sigma_{*,1}^{2-\frac{2}{L}}$ at the balanced
 126 minimum. In Lemma 8, we show that the sharpness at the balanced minimum is the flattest, and
 127 hence $L\sigma_{*,1}^{2-\frac{2}{L}}$ represents the smallest sharpness value among all global minima. Thus, if η is set
 128 such that $\eta > 2/\lambda_1$, oscillations in the loss will occur, as the step size is large enough to induce oscil-
 129 lations even in the flattest region. Interestingly, notice that all non-zero eigenvalues are a function of
 130 network depth. For a deeper network, the sharpness will be larger, implying that a smaller learning
 131 rate can be used to drive the DLN into EOS. This provides a unique perspective on how the learning
 132 rate should be chosen as networks become deeper and explains the observation made by [1], who
 133 observed that sharpness scales with the depth of the network. Equipped with the eigenvalues, we
 134 show in the following result that oscillations occur in a two-period orbit along the i -th eigenvector
 135 direction of the balanced minimum, given that the learning rate is set to be greater than $2/\lambda_i$.

136 **Theorem 1** (Stable Subspace Oscillations). Let $\alpha' := \left(\ln \left(\frac{2\sqrt{2}}{\eta\lambda_1} \right) \cdot \frac{\sigma_{*,1}^{4/L}}{L^2 \cdot 2^{\frac{2(L-3)}{L}}} \right)^{1/4}$. Consider running GD
 137 on the loss in (1) with initialization scale $0 < \alpha < \alpha'$. If $\eta = \frac{2}{K}$ with $\lambda_i \leq K < \lambda_{i+1}$, then 2-period orbit
 138 oscillation occurs in the direction of Δ_i , where λ_i and Δ_i denote the i -th largest eigenvalue and eigenvector of
 139 the Hessian at the balanced minimum, respectively.

140 The complete proof is provided in Appendix C.1, where we derive all eigenvectors at the balanced
 141 minimum and demonstrate that the necessary conditions from Lemma 12 (restated from [16]) are
 142 satisfied for a two-period orbit. The condition on the initialization scale is chosen to ensure balanced
 143 behavior, as demonstrated in Lemma 2. To understand Theorem 1 more clearly, consider the first
 144 eigenvector of the Hessian, which we derived to be

$$\Delta_1 = \frac{1}{\sqrt{L}} \cdot \text{vec} \left(\mathbf{u}_{*,1} \mathbf{v}_{*,1}^\top, \mathbf{v}_{*,1} \mathbf{v}_{*,1}^\top, \dots, \mathbf{v}_{*,1} \mathbf{v}_{*,1}^\top \right),$$

145 where $\mathbf{u}_{*,1}, \mathbf{v}_{*,1} \in \mathbb{R}^d$ are the first left and right singular vectors of \mathbf{M}_* , respectively. By Propo-
 146 sition 2, we know that the each weight layer takes the form $\mathbf{W}_\ell = \mathbf{V}_* \Sigma_\ell \mathbf{V}_*^\top$ for all $\ell \in [L - 1]$
 147 and $\mathbf{W}_L = \mathbf{U}_* \Sigma_L \mathbf{V}_*^\top$ at convergence, starting from the unbalanced initialization. By stacking and
 148 flattening these weights, consider the direction

$$\tilde{\Delta} := \sum_{i=1}^d \text{vec} \left(\sigma_{L,i} \cdot \mathbf{u}_{*,i} \mathbf{v}_{*,i}^\top, \sigma_{L-1,i} \cdot \mathbf{v}_{*,i} \mathbf{v}_{*,i}^\top, \dots, \sigma_{1,i} \cdot \mathbf{v}_{*,i} \mathbf{v}_{*,i}^\top \right).$$

149 Since $\tilde{\Delta}^\top \Delta_1$ is only non-zero in the rank-1 components of $\tilde{\Delta}$, this implies that if $\lambda_1 \leq K < \lambda_2$
 150 from Theorem 1, the oscillations only occur in the rank-1 components of the weights. The following
 151 result substantiates this claim by demonstrating that, with an appropriately chosen learning rate,
 152 oscillations occur in the singular values in the top- p directions given that $p \leq r$.

153 **Theorem 2** (Rank- p Periodic Subspace Oscillations). Let $\mathbf{M}_* = \mathbf{U}_* \Sigma_* \mathbf{V}_*^\top$ denote the SVD of the target
 154 matrix and define $S_p := L\sigma_{*,p}^{2-\frac{2}{L}}$ and $K'_p := \max \left\{ S_{p+1}, \frac{S_p}{2\sqrt{2}} \right\}$. If we run GD on the deep matrix factoriza-
 155 tion loss with initialization scale $\alpha < \alpha'$ from Theorem 1 and learning rate $\eta = \frac{2}{K}$, where $K'_p < K < S_p$,
 156 then under strict balancing, the top- p singular values of the end-to-end DLN oscillates in a 2-period orbit

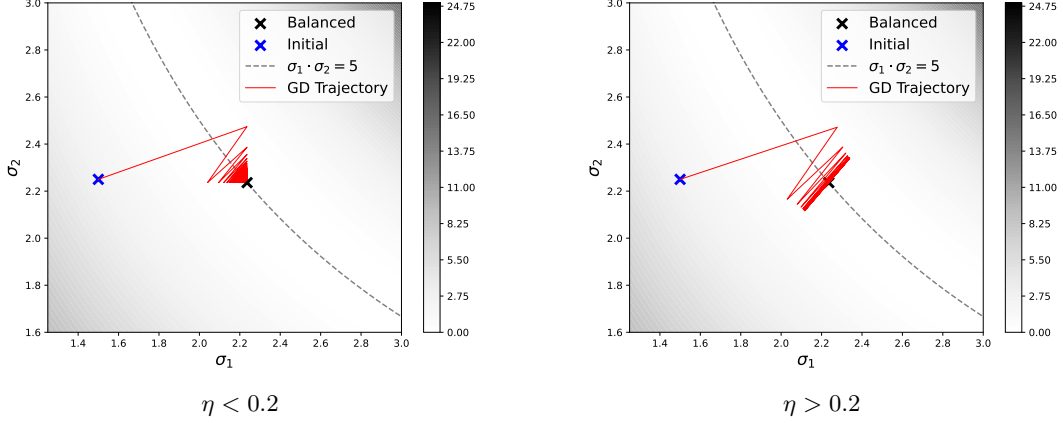


Figure 4: Illustration of the GD trajectories for two different learning rates for minimizing the function $f(\sigma_1, \sigma_2) = \frac{1}{2}(\sigma_2 \cdot \sigma_1 - 5)^2$, starting from an unbalanced initial point. The sharpness at the balanced minimum is 10, and so the learning rate needed to enter EOS is $\eta = 0.2$. These plots show that while GD initially arrives at an unbalanced solution in both cases, the iterates oscillate about the other minima to arrive at the balanced solution within the EOS regime.

157 ($j \in \{1, 2\}$) around the balanced minimum and admits the following decomposition:

$$\mathbf{W}_{L:1} = \underbrace{\sum_{i=1}^p \rho_{i,j}^L \cdot \mathbf{u}_{*,i} \mathbf{v}_{*,i}^\top}_{\text{oscillation subspace}} + \underbrace{\sum_{k=p+1}^d \sigma_{*,k} \cdot \mathbf{u}_{*,k} \mathbf{v}_{*,k}^\top}_{\text{stationary subspace}}, \quad j \in \{1, 2\}, \quad \forall \ell \in [L-1], \quad (3)$$

158 where $\rho_{i,1} \in (0, \sigma_{*,i}^{1/L})$ and $\rho_{i,2} \in (\sigma_{*,i}^{1/L}, (2\sigma_{*,i})^{1/L})$ are the two real roots of the polynomial $g(\rho_i) = 0$ and

$$g(\rho_i) = \rho_i^L \cdot \frac{1 + (1 + \eta L(\sigma_{*,i} - \rho_i^L) \cdot \rho_i^{L-2})^{2L-1}}{1 + (1 + \eta L(\sigma_{*,i} - \rho_i^L) \cdot \rho_i^{L-2})^{L-1}} - \sigma_{*,i}.$$

159 In contrast to Theorem 1, Theorem 2 explicitly identifies the subspaces that exhibit a two-period orbit
 160 based on the range of the learning rate. It also provides a rough characterization of the oscillation
 161 amplitude, which is determined by $\rho_{i,1}$ and $\rho_{i,2}$ —values below and above the balanced minimum,
 162 respectively. Since there is no closed-form solution for an arbitrary higher-order polynomial, $\rho_{i,1}$
 163 and $\rho_{i,2}$ are defined as solutions to the polynomial $g(\rho_i)$. Overall, this aims to theoretically explain
 164 why (i) oscillations occur primarily within the top subspaces of the network, as observed by [2],
 165 and (ii) oscillations are more pronounced in the directions of stronger features, as measured by the
 166 magnitudes of their singular values.

167 Notice that Theorem 2 demonstrates the existence of a two-period orbit only around the balanced
 168 minimum. While this assumption was initially made for ease of analysis, we empirically observe
 169 that the two-period orbit actually *only* occurs around the balanced solution. To illustrate this claim,
 170 in Figure 4, we provide a plot of the GD trajectory for minimizing a two-layer scalar loss $f(\sigma_1, \sigma_2) =$
 171 $\frac{1}{2}(\sigma_2 \cdot \sigma_1 - 5)^2$, starting from an unbalanced initial point $(\sigma_1, \sigma_2) = (1.5, 2.25)$. Notice that, by
 172 Lemma 1, the sharpness around the balanced minimum is $L\sigma_{*,1}^{2-2/L} = 10$, and thus the necessary
 173 learning rate to enter the EOS regime is $\eta = 0.2$. We plot the GD trajectory under two cases for the
 174 learning rate: (i) slightly below the EOS learning rate, $\eta = 0.1999$, and (ii) slightly above it, $\eta =$
 175 0.2010 . When $\eta = 0.2010$, GD first arrives at an unbalanced solution, then oscillates until it reaches
 176 the balanced minimum, where it sustains a two-period orbit around the balanced solution. The
 177 other minima are too narrow to sustain the oscillations induced by the large learning rate, causing
 178 the GD iterates to bounce out of those minima and settle at the flattest, balanced solution. When
 179 the learning rate is slightly below $\eta = 0.2$, it remains large enough to induce oscillations around

180 other unbalanced minima, but ultimately GD converges to the balanced solution, where it exhibits
 181 no oscillations, as predicted by Theorem 2. This empirical observation suggests that two-period
 182 oscillations and balancing occur simultaneously, which we leave for future investigation.

183 Finally, we conclude by remarking that our result also aims to generalize the recent theoretical find-
 184 ings of [16], where they proved the existence of a certain class of scalar functions $f(x)$ for which
 185 GD does not diverge even when operating beyond the stability threshold. They demonstrated that
 186 there exists a range in which the loss oscillates around the local minima with a certain periodic-
 187 ity. These oscillations gradually progress into higher periodic orbits (e.g., 2, 4, 8 periods), transition
 188 into chaotic behavior, and ultimately result in divergence. In our work, we prove that this oscillatory
 189 behavior beyond the stability threshold also occurs in DLNs.

190 3.2. Assumptions and Analytical Tools

191 This section presents the two main tools used in our analyses: the singular vector stationary set and
 192 singular value balancedness. First, we present the singular vector stationary set, which allows us
 193 to encompass a wider range of initialization schemes. This set defines a broad class of initialization
 194 for which singular vector alignment occurs, simplifying the dynamics to only singular values.

195 **Proposition 1** (Singular Vector Stationary Set). *Consider the deep matrix factorization loss in Equa-
 196 tion (1). Let $\mathbf{M}_\star = \mathbf{U}_\star \Sigma_\star \mathbf{V}_\star^\top$ and $\mathbf{W}_\ell(t) = \mathbf{U}_\ell(t) \Sigma_\ell(t) \mathbf{V}_\ell^\top(t)$ denote the compact SVD for the target
 197 matrix and the ℓ -th layer weight matrix at time t , respectively. For any time $t \geq 0$, if $\dot{\mathbf{U}}_\ell(t) = \dot{\mathbf{V}}_\ell(t) = 0$ for
 198 all $\ell \in [L]$, then the singular vector stationary points for each weight matrix are given by*

$$\text{SVS}(f(\Theta)) = \begin{cases} (\mathbf{U}_L, \mathbf{V}_L) &= (\mathbf{U}_\star, \mathbf{Q}_L), \\ (\mathbf{U}_\ell, \mathbf{V}_\ell) &= (\mathbf{Q}_{\ell+1}, \mathbf{Q}_\ell), \quad \forall \ell \in [2, L-1], \\ (\mathbf{U}_1, \mathbf{V}_1) &= (\mathbf{Q}_2, \mathbf{V}_\star), \end{cases}$$

199 where $\{\mathbf{Q}_\ell\}_{\ell=2}^L$ are any set of orthogonal matrices.

200 The singular vector stationary set states that for any set of weights where the gradients with respect
 201 to the singular vectors become zero, the singular vectors become fixed points for subsequent iter-
 202 ations. Once the singular vectors become stationary, running GD further isolates the dynamics on
 203 the singular values. Hence, throughout our analysis, we re-write and consider the loss

$$\frac{1}{2} \|\mathbf{W}_{L:1}(t) - \mathbf{M}^\star\|_F^2 = \frac{1}{2} \|\Sigma_{L:1} - \Sigma^\star\|_F^2 = \frac{1}{2} \sum_{i=1}^r (\sigma_i(\Sigma_{L:1}(t)) - \sigma_{\star,i})^2, \quad (4)$$

204 where $\Sigma_{L:1}$ are the singular values of $\mathbf{W}_{L:1}$. This allows us to decouple the dynamics of the singular
 205 vectors and singular values, focusing on the periodicity that occurs in the singular values within the
 206 EOS regime. In Propositions 2 and 3, we prove that both the unbalanced and balanced initializations
 207 belong to this set respectively, with an illustration in Figure 3. Specifically, we show that the singular
 208 vectors belongs to the singular vector stationary set after GD iteration $t = 1$ (far before entering the
 209 EOS regime) with $\mathbf{Q}_\ell = \mathbf{V}_\star$, allowing us to consider the loss in Equation (4). Next, we present a
 210 result to validate our use of the strictly balanced assumption on the unbalanced initialization case
 211 by showing that the singular values become increasingly balanced throughout the GD iterations.

212 **Lemma 2** (Balancing). *Let $\sigma_{\star,i}$ and $\sigma_{\ell,i}(t)$ denote the i -th singular value of $\mathbf{M}_\star \in \mathbb{R}^{d \times d}$ and $\mathbf{W}_\ell(t)$,
 213 respectively and define $S_i := L \sigma_{\star,i}^{2-\frac{2}{L}}$. Consider GD on the i -th index of the simplified loss in (4) with the
 214 unbalanced initialization and learning rate $\frac{2}{S_i} < \eta < \frac{2\sqrt{2}}{S_i}$. If the initialization scale α satisfies $0 < \alpha <$
 215 $\left(\ln \left(\frac{2\sqrt{2}}{\eta S_i} \right) \cdot \frac{\sigma_{\star,i}^{4/L}}{L^{2.2} \frac{2L-3}{L}} \right)^{1/4}$, then there exists a constant $c \in (0, 1]$ such that for all $\ell \in [L-1]$, we have
 216 $\left| \sigma_{L,i}^2(t+1) - \sigma_{\ell,i}^2(t+1) \right| < c \left| \sigma_{L,i}^2(t) - \sigma_{\ell,i}^2(t) \right|$.*

217 This result has been shown to hold similarly for two-layer matrix factorization [16, 34, 35], and our
 218 analysis extends it to the deep case. Lemma 2 considers the scalar loss for a single singular value

219 index and states that, as long as α is chosen below a threshold dependent on $\sigma_{*,i}$, the i -th singular
 220 value will become increasingly balanced. To ensure that balancing occurs for all singular values of
 221 the loss in (4), we can select the learning rate to induce oscillations in all singular values (assuming
 222 they remain below the divergence limit) and choose α with $\sigma_{*,1}$ such that it is the smallest α that
 223 satisfies the condition for all singular values $\sigma_{*,i}$.

224 If the constant were $c < 1$, note that the balancing gap
 225 would approach zero infinitesimally. However, our analy-
 226 sis currently only shows that $c < 1$ when the product of singu-
 227 lar values across all layers $\sigma_i(\Sigma_{L:1}) < \sigma_{*,i}$ and but $c = 1$
 228 when $\sigma_i(\Sigma_{L:1}) > \sigma_{*,i}$. Since we start from a small initializa-
 229 tion scale, we generally mostly operate within the regime
 230 $\sigma_i(\Sigma_{L:1}) < \sigma_{*,i}$, and only transition to the latter regime
 231 when oscillations occur. Note that $\sigma_i(\Sigma_{L:1}) = \sigma_{*,i}$ cannot
 232 occur since the learning rate is chosen to be within the EOS
 233 regime – equality can only arise in the stable regime, where
 234 balancing does not occur. In Figure 5, we plot the balancing
 235 gap between the top-3 singular values of a weight matrix
 236 initialized to zero and those initialized to α for a rank-3
 237 matrix. This plot shows that the gap decreases and goes to
 238 zero empirically, and this is consistently the case across all
 239 of our experiments, with additional results provided in Appendix B. This provides empirical evi-
 240 dence that our analysis can be further improved such that $c < 1$ for both cases. To this end, we use
 241 this insights to assume that strict balancing holds for both the considered initialization schemes.
 242 This allows us to write the loss of the singular values into the form $\sigma_i(\Sigma_{L:1}(t)) = \sigma_i^L(t)$, which
 243 allows us to focus on the dynamics in the singular values.

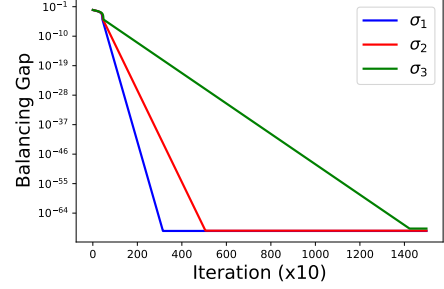


Figure 5: Plot of $|\sigma_{L,i}^2(t) - \sigma_{\ell,i}^2(t)|$ showing strict balancing.

244 3.3. Relation to Diagonal Linear Networks

245 In this section, we derive the necessary conditions and characteristics of two-period oscillations in
 246 diagonal linear networks to establish their similarities with DLNs.

247 **Theorem 3** (Subspace Oscillation for Diagonal Linear Networks). *Consider an L -layer diagonal linear*
 248 *network on the loss*

$$\mathcal{L}(\{\mathbf{s}_\ell\}_{\ell=1}^L) := \frac{1}{2} \|\mathbf{s}_1 \odot \dots \odot \mathbf{s}_L - \mathbf{s}_*\|_2^2, \quad (5)$$

249 where $\mathbf{s}_* \in \mathbb{R}^d$ be an r -sparse vector with ordered coordinates such that $s_{*,1} > \dots > s_{*,d}$ and define $S_p :=$
 250 $L s_{*,p}^{2-\frac{2}{L}}$ and $\alpha' := \left(\ln \left(\frac{2\sqrt{2}}{\eta L s_{*,1}^{2-\frac{2}{L}}} \right) \cdot \frac{s_{*,1}^{\frac{4}{L}}}{L^2 \cdot 2^{\frac{2L-3}{L}}} \right)^{\frac{1}{4}}$. For any $p < r - 1$ and $\alpha < \alpha'$, suppose we run GD
 251 on Equation (5) with learning rate $\eta = \frac{2}{K}$, where $S_p \geq K > S_{p+1}$ with initialization $\mathbf{s}_\ell = \alpha \mathbf{1}_d$ for all
 252 $\ell \in [L - 1]$ and $\mathbf{s}_L = \mathbf{0}_d$. Then, under strict balancing, the top- p coordinates of \mathbf{s}_ℓ oscillate within a 2-period
 253 fixed orbit around the minima in the form

$$s_{\ell,i}(t) = \rho_{i,j}(t), \quad \forall i < p, \forall \ell \in [L],$$

254 where $\rho_{i,j}(t) \in \{\rho_{i,1}, \rho_{i,2}\}$, $\rho_{i,1} \in \left(0, s_{*,i}^{1/L}\right)$ and $\rho_{i,2} \in \left(s_{*,i}^{1/L}, (2s_{*,i})^{1/L}\right)$ are two real roots of the polyno-
 255 mial $h(\rho) = 0$:

$$h(\rho) = \rho^L \cdot \frac{1 + (1 + \eta L(s_{*,i} - \rho^L) \cdot \rho^{L-2})^{2L-1}}{1 + (1 + \eta L(s_{*,i} - \rho^L) \cdot \rho^{L-2})^{L-1}} - s_{*,i}.$$

256 From Lemma 1, we observe that DLNs exhibit additional dominant curvature directions that are not
 257 present in diagonal linear networks—specifically, the eigenvalues corresponding to the “interaction
 258 with other singular values” are absent in diagonal linear networks. These eigenvalues arise due to

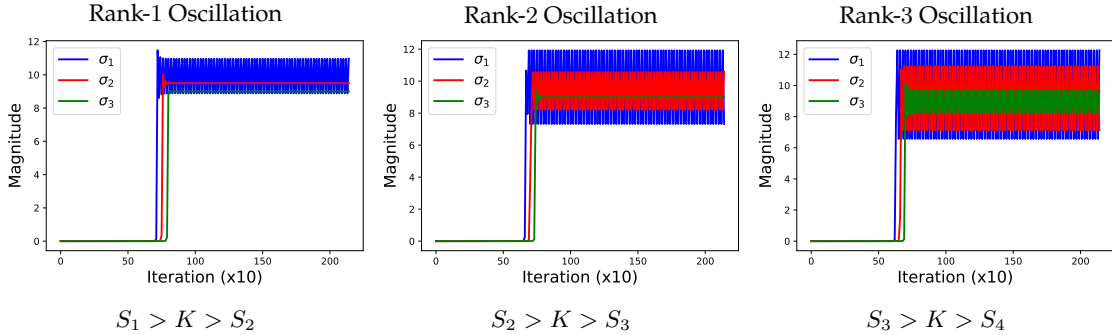


Figure 6: Evolution of the singular values of the end-to-end 3-layer network for fitting a rank-3 target matrix with singular values 10, 9.5, and 9. We use a learning rate of $\eta = 2/S_i$ with $S_i := L\sigma_{*,i}^{2-2/L}$. The oscillations occur exactly with learning rate ranges specified in Theorem 2.

259 the zero off-diagonal elements of the singular value diagonal matrix in (4). However, despite these
 260 extra directions, Theorem 3 demonstrates that the behavior of diagonal linear networks and DLNs is
 261 essentially the same. This can be understood using the argument from Theorem 1: the eigenvectors
 262 corresponding to these directions are always orthogonal to the flattened weights $\tilde{\Delta}$, thereby making
 263 the behaviors of the two network types synonymous, even in the EOS regime.

264 4. Experimental Results

265 4.1. Subspace Oscillations in Deep Networks

266 Firstly, we provide experimental results corroborating Theorem 2. We let the target matrix be
 267 $\mathbf{M}_* \in \mathbb{R}^{50 \times 50}$ with rank 3, with dominant singular values $\sigma_* = 10, 9.5, 9$. For the DLN, we con-
 268 sider a 3-layer network, with each layer as $\mathbf{W}_\ell \in \mathbb{R}^{50 \times 50}$ and use an initialization scale of $\alpha = 0.01$.
 269 In Figure 6, we present the behaviors of the singular values of
 270 the end-to-end network under different learning rate regimes.
 271 Recall that by Theorem 2, the i -th singular value undergoes
 272 periodic oscillations when K is set to be $S_i < K < S_{i+1}$,
 273 where $S_i = L\sigma_{*,i}^{2-2/L}$. Figure 6 illustrates this clearly – we only
 274 observe oscillations in the i -th coordinate depending on the
 275 learning rate. Interestingly, notice that σ_2 also begins to os-
 276 cillate in the rank-1 oscillation region before settling at a min-
 277 imum. This occurs because, while the learning rate is large
 278 enough to catapult out of a minimum, it is not sufficiently large
 279 to induce periodic oscillations.

280 In Figure 7, we present an experiment demonstrating the rela-
 281 tionship between the oscillation range and the learning rate by
 282 plotting the amplitude of the singular value oscillations in the
 283 end-to-end network. The oscillations begin to occur starting
 284 from each region $\eta = 2/S_i$, and the oscillation range (or amplitude) increases as the learning rate
 285 increases. This can also be observed in Figure 6; the amplitude of σ_1 increases as we move from the
 286 rank-1 to the rank-3 oscillation region.

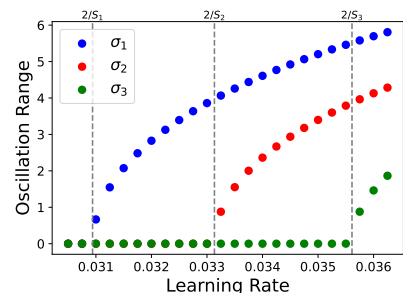
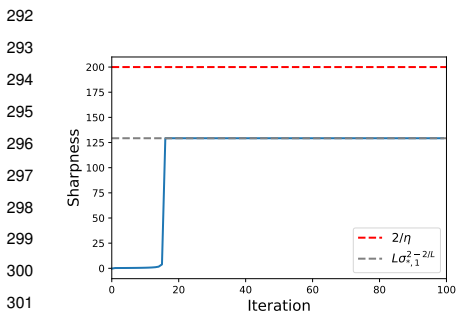


Figure 7: Oscillation range as a function of the learning rate.

287 4.2. Similarities and Differences Between Linear and Nonlinear Nets at EOS

288 **Mild Sharpening.** “Mild” sharpening refers to the sharpness not rising to $2/\eta$ throughout learn-
 289 ing, and generally occurs in tasks with low complexity as discussed in Caveat 2 of [1]. We il-

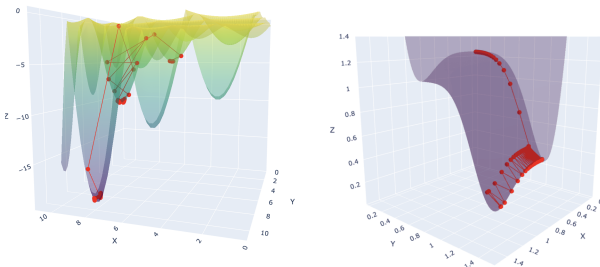
290 illustrate mild sharpening in Figure 10, where we plot sharpness in two settings: (i) regression
 291 with simple images and (ii) classification with an MLP using a subset of the CIFAR-10 dataset.



303 Figure 8: DLNs do not enter EOS
 304 regime if $L\sigma_{*1}^{2-\frac{2}{L}} < 2/\eta$.

307 The intrinsic dimension update in neural networks for such low complexity tasks is usually smaller
 308 [36] which could cause the sharpness to be small. Similar observations can also be seen in DLNs. In
 309 Figure 8, we show that the sharpness reaches $L\sigma_{*,1}^{2-\frac{2}{L}}$, where $\sigma_{*,1}$ is the singular value of the target
 310 matrix. Whenever $L\sigma_{*,1}^{2-\frac{2}{L}} < 2/\eta$, the network will not enter the EOS regime. This can be viewed
 311 as low-complexity learning, as $\sigma_{*,1}$ corresponds to the magnitude of the strongest feature of the
 312 target matrix. Hence, when $\sigma_{*,1}$ is not large enough, the sharpness will not rise to $2/\eta$. While these
 313 observations do not fully explain mild sharpening, our experiments demonstrate that interpreting
 314 sharpness as a measure of complexity, combined with our findings from DLNs, marks an important
 315 first step toward fully understanding this phenomenon.

316 **Difference in Oscillation Behaviors.** Here, we discuss the differences in oscillations that arise in
 317 DLNs compared to catapults that occur in practical deep nonlinear networks. The main differ-
 318 ence lies in the loss landscape—at convergence, the Hessian for DLNs is positive semi-definite,
 319 as shown in Lemma 1, meaning there are only directions of positive curvature and flat direc-
 320 tions (in the null space of the Hessian). In this landscape, oscillations occur because the basin
 321 walls bounce off, without the direction of escape. However, in deep nonlinear networks, it
 322 has been frequently observed that the Hessian at the minima has negative eigenvalues [37, 38].
 323 This enables an escape direction along the negative curvature, preventing sustained oscillations.
 324 In Figure 9, we demonstrate these two differences by visualizing the loss land-
 325 scapes and the iterates throughout GD marked in red. The Holder table function Figure 9 (left)
 326 exhibits numerous local minima, causing the loss to exhibit a sharp “catapult” when a large learn-
 327 ing rate is used. In contrast, for DLNs (shown in the right) the loss oscillates in
 328 a periodic orbit around the minima since there are no spurious local minima [39–
 329 43].



336 Lastly, [5] studies self-stabilization, where sharpness decreases below $2/\eta$
 337 after initially exceeding $2/\eta$. Their analysis requires assumptions such as
 338 $\nabla L(\theta) \cdot u(\theta) = 0$ and $\nabla S(\theta)$ lies in the null space of the Hessian, where $S(\theta)$ and $u(\theta)$
 339 denotes the sharpness and its corresponding
 340
 341

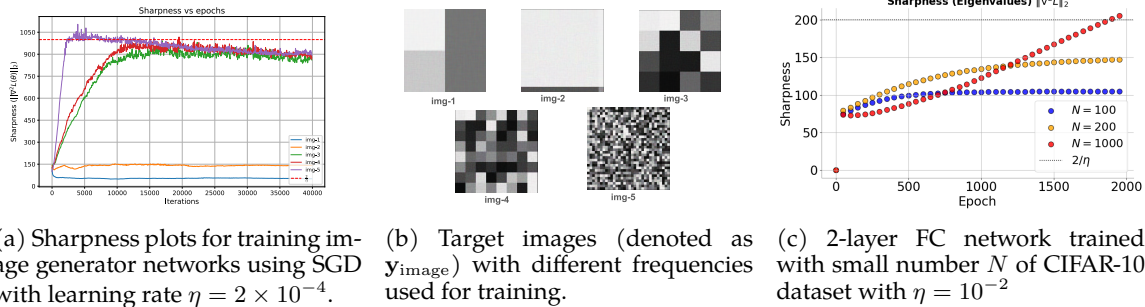


Figure 10: Illustration of Caveat 2 by [1] on how mild sharpening occurs on simple datasets and network. (a) Regression task showing the evolution of the sharpness when an UNet (with fixed initialization) is trained to fit a single image shown in (b). (c) Evolution of the minimal progressive sharpening on a classification task of a 2-layer MLP trained on a subset of CIFAR-10.

342 eigenvector respectively. These assumptions do not hold exactly in DLNs. Rather, the sharpness
 343 oscillates about $2/\eta$ as shown in Figure 2 as the condition for stable oscillation holds along each
 344 eigenvector of the Hessian.

345 5. Conclusion, Limitations and Future Work

346 In this paper, we presented a fine-grained analysis of the learning dynamics of deep matrix factor-
 347 ization with the aim of understanding unexplained phenomena in deep nonlinear networks within
 348 the EOS regime. Our analysis revealed that within EOS, DLNs exhibit periodic oscillations in small
 349 subspaces, where the subspace dimension is exactly characterized by the learning rate. There are
 350 two limitations to our work: we require (i) the dynamics converge to the singular vector station-
 351 ary set, and (ii) strict balancing of the singular values. However, we provide thorough empirical
 352 evidence validating the use of these assumptions, along with more results in Appendix B. For the
 353 balancing assumption, we leave for future work on alleviating the assumption of strict balancing,
 354 and rigorously show that this holds before entering the EOS regime.

References

- 355
- 356 [1] Jeremy Cohen, Simran Kaur, Yuanzhi Li, J Zico Kolter, and Ameet Talwalkar. Gradient de-
357 scent on neural networks typically occurs at the edge of stability. In *International Conference on*
358 *Learning Representations*, 2021. URL <https://openreview.net/forum?id=jh-rTtvkGeM>.
- 359 [2] Libin Zhu, Chaoyue Liu, Adityanarayanan Radhakrishnan, and Mikhail Belkin. Catapults in
360 SGD: spikes in the training loss and their impact on generalization through feature learning.
361 *arXiv preprint arXiv:2306.04815*, 2023.
- 362 [3] Soufiane Hayou, Nikhil Ghosh, and Bin Yu. LoRA+: Efficient low rank adaptation of
363 large models. In *Forty-first International Conference on Machine Learning*, 2024. URL <https://openreview.net/forum?id=NEv8YqBR00>.
364
- 365 [4] Aitor Lewkowycz, Yasaman Bahri, Ethan Dyer, Jascha Sohl-Dickstein, and Guy Gur-Ari.
366 The large learning rate phase of deep learning: the catapult mechanism. *arXiv preprint*
367 *arXiv:2003.02218*, 2020.
- 368 [5] Alex Damian, Eshaan Nichani, and Jason D. Lee. Self-stabilization: The implicit bias of gra-
369 dient descent at the edge of stability. In *The Eleventh International Conference on Learning Repre-*
370 *sentations*, 2023. URL <https://openreview.net/forum?id=nhKHA59gXz>.
- 371 [6] Nitish Shirish Keskar, Dheevatsa Mudigere, Jorge Nocedal, Mikhail Smelyanskiy, and Ping
372 Tak Peter Tang. On large-batch training for deep learning: Generalization gap and sharp min-
373 ima. In *International Conference on Learning Representations*, 2017. URL <https://openreview.net/forum?id=H1oyRLYgg>.
374
- 375 [7] Pavel Izmailov, Dmitrii Podoprikin, Timur Garipov, Dmitry Vetrov, and Andrew Gordon
376 Wilson. Averaging weights leads to wider optima and better generalization. *arXiv preprint*
377 *arXiv:1803.05407*, 2019. URL <https://arxiv.org/abs/1803.05407>.
- 378 [8] Henning Petzka, Michael Kamp, Linara Adilova, Cristian Sminchisescu, and Mario Boley. Rel-
379 ative flatness and generalization. In *Advances in Neural Information Processing Systems*, 2021.
380 URL https://openreview.net/forum?id=sygv07ctb_.
- 381 [9] Pierre Foret, Ariel Kleiner, Hossein Mobahi, and Behnam Neyshabur. Sharpness-aware min-
382 imization for efficiently improving generalization. In *International Conference on Learning Rep-*
383 *resentations*, 2021. URL <https://openreview.net/forum?id=6Tm1mpos1rM>.
- 384 [10] Khashayar Gatmiry, Zhiyuan Li, Tengyu Ma, Sashank J. Reddi, Stefanie Jegelka, and Ching-
385 Yao Chuang. What is the inductive bias of flatness regularization? A study of deep matrix
386 factorization models. In *Thirty-seventh Conference on Neural Information Processing Systems*, 2023.
387 URL <https://openreview.net/forum?id=2hQ7MBQApp>.
- 388 [11] Xingyu Zhu, Zixuan Wang, Xiang Wang, Mo Zhou, and Rong Ge. Understanding edge-of-
389 stability training dynamics with a minimalist example. In *The Eleventh International Conference*
390 *on Learning Representations*, 2023. URL <https://openreview.net/forum?id=p7EagBsMAEO>.
- 391 [12] Yuqing Wang, Zhenghao Xu, Tuo Zhao, and Molei Tao. Good regularity creates large learn-
392 ing rate implicit biases: edge of stability, balancing, and catapult. In *NeurIPS 2023 Workshop*
393 *on Mathematics of Modern Machine Learning*, 2023. URL <https://openreview.net/forum?id=6015A3h2y1>.
394
- 395 [13] Itai Kreisler, Mor Shpigel Nacson, Daniel Soudry, and Yair Carmon. Gradient descent mono-
396 tonically decreases the sharpness of gradient flow solutions in scalar networks and beyond. In
397 *International Conference on Machine Learning*, pages 17684–17744. PMLR, 2023.
- 398 [14] Atish Agarwala, Fabian Pedregosa, and Jeffrey Pennington. Second-order regression models
399 exhibit progressive sharpening to the edge of stability. *arXiv preprint arXiv:2210.04860*, 2022.

- 400 [15] Mathieu Even, Scott Pesme, Suriya Gunasekar, and Nicolas Flammarion. (S)GD over diag-
401 onal linear networks: Implicit bias, large stepsizes and edge of stability. *Advances in Neural*
402 *Information Processing Systems*, 36, 2024.
- 403 [16] Lei Chen and Joan Bruna. Beyond the edge of stability via two-step gradient updates, 2023.
- 404 [17] Andrew M. Saxe, James L. McClelland, and Surya Ganguli. Exact solutions to the nonlinear
405 dynamics of learning in deep linear neural networks. In *2nd International Conference on Learning*
406 *Representations, ICLR*, 2014. URL <http://arxiv.org/abs/1312.6120>.
- 407 [18] Sanjeev Arora, Nadav Cohen, and Elad Hazan. On the optimization of deep networks: Implicit
408 acceleration by overparameterization. In *International conference on machine learning*, pages 244–
409 253. PMLR, 2018.
- 410 [19] Sanjeev Arora, Nadav Cohen, Wei Hu, and Yuping Luo. Implicit regularization in
411 deep matrix factorization. In *Advances in Neural Information Processing Systems*, vol-
412 ume 32, 2019. URL [https://proceedings.neurips.cc/paper_files/paper/2019/file/](https://proceedings.neurips.cc/paper_files/paper/2019/file/c0c783b5fc0d7d808f1d14a6e9c8280d-Paper.pdf)
413 [c0c783b5fc0d7d808f1d14a6e9c8280d-Paper.pdf](https://proceedings.neurips.cc/paper_files/paper/2019/file/c0c783b5fc0d7d808f1d14a6e9c8280d-Paper.pdf).
- 414 [20] Chong You, Zhihui Zhu, Qing Qu, and Yi Ma. Robust recovery via implicit bias of discrepant
415 learning rates for double over-parameterization. *Advances in Neural Information Processing Sys-*
416 *tems*, 33:17733–17744, 2020.
- 417 [21] Sheng Liu, Zhihui Zhu, Qing Qu, and Chong You. Robust training under label noise by over-
418 parameterization. In *International Conference on Machine Learning*, pages 14153–14172. PMLR,
419 2022.
- 420 [22] Xitong Zhang, Ismail R Alkhouri, and Rongrong Wang. Structure-preserving network com-
421 pression via low-rank induced training through linear layers composition. *arXiv preprint*
422 *arXiv:2405.03089*, 2024.
- 423 [23] Scott Pesme and Nicolas Flammarion. Saddle-to-saddle dynamics in diagonal linear networks.
424 *Advances in Neural Information Processing Systems*, 36:7475–7505, 2023.
- 425 [24] Arthur Jacot, François Ged, Berfin Şimşek, Clément Hongler, and Franck Gabriel. Saddle-to-
426 saddle dynamics in deep linear networks: Small initialization training, symmetry, and sparsity.
427 *arXiv preprint arXiv:2106.15933*, 2022.
- 428 [25] Peng Wang, Xiao Li, Can Yaras, Zhihui Zhu, Laura Balzano, Wei Hu, and Qing Qu. Under-
429 standing deep representation learning via layerwise feature compression and discrimination.
430 *arXiv preprint arXiv:2311.02960*, 2024. URL <https://arxiv.org/abs/2311.02960>.
- 431 [26] Yedi Zhang, Andrew M Saxe, and Peter E. Latham. When are bias-free reLU networks like
432 linear networks? In *High-dimensional Learning Dynamics 2024: The Emergence of Structure and*
433 *Reasoning*, 2024. URL <https://openreview.net/forum?id=LdYBMeWOG3>.
- 434 [27] Can Yaras, Peng Wang, Wei Hu, Zhihui Zhu, Laura Balzano, and Qing Qu. The law of parsimony
435 in gradient descent for learning deep linear networks. *arXiv preprint arXiv:2306.01154*,
436 2023.
- 437 [28] Edward Ott. *Chaos in Dynamical Systems*. Cambridge University Press, 2 edition, 2002.
- 438 [29] Aditya Vardhan Varre, Maria-Luiza Vladarean, Loucas PILLAUD-VIVIEN, and
439 Nicolas Flammarion. On the spectral bias of two-layer linear networks. In *Ad-*
440 *vances in Neural Information Processing Systems*, volume 36, pages 64380–64414,
441 2023. URL [https://proceedings.neurips.cc/paper_files/paper/2023/file/](https://proceedings.neurips.cc/paper_files/paper/2023/file/cad2fd66cf88226d868f90a7cbaa4a53-Paper-Conference.pdf)
442 [cad2fd66cf88226d868f90a7cbaa4a53-Paper-Conference.pdf](https://proceedings.neurips.cc/paper_files/paper/2023/file/cad2fd66cf88226d868f90a7cbaa4a53-Paper-Conference.pdf).

- 443 [30] Zhenghao Xu, Yuqing Wang, Tuo Zhao, Rachel Ward, and Molei Tao. Provable acceleration of
444 nesterov’s accelerated gradient for rectangular matrix factorization and linear neural networks.
445 *arXiv preprint arXiv:2410.09640*, 2024.
- 446 [31] Gauthier Gidel, Francis Bach, and Simon Lacoste-Julien. Implicit regularization of discrete
447 gradient dynamics in linear neural networks. In *Advances in Neural Information Processing Sys-*
448 *tems*, volume 32, 2019. URL [https://proceedings.neurips.cc/paper_files/paper/2019/](https://proceedings.neurips.cc/paper_files/paper/2019/file/f39ae9ff3a81f499230c4126e01f421b-Paper.pdf)
449 [file/f39ae9ff3a81f499230c4126e01f421b-Paper.pdf](https://proceedings.neurips.cc/paper_files/paper/2019/file/f39ae9ff3a81f499230c4126e01f421b-Paper.pdf).
- 450 [32] Hung-Hsu Chou, Carsten Gieshoff, Johannes Maly, and Holger Rauhut. Gradient descent for
451 deep matrix factorization: Dynamics and implicit bias towards low rank. *Applied and Compu-*
452 *tational Harmonic Analysis*, 68:101595, 2024.
- 453 [33] Soo Min Kwon, Zekai Zhang, Dogyoon Song, Laura Balzano, and Qing Qu. Efficient low-
454 dimensional compression of overparameterized models. In *Proceedings of The 27th International*
455 *Conference on Artificial Intelligence and Statistics*, volume 238 of *Proceedings of Machine Learning*
456 *Research*, pages 1009–1017. PMLR, 02–04 May 2024. URL [https://proceedings.mlr.press/](https://proceedings.mlr.press/v238/min-kwon24a.html)
457 [v238/min-kwon24a.html](https://proceedings.mlr.press/v238/min-kwon24a.html).
- 458 [34] Yuqing Wang, Minshuo Chen, Tuo Zhao, and Molei Tao. Large learning rate tames homogene-
459 ity: Convergence and balancing effect. *arXiv preprint arXiv:2110.03677*, 2021.
- 460 [35] Tian Ye and Simon S Du. Global convergence of gradient descent for asymmetric low-rank
461 matrix factorization. *Advances in Neural Information Processing Systems*, 34:1429–1439, 2021.
- 462 [36] Chunyuan Li, Heerad Farkhoor, Rosanne Liu, and Jason Yosinski. Measuring the intrinsic
463 dimension of objective landscapes. *arXiv preprint arXiv:1804.08838*, 2018.
- 464 [37] Behrooz Ghorbani, Shankar Krishnan, and Ying Xiao. An investigation into neural net opti-
465 mization via hessian eigenvalue density. In *International Conference on Machine Learning*, pages
466 2232–2241. PMLR, 2019.
- 467 [38] Levent Sagun, Leon Bottou, and Yann LeCun. Eigenvalues of the hessian in deep learning:
468 Singularity and beyond. *arXiv preprint arXiv:1611.07476*, 2016.
- 469 [39] Rong Ge, Jason D Lee, and Tengyu Ma. Matrix completion has no spurious local minimum.
470 *Advances in neural information processing systems*, 29, 2016.
- 471 [40] Kenji Kawaguchi. Deep learning without poor local minima. *Advances in neural information*
472 *processing systems*, 29, 2016.
- 473 [41] Haihao Lu and Kenji Kawaguchi. Depth creates no bad local minima. *arXiv preprint*
474 *arXiv:1702.08580*, 2017.
- 475 [42] Li Zhang. Depth creates no more spurious local minima. *arXiv preprint arXiv:1901.09827*, 2019.
- 476 [43] Chulhee Yun, Suvrit Sra, and Ali Jadbabaie. Small nonlinearities in activation functions create
477 bad local minima in neural networks. *arXiv preprint arXiv:1802.03487*, 2018.
- 478 [44] Stanislaw Jastrzebski, Maciej Szymczak, Stanislav Fort, Devansh Arpit, Jacek Tabor,
479 Kyunghyun Cho, and Krzysztof Geras. The break-even point on optimization trajectories of
480 deep neural networks. *arXiv preprint arXiv:2002.09572*, 2020.
- 481 [45] Stanisław Jastrzębski, Zachary Kenton, Nicolas Ballas, Asja Fischer, Yoshua Bengio, and Amos
482 Storkey. On the relation between the sharpest directions of dnn loss and the sgd step length.
483 *arXiv preprint arXiv:1807.05031*, 2018.
- 484 [46] Sanjeev Arora, Zhiyuan Li, and Abhishek Panigrahi. Understanding gradient descent on the
485 edge of stability in deep learning. In *International Conference on Machine Learning*, pages 948–
486 1024. PMLR, 2022.

- 487 [47] Kaifeng Lyu, Zhiyuan Li, and Sanjeev Arora. Understanding the generalization benefit of
488 normalization layers: Sharpness reduction. *Advances in Neural Information Processing Systems*,
489 35:34689–34708, 2022.
- 490 [48] Kwangjun Ahn, Sébastien Bubeck, Sinho Chewi, Yin Tat Lee, Felipe Suarez, and Yi Zhang.
491 Learning threshold neurons via edge of stability. *Advances in Neural Information Processing*
492 *Systems*, 36, 2024.
- 493 [49] Zixuan Wang, Zhouzi Li, and Jian Li. Analyzing sharpness along gd trajectory: Progressive
494 sharpening and edge of stability. *Advances in Neural Information Processing Systems*, 35:9983–
495 9994, 2022.
- 496 [50] Jingfeng Wu, Vladimir Braverman, and Jason D Lee. Implicit bias of gradient descent for
497 logistic regression at the edge of stability. *Advances in Neural Information Processing Systems*, 36,
498 2024.
- 499 [51] Minhak Song and Chulhee Yun. Trajectory alignment: understanding the edge of stability
500 phenomenon via bifurcation theory. *arXiv preprint arXiv:2307.04204*, 2023.
- 501 [52] Dayal Singh Kalra, Tianyu He, and Maissam Barkeshli. Universal sharpness dynamics in neural
502 network training: Fixed point analysis, edge of stability, and route to chaos. *arXiv preprint*
503 *arXiv:2311.02076*, 2023.
- 504 [53] Libin Zhu, Chaoyue Liu, Adityanarayanan Radhakrishnan, and Mikhail Belkin. Quadratic
505 models for understanding neural network dynamics. *arXiv preprint arXiv:2205.11787*, 2022.
- 506 [54] Xuxing Chen, Krishnakumar Balasubramanian, Promit Ghosal, and Bhavya Agrawalla. From
507 stability to chaos: Analyzing gradient descent dynamics in quadratic regression. *arXiv preprint*
508 *arXiv:2310.01687*, 2023.
- 509 [55] Daniel Gissin, Shai Shalev-Shwartz, and Amit Daniely. The implicit bias of depth: How incre-
510 mental learning drives generalization. In *International Conference on Learning Representations*,
511 2020. URL <https://openreview.net/forum?id=H1ljOnNFwB>.
- 512 [56] Hung-Hsu Chou, Carsten Gieshoff, Johannes Maly, and Holger Rauhut. Gradient descent
513 for deep matrix factorization: Dynamics and implicit bias towards low rank. *Applied and*
514 *Computational Harmonic Analysis*, 68:101595, 2024. ISSN 1063-5203. doi: <https://doi.org/10.1016/j.acha.2023.101595>. URL <https://www.sciencedirect.com/science/article/pii/S1063520323000829>.
- 517 [57] Can Yaras, Peng Wang, Laura Balzano, and Qing Qu. Compressible dynamics in deep overpa-
518 rameterized low-rank learning & adaptation. In *Forty-first International Conference on Machine*
519 *Learning*, 2024. URL <https://openreview.net/forum?id=uDkXoZMzBv>.
- 520 [58] Edward J Hu, yelong shen, Phillip Wallis, Zeyuan Allen-Zhu, Yanzhi Li, Shean Wang,
521 Lu Wang, and Weizhu Chen. LoRA: Low-rank adaptation of large language models. In *Inter-*
522 *national Conference on Learning Representations*, 2022. URL [https://openreview.net/forum?](https://openreview.net/forum?id=nZeVKeeFYf9)
523 [id=nZeVKeeFYf9](https://openreview.net/forum?id=nZeVKeeFYf9).
- 524 [59] Alex Wang, Amanpreet Singh, Julian Michael, Felix Hill, Omer Levy, and Samuel R. Bowman.
525 GLUE: A multi-task benchmark and analysis platform for natural language understanding.
526 In *International Conference on Learning Representations*, 2019. URL [https://openreview.net/](https://openreview.net/forum?id=rJ4km2R5t7)
527 [forum?id=rJ4km2R5t7](https://openreview.net/forum?id=rJ4km2R5t7).
- 528 [60] Leon Mirsky. A trace inequality of John von Neumann. *Monatshefte für mathematik*, 79(4):
529 303–306, 1975.
- 530 [61] Pierre Marion and Lénaïc Chizat. Deep linear networks for regression are implicitly regular-
531 ized towards flat minima. *arXiv preprint arXiv:2405.13456*, 2024.

532

533

534

Appendix

535 Contents

536	1. Introduction	1
537	2. Notation and Problem Setup	3
538	3. Deep Matrix Factorization Beyond the Edge of Stability	4
539	3.1. Main Results	4
540	3.2. Assumptions and Analytical Tools	7
541	3.3. Relation to Diagonal Linear Networks	8
542	4. Experimental Results	9
543	4.1. Subspace Oscillations in Deep Networks	9
544	4.2. Similarities and Differences Between Linear and Nonlinear Nets at EOS	9
545	5. Conclusion, Limitations and Future Work	11
546	A Discussion on Related Work	16
547	B Additional Results	17
548	B.1. Experimental Details	17
549	B.2. Initialization Outside Singular Vector Invariant Set	19
550	B.3. Balancing of Singular Values	19
551	B.4. Additional Experiments for Balancing, Singular Vector Invariance, and Theory	21
552	B.5. Periodic and Free Oscillations	23
553	B.6. Investigation of Oscillations in Low-Rank Adaptors	25
554	C Deferred Proofs	29
555	C.1. Deferred Proofs for Oscillations	29
556	C.2. Deferred Proofs for Singular Vector Invariance	53
557	C.3. Auxiliary Results	55

558 A. Discussion on Related Work

559 **Implicit Bias of Edge of Stability.** Edge of stability was first coined by [1], where they showed
560 that the Hessian of the training loss plateaus around $2/\eta$ when deep models were trained using
561 GD. However, [44, 45] previously demonstrated that the step size influences the sharpness along
562 the optimization trajectory. Due to the important practical implications of the edge of stability, there
563 has been an explosion of research dedicated to understanding this phenomenon and its implicit reg-
564 ularization properties. Here, we survey a few of these works. [5] explained edge of stability through

565 a mechanism called “self-stabilization”, where they showed that during the momentary divergence
 566 of the iterates along the sharpest eigenvector direction of the Hessian, the iterates also move along
 567 the negative direction of the gradient of the curvature, which leads to stabilizing the sharpness to
 568 $2/\eta$. [14] proved that second-order regression models (the simplest class of models after the lin-
 569 earized NTK model) demonstrate progressive sharpening of the NTK eigenvalue towards a slightly
 570 different value than $2/\eta$. [46] mathematically analyzed the edge of stability, where they showed that
 571 the GD updates evolve along some deterministic flow on the manifold of the minima. [47] showed
 572 that the normalization layers had an important role in the edge of stability – they showed that these
 573 layers encouraged GD to reduce the sharpness of the loss surface and enter the EOS regime. [48] es-
 574 tablished the phenomenon in two-layer networks and find phase transitions for step-sizes in which
 575 networks fail to learn “threshold” neurons. [49] also analyze a two-layer network, but provide a
 576 theoretical proof for the change in sharpness across four different phases. [15] analyzed the edge
 577 of stability in diagonal linear networks and found that oscillations occur on the sparse support of
 578 the vectors. Lastly, [50] analyzed the convergence at the edge of stability for constant step size GD
 579 for logistic regression on linearly separable data.

580 **Edge of Stability in Toy Functions.** To analyze the edge of stability in slightly simpler settings,
 581 many works have constructed scalar functions to analyze the prevalence of this phenomenon. For
 582 example, [16] studied a certain class of scalar functions and identified conditions in which the func-
 583 tion enters the edge of stability through a two-step convergence analysis. [12] showed that the edge
 584 of stability occurs in specific scalar functions, which satisfies certain regularity conditions and de-
 585 veloped a global convergence theory for a family of non-convex functions without globally Lipschitz
 586 continuous gradients. [11] analyzed local oscillatory behaviors for 4-layer scalar networks with bal-
 587 anced initialization. [51, 52] provide analyses of learning dynamics at the EOS in simplified settings
 588 such as two-layer networks. [53, 54] study GD dynamics for quadratic models in large learning rate
 589 regimes. Overall, all of these works showed that the necessary condition for the edge of stability
 590 to occur is that the second derivative of the loss function is non-zero, even though they assumed
 591 simple scalar functions. Our work takes one step further to analyze the prevalence of the edge of sta-
 592 bility in DLNs. Although our loss simplifies to a loss in terms of the singular values, they precisely
 593 characterize the dynamics of the DLNs for the deep matrix factorization problem.

594 **Deep Linear Networks.** Over the past decade, many existing works have analyzed the learning
 595 dynamics of DLNs as a surrogate for deep nonlinear networks to study the effects of depth and im-
 596 plicit regularization [17–19, 22]. Generally, these works focus on unveiling the dynamics of a phe-
 597 nomenon called “incremental learning”, where small initialization scales induce a greedy singular
 598 value learning approach [17, 33, 55], analyzing the learning dynamics via gradient flow [17, 19, 56],
 599 or showing that the DLN is biased towards low-rank solution [19, 33, 57], amongst others. How-
 600 ever, these works do not consider the occurrence of the edge of stability in such networks. On the
 601 other hand, while works such as those by [57] and [33] have similar observations in that the weight
 602 updates occur within an invariant subspace as shown by Proposition 2, they do not analyze the edge
 603 of stability regime.

604 B. Additional Results

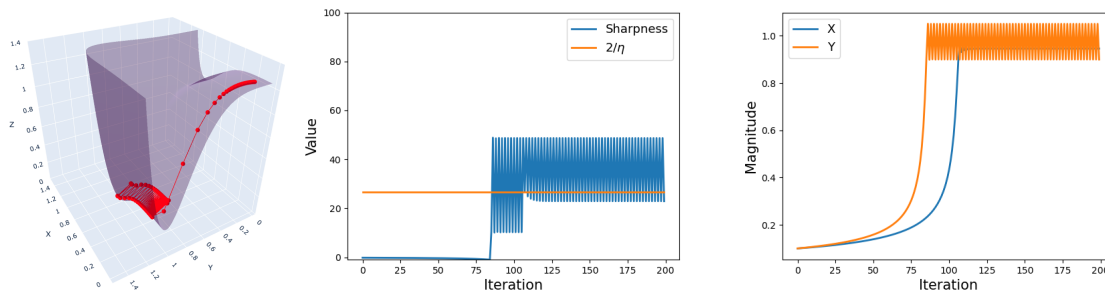
605 B.1. Experimental Details

606 In this section, we provide additional details regarding the experiments used to generate the figures
 607 in the main text. For Figure 1, we consider a rank-3 target matrix $\mathbf{M}_* \in \mathbb{R}^{5 \times 5}$ with ordered singular
 608 values 10, 6, 3. We use a 3-layer DLN to fit the target matrix. Since $\sigma_{*,1} = 10$, the network enters the
 609 EOS regime at

$$\eta = \frac{2}{L\sigma_{*,1}^{2-2/L}} = 0.0309.$$

610 We show that there exists a two-period orbit after $0.0309/2 = 0.0154$, as we do not have a scaling of
 611 $1/2$ in the objective function for the code used to generate the figures.

Oscillation along Y-axis: $2/\lambda_2 > \eta > 2/\lambda_1$



Oscillation along both X and Y-axis: $\eta > 2/\lambda_2$

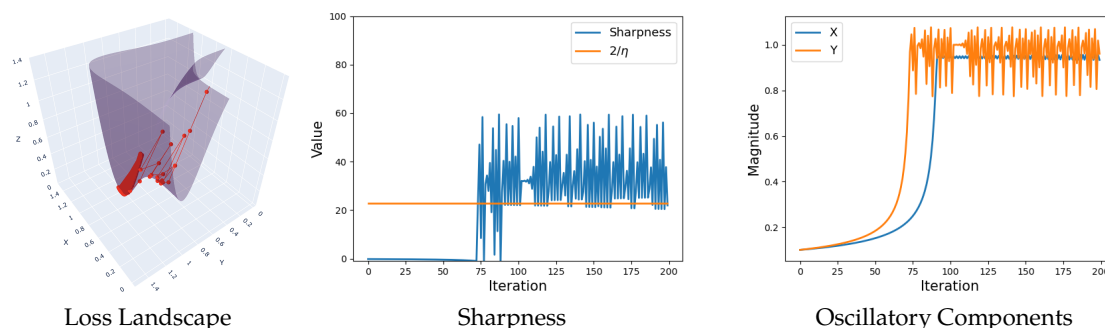


Figure 11: Demonstration of the EOS dynamics of a 2-dimensional depth-4 scalar network as shown in Equation (6). X, Y axes are the eigenvectors of the Hessian with eigenvalues λ_1 and λ_2 respectively. Top: when $\eta > 2/\lambda_1$, the X component remains fixed, while the Y component oscillates with a periodicity of 2. Bottom: for $\eta > 2/\lambda_2$, the iterates oscillate in both directions.

612 In Figure 9 and 11, we compared the landscape of DLNs with that of a more complicated non-convex
 613 function such as the Holder table function. To mimic the DLN, we considered the loss function

$$z = L(x, y) = (x^4 - 0.8)^2 + (y^4 - 1)^2, \quad (6)$$

614 which corresponds to a 4-layer network. Here the eigenvector of the Hessian at the global minima
 615 coincides with the x, y -axis. We calculate the eigenvalues λ_1 and λ_2 at the minimum $(0.8^{0.25}, 1)$ and
 616 plot the dynamics of the iterates for step size range $\frac{2}{\lambda_2} > \eta > \frac{2}{\lambda_1}$ and $\eta > \frac{2}{\lambda_2}$. When $\frac{2}{\lambda_2} > \eta > \frac{2}{\lambda_1}$ the
 617 x -coordinate stays fixed at the minima $0.8^{0.25}$ and the y -coordinate oscillates around its minimum at
 618 $y = 1$. This is evident in the landscape figure. Similarly, when $\eta > \frac{2}{\lambda_2}$, oscillations occur in both the
 619 x and y direction. The loss landscape $z = L(x, y)$ does not have spurious local minima, so sustained
 620 oscillations take place in the loss basin.

621 For the non-convex landscape as shown in Figure 9 and 12, we consider the Holder table function:

$$f(x, y) = - \left| \sin(x) \cos(y) \exp \left(1 - \frac{\sqrt{x^2 + y^2}}{\pi} \right) \right|.$$

622 By observation, we initialize near a sharp minima and run GD with an increasing learning rate step
 623 size as shown in the lefthand side of Figure 12. When the learning rate is fixed, we observe that
 624 oscillations take place inside the local valley, but when learning rate is increased, it jumps out of the
 625 local valley to find a flatter basin. Similar to the observations by [1], the sharpness of the GD iterates
 626 are “regulated” by the threshold $2/\eta$, as it seems to closely follow this value as shown in Figure 12.

627 Overall, these examples aim to highlight the difference in linear and complex loss landscapes. The
 628 former consists of *only* saddles and global minima, and hence (stably) oscillate about the global

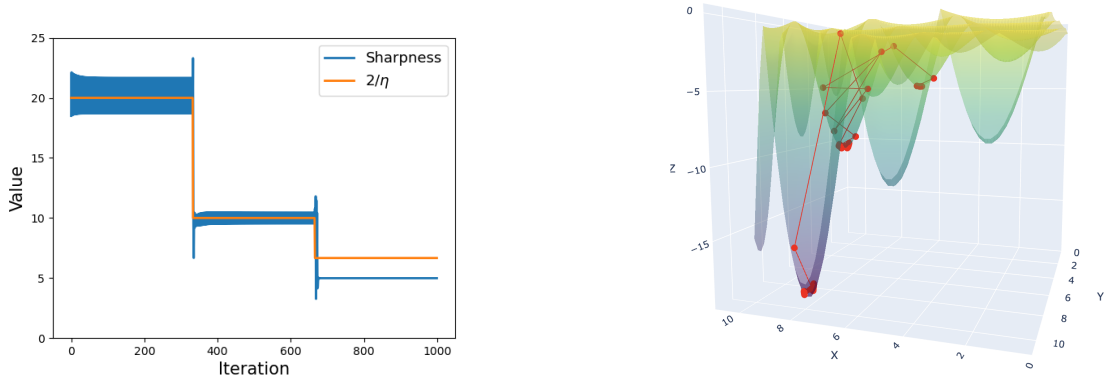


Figure 12: EOS dynamics at various step learning rates from the Holder table function. Left: plot of the learning rate steps and sharpness, showing that sharpness follows the EOS limit $2/\eta$. Right: Plot showing that the iterates catapult out of a local basin when the learning rate is increased and jumps out to a surface where the sharpness is about $2/\eta$.

629 minimum. However, in more complicated non-convex landscapes, sharpness regularization due to
 630 large learning rates enable catapulting to flatter loss basins, where sharpness is smaller than $2/\eta$.

631 B.2. Initialization Outside Singular Vector Invariant Set

632 In this section, we present an initialization example that is outside the singular vector stationary set.
 633 We consider the following initialization:

$$\mathbf{W}_L(0) = \mathbf{0}, \quad \mathbf{W}_\ell(0) = \alpha \mathbf{P}_\ell, \quad \forall \ell \in [L-1], \quad (7)$$

634 where $\mathbf{P}_\ell \in \mathbb{R}^{d \times d}$ is an orthogonal matrix. Note that here for $\ell > 1$, the singular vectors do not align
 635 and lies outside the SVS set we defined in Proposition 2. We consider the deep matrix factorization
 636 problem with a target matrix $\mathbf{M}_* \in \mathbb{R}^{d \times d}$, where $d = 100$, $r = 5$, and $\alpha = 0.01$. We empirically
 637 obtain that the decomposition after convergence admits the form:

$$\mathbf{W}_L(t) = \mathbf{U}^* \begin{bmatrix} \boldsymbol{\Sigma}_L(t) & \mathbf{0} \\ \mathbf{0} & \mathbf{0} \end{bmatrix} \left[\left(\prod_{i=L-1}^1 \mathbf{P}_i \right) \mathbf{V}^* \right]^\top, \quad (8)$$

$$\mathbf{W}_\ell(t) = \left[\left(\prod_{i=\ell}^1 \mathbf{P}_i \right) \mathbf{V}^* \right] \begin{bmatrix} \boldsymbol{\Sigma}_\ell(t) & \mathbf{0} \\ \mathbf{0} & \alpha \mathbf{I}_{d-r} \end{bmatrix} \left[\left(\prod_{i=\ell-1}^1 \mathbf{P}_i \right) \mathbf{V}^* \right]^\top, \quad \forall \ell \in [2, L-1], \quad (9)$$

$$\mathbf{W}_1(t) = \mathbf{P}_1 \mathbf{V}^* \begin{bmatrix} \boldsymbol{\Sigma}_1(t) & \mathbf{0} \\ \mathbf{0} & \alpha \mathbf{I}_{d-r} \end{bmatrix} \mathbf{V}^{*\top}, \quad (10)$$

638 where $\mathbf{W}_L(0) = \mathbf{0}$ and $\mathbf{W}_\ell(0) = \alpha \mathbf{P}_\ell, \forall \ell \in [L-1]$. The decomposition after convergence lies in
 639 the SVS set as the singular vectors now align with each other. This demonstrates an example where
 640 even when the initialization is made outside the SVS set, GD aligns the singular vectors such that
 641 after certain iterations it lies in the SVS set.

642 B.3. Balancing of Singular Values

643 In this section, we present additional experimental results on Lemma 2 and how close the iterates
 644 become for different initialization scales. To this end, we consider the same setup from the previous
 645 section, where we have a target matrix $\mathbf{M}_* \in \mathbb{R}^{d \times d}$, where $d = 100$, $r = 5$, and varying initialization
 646 α . In Figure 14, we observe that for larger values of α , the balancing quickly occurs, whereas for
 647 smaller values of α , the balancing is almost immediate. This is also highlight that our bound on
 648 α in Lemma 2 may be an artifact of our analysis, and can choose larger values of α in practice.

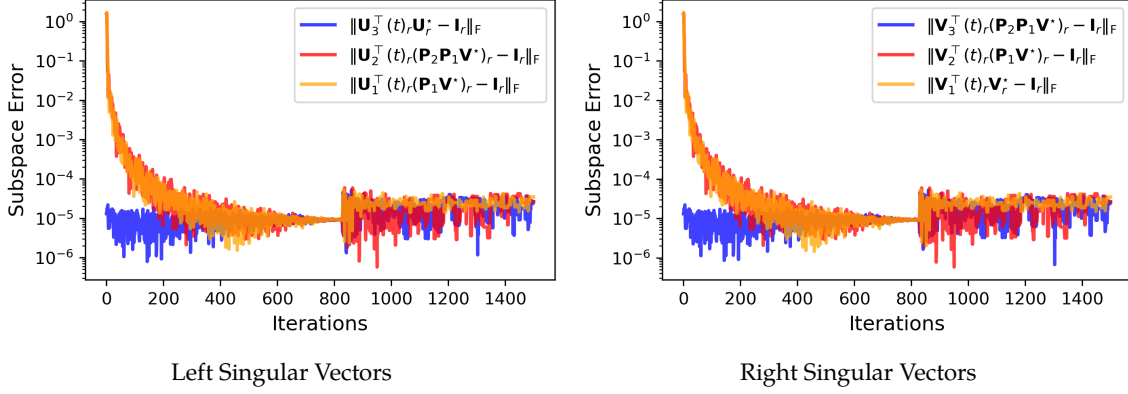


Figure 13: Empirical verification of the decomposition for initialization with orthogonal matrices (lying outside SVS set) in that after some GD iterations, the singular vectors of the intermediate matrices align to lie within SVS set, displaying singular vector invariance.

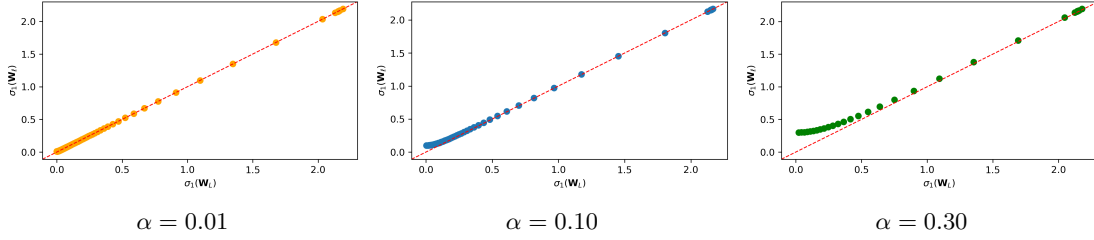


Figure 14: Observing the balancedness between the singular value initialized to 0 and a singular value initialized to α . The scattered points are successive GD iterations (going left to right). The initial gap between the two values is larger for a larger α , but quickly gets closer over more GD iterations.

649 **Balancing in the Stable Regime.** Here, we discuss the difference in the balancing of singular values
650 within the stable regime versus the EOS regime. In Figure 4, we noted that strict balancing and the
651 two-period orbit occur simultaneously, which we used as a basis for considering strict balancing in
652 our analyses. However, we observe that strict balancing does not actually occur within the stable
653 regime. To illustrate this, we present additional contour plots in Figure 15, following the setup in
654 Figure 4. When starting from an unbalanced initialization, GD tends to converge to any solution
655 that minimizes the objective function to zero (i.e., $\sigma_1\sigma_2 = 5$), which is not necessarily the balanced
656 solution.

657 In Figure 16, we plot the balancing gap between the singular value initialized to zero and the one
658 initialized to α for fitting a rank-3 matrix with singular values 10, 9.5, and 9 using a 3-layer DLN.
659 In the stable regime, where oscillations do not occur, the balancing gap plateaus. However, when
660 the learning rate is large enough to induce oscillations in the first singular value of the DLN, the
661 balancing gap for the first singular value strictly goes to zero. Similarly, when oscillations occur in
662 the second singular value, the balancing gap at the second index also goes to zero. This suggests
663 that the balancing gap strictly goes to zero only in the presence of oscillations (i.e., within the EOS
664 regime).

665 We provide intuition for why balancing does not occur in the stable regime as it does in the EOS
666 regime. In the proof for Lemma 2, we define the balancing dynamics between singular value σ_i and

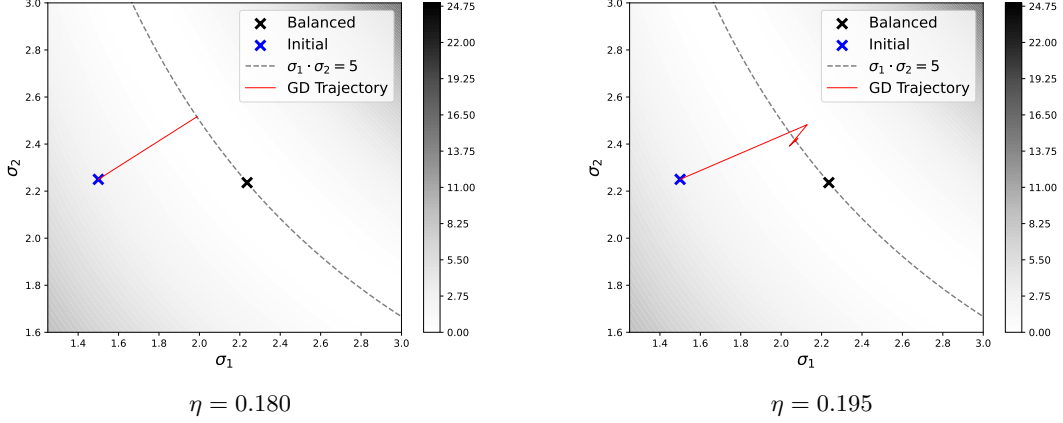


Figure 15: Illustration of the GD trajectories for two different learning rates for minimizing the function $f(\sigma_1, \sigma_2) = \frac{1}{2}(\sigma_2 \cdot \sigma_1 - 5)^2$, starting from an unbalanced initial point. The sharpness at the balanced minimum is 10, and so the learning rate needed to enter EOS is $\eta = 0.2$.

667 σ_j at iteration t as

$$\begin{aligned}
 b_{i,j}^{(t+1)} &:= \left(\sigma_i^{(t+1)}\right)^2 - \left(\sigma_j^{(t+1)}\right)^2 \\
 &= b_{i,j}^{(t)} \left(1 - \eta^2 (\pi^{(t)} - \sigma_\star)^2 \frac{(\pi^{(t)})^2}{\left(\sigma_i^{(t)}\right)^2 \left(\sigma_j^{(t)}\right)^2} \right),
 \end{aligned}$$

668 where $\pi^{(t)}$ denotes the product of the singular values across all layers at time t . Then, notice that in
 669 the stable regime, as soon as we reach a solution such that $\pi^{(t)} = \sigma_\star$, we obtain $b_{i,j}^{(t+1)} = b_{i,j}^{(t)}$, and so
 670 the balancing gap must plateau. However, in the EOS regime, we can never achieve $\pi^{(t)} = \sigma_\star$ due
 671 to oscillations, which allows the balancing gap to further decrease.

672 B.4. Additional Experiments for Balancing, Singular Vector Invariance, and 673 Theory

674 Our theory relied on two tools and assumptions: balancing of singular values and stationarity of
 675 the singular vectors. In this section, we investigate how the dynamics at EOS are affected if these
 676 two assumptions do not hold.

677 **Balancing.** By Lemma 2, recall that balancing only holds as long as α chosen below a certain thresh-
 678 old. To this end, we consider the dynamics of a 3-layer DLN to fit a target matrix $\mathbf{M}_\star \in \mathbb{R}^{10 \times 10}$ of
 679 rank-3 with ordered singular values 10, 8, 6. We use a learning rate of $\eta = 0.0166$, which corre-
 680 sponds to oscillations in the top-2 singular values. In Figure 17, we show the dynamics of when the
 681 initialization scale is $\alpha = 0.01$ and $\alpha = 0.5$, where balancing holds theoretically for the former but
 682 not for the latter. Clearly, we observe that balancing does not hold for $\alpha = 0.5$. However, examining
 683 the middle plots reveals that the oscillations in the singular values still have the same amplitude in
 684 both cases and for both singular values. This suggests that balancing is merely a tool for analysis,
 685 as the oscillations of interest remain prevalent in both scenarios.

686 **Singular Vector Stationarity.** Throughout this paper, we considered two initializations in Equa-
 687 tion (?), where balancing holds immediately and one where balancing holds for a sufficiently small
 688 initialization scale. In this section, we investigate different initializations with aim to observe (i) if
 689 they do not converge to the SVS set and (ii) how they affect the oscillations if they do not belong to

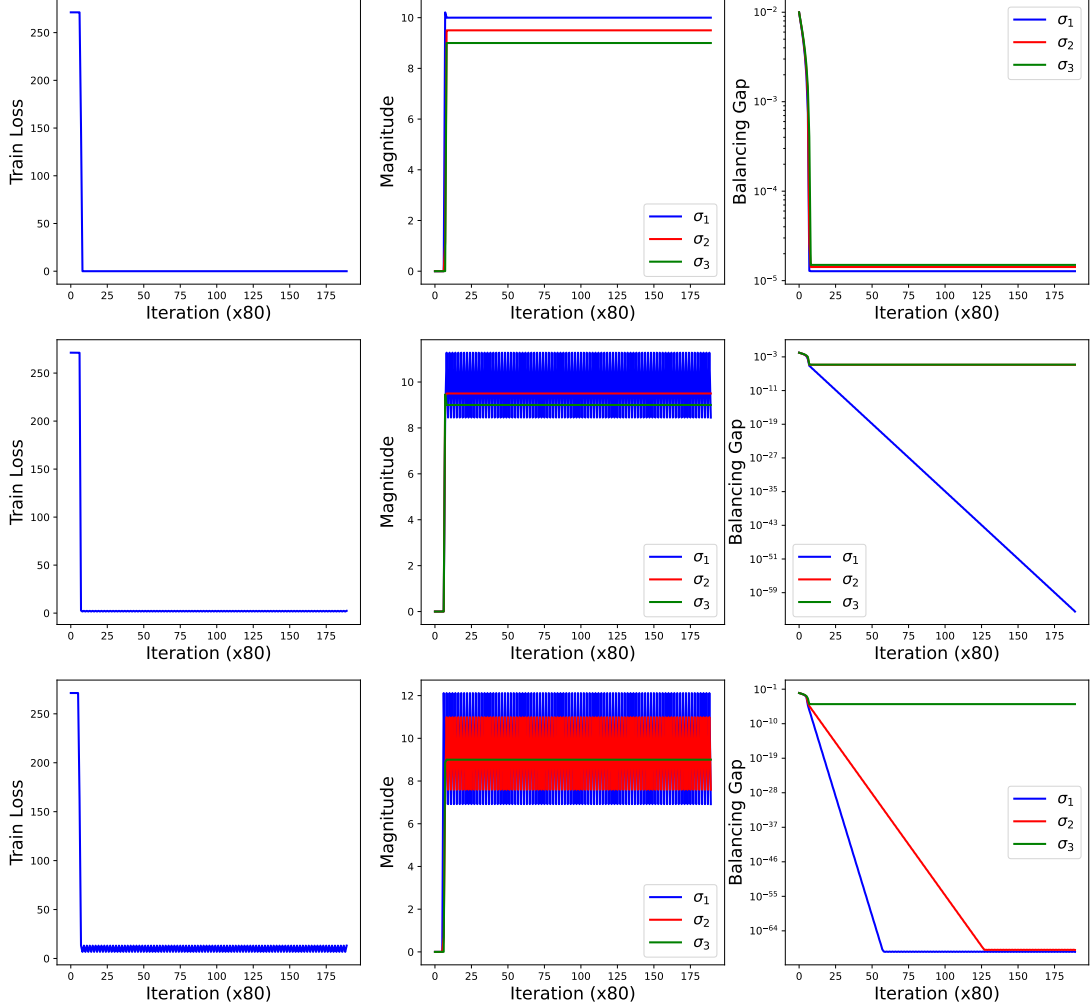


Figure 16: Plots of the training loss, singular value magnitude, and the balancing gap over iterations for different learning rates: $\eta = 0.030, 0.032, 0.034$ (top to bottom). When the learning rate is stable ($\eta < 0.031$ since the top singular value is $\sigma_{*,1} = 10$), the balancing gap plateaus, whereas the balancing gap goes strictly to zero when the oscillations occur.

690 the SVS set. To this end, we consider the following:

$$\mathbf{W}_L(0) = \mathbf{0}, \quad \mathbf{W}_\ell(0) = \alpha \mathbf{I}_d, \quad \forall \ell \in [L-1], \quad (\text{Original})$$

$$\mathbf{W}_L(0) = \mathbf{0}, \quad \mathbf{W}_\ell(0) = \alpha \mathbf{P}_\ell, \quad \forall \ell \in [L-1], \quad (\text{Orthogonal})$$

$$\mathbf{W}_L(0) = \mathbf{0}, \quad \mathbf{W}_\ell(0) = \alpha \mathbf{H}_\ell, \quad \forall \ell \in [L-1], \quad (\text{Random})$$

691 where \mathbf{P}_ℓ is an orthogonal matrix and \mathbf{H}_ℓ is a random matrix with Gaussian entries. For all of these
692 initialization schemes, we consider the same setup as in the balancing case, with an initialization
693 scale of $\alpha = 0.01$. To observe if singular vector stationarity holds, we consider the subspace distance
694 as follows:

$$\text{Subspace Distance} = \|\mathbf{U}_{\ell-1,r}^\top \mathbf{V}_{\ell,r} - \mathbf{I}_r\|_F, \quad (11)$$

695 where $\mathbf{U}_{\ell,r}$ and $\mathbf{V}_{\ell,r}$ are the top- r left and right singular vectors of layer \mathbf{W}_ℓ , respectively. Since
696 Proposition 1 implies that the intermediate singular vectors cancel, the initialization converges to
697 the SVS set if the subspace distance goes to zero. In Figure 18, we plot the dynamics for all of the
698 initializations. Generally, we observe that the subspace distance for all cases go to zero, validating
699 the use of the SVS set for analysis purposes.

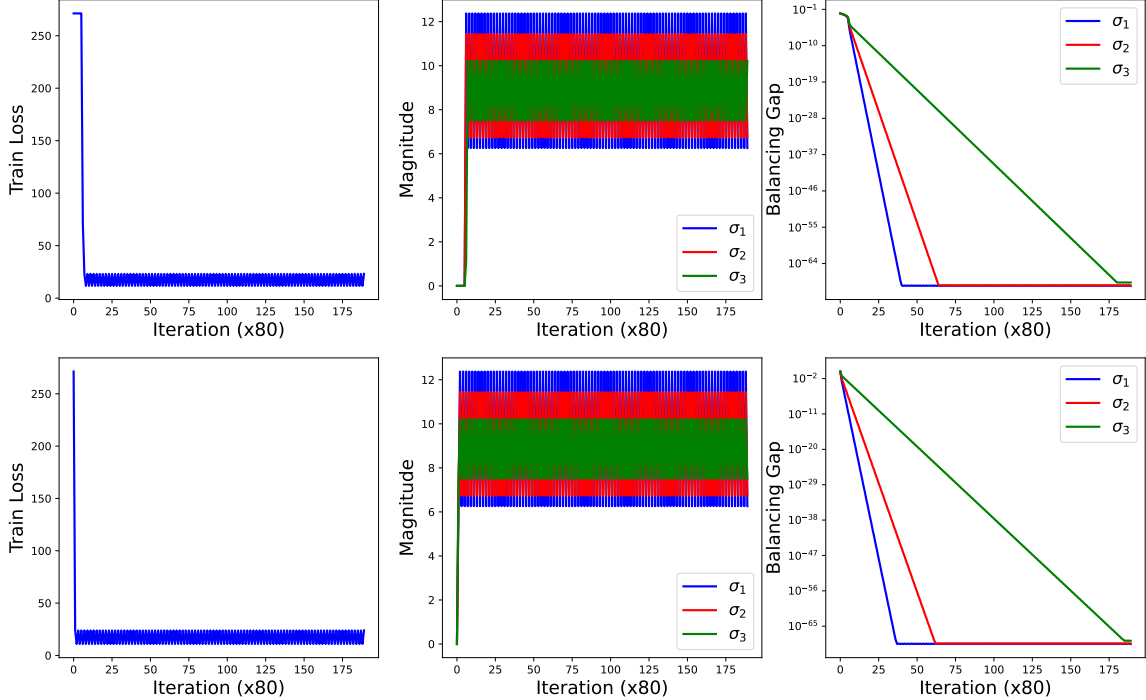


Figure 17: Top: EOS dynamics of a 3-layer DLN with initialization scale $\alpha = 0.01$, where balancing theoretically holds. Bottom: EOS dynamics of the DLN with initialization scale $\alpha = 0.5$. While the balancing does not hold for $\alpha = 0.5$, the oscillations in the singular values are still prevalent, with the same amplitude.

700 **Additional Results.** In this section, we provide more experimental results to corroborate our theory. Recall that in Lemma 1, we proved that the learning rate needed to enter the EOS is a function of the depth, and that deeper networks can enter EOS using a smaller learning rate. To verify this claim, we provide an additional experiment where the target matrix is $\mathbf{M}_* \in \mathbb{R}^{5 \times 5}$ with the top singular value set to $\sigma_{*,1} = 0.5$. We use an initialization scale of $\alpha = 0.01$. In Figure 19, we can clearly see that shallower networks need a larger learning rate, and vice versa to enter EOS. Here, black refers to stable learning and white refers to regions in which oscillations occur (EOS regime).

707 B.5. Periodic and Free Oscillations

708 In this section, we present additional experiments on oscillation and catapults in both deep linear
709 and nonlinear networks to supplement the results in the main paper. First, we consider a 3-layer
710 MLP without bias terms for the weights, with each hidden layer consisting of 1000 units. The network
711 is trained using MSE loss with a learning rate of $\eta = 4$, along with random weights scaled
712 by $\alpha = 0.01$ and full-batch gradient descent on a 5K subset of the MNIST dataset, following [1].
713 The motivation for omitting bias terms comes from the findings of [26], where they provably show
714 that a ReLU network without bias terms behaves similarly to a linear network. With this in mind,
715 we aimed to investigate how oscillations manifest in comparison to deep linear networks (DLNs).
716 In Figure 20, we plot the training loss, top-5 singular values, and sharpness throughout training.
717 Interestingly, despite the non-convexity of the loss landscape, the oscillations appear to be almost
718 periodic across all three plots. It would be of great interest to theoretically study the behavior of
719 EOS for this network architecture and determine whether our analyses extend to this case as well.

720 Next, we consider the DLN setting to corroborate our result from Theorem 2. We consider modeling
721 rank-3 target matrix with singular values $\sigma_{*,i} = \{10, 9, 8\}$ with a 3-layer DLN with initialization scale
722 $\alpha = 0.1$. By computing the sharpness under these settings, notice that $2/\lambda_1 = L\sigma_{*,1}^{2-\frac{2}{L}} \approx 0.01547$

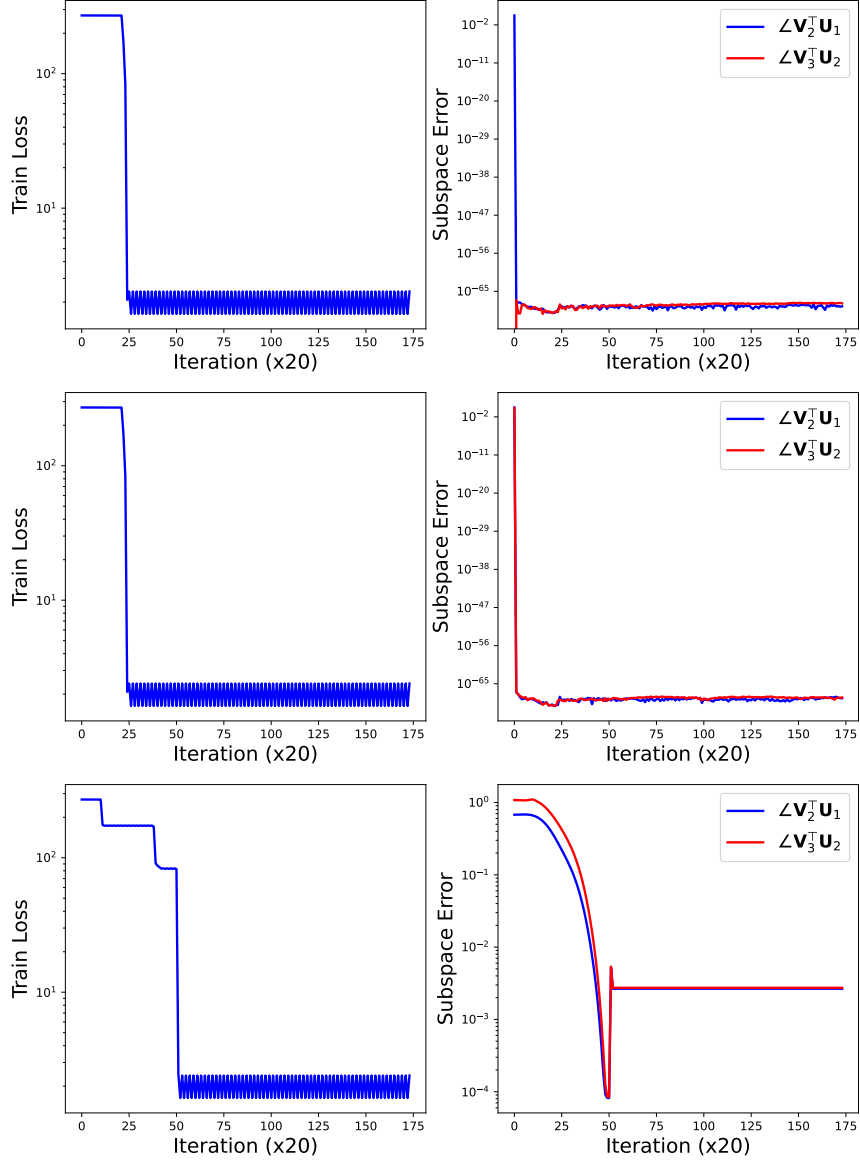


Figure 18: EOS dynamics of a 3-layer DLN for different initializations where it all converges to the SVS set. The subspace distance is defined in Equation (11). Top: Dynamics with the original identity initialization. Middle: Dynamics with orthogonal initialization. Bottom: Dynamics with random initialization.

723 and $2/\lambda_2 \approx 0.01657$. In Figure 21, we use learning rates near these values, and plot the oscillations
 724 in the singular values. Here, we can see that the oscillations follow exactly our theory.

725 Lastly, we provide additional experiments demonstrating stronger oscillation in feature directions
 726 as measured by the singular values. To this end, we consider a 4-layer MLP with ReLU activations
 727 with hidden layer size in each unit of 200 for classification on a subsampled 20K set on MNIST and
 728 CIFAR-10. In Figure 22, we show that the oscillations in the training loss are artifacts of jumps only
 729 in the top singular values, which is also what we observe in the DLN setting.

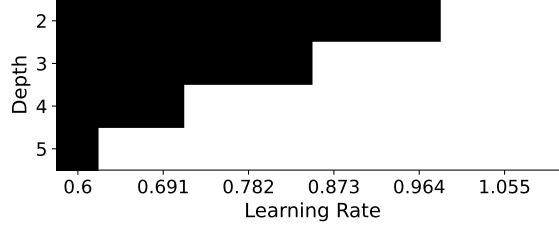


Figure 19: Demonstrating that deeper networks requires a smaller learning rate to enter the EOS regime for DLNs, as implied by Lemma 2, for a target matrix with top singular value $\sigma_{*,1} = 0.5$ and initialization $\alpha = 0.01$. Black refers to stable learning and white refers to regions in which oscillations in the loss and singular values occur. The EOS limit exactly matches $\eta = \frac{2}{L\sigma_{*,i}^{2-\frac{2}{L}}}$.

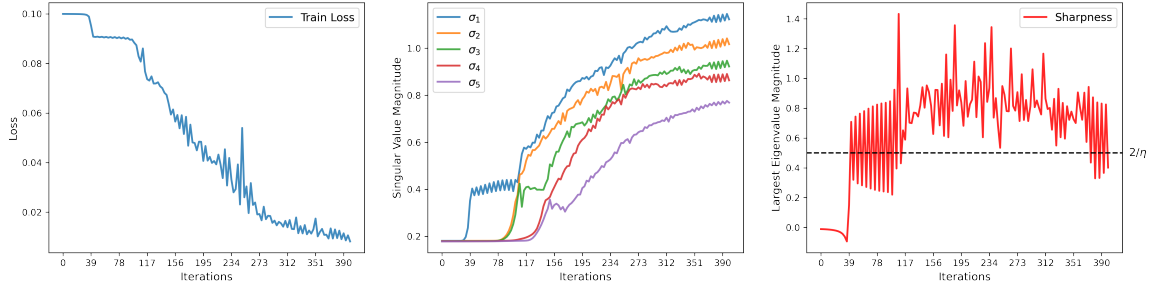


Figure 20: Plot of the training loss, singular values, and sharpness for an MLP network with no bias. Similar to the DLN case, there are oscillations in each of the plots throughout iterations.

730 B.6. Investigation of Oscillations in Low-Rank Adaptors

731 Previously, we investigated the differences in oscillations (i.e., oscillations versus catapults) in deep
 732 linear and nonlinear networks, and how changes in the landscape present one behavior or the other.
 733 Low-rank adaptation (LoRA) [58] has arguably become one of the most popular methods for fine-
 734 tuning deep neural networks. By viewing the adaptations as individual low-rank matrix factor-
 735 ization problems, then this formulation closely aligns with our theoretical setup with a depth of
 736 2. Here we pose the question (i) does oscillations may appear in such a setup and (ii) what these
 737 oscillations may imply in terms of generalization.

738 Briefly, the main idea behind LoRA is that rather than training from scratch, we can update two
 739 low-rank factor matrices to “append” onto an existing weight matrix. That is, give a pre-trained
 740 weight matrix $\mathbf{W}_0 \in \mathbb{R}^{d_1 \times d_2}$, LoRA involves updating two low-rank factors commonly referred to
 741 as “adaptors”:

$$\underbrace{\mathbf{W}_*}_{\text{new weight}} = \underbrace{\mathbf{W}_0}_{\text{pre-trained weight}} + \underbrace{\mathbf{A}\mathbf{B}^\top}_{\text{adaptors}}.$$

742 For a sufficiently small rank r , upon training only $\mathbf{A} \in \mathbb{R}^{d_1 \times r}$ and $\mathbf{B} \in \mathbb{R}^{d_2 \times r}$, $\mathbf{W}_* \in \mathbb{R}^{d_1 \times d_2}$ is used
 743 for inference.

744 For the experimental settings, we follow the setup used by [57] and consider a pre-trained
 745 BERT [59] base model and apply adaptation on all attention and feedforward weights in the
 746 transformer, resulting in 72 adapted layers in total. For initialization, we use random weights
 747 and scale them using an initialization scale of $\alpha = 10^{-3}$ for the adaptors and randomly
 748 sample 512 examples from the STS-B [59] dataset for fine-tuning. We choose a batch size
 749 of 64 with a maximum sequence length of 128 tokens. First, we experiment how large the
 750 rank of the adaptors must be to drive the entire network to EOS. Using a learning rate of
 751 $\eta = 10^{-4}$, Figure 23 shows oscillatory behavior across all ranks. However, this behavior
 752 may also be an artifact of the stochasticity induced by updating with only a batch of samples.

753

754 In Figure 24, we present the training loss and Pearson correlation
755 relation for different learning rates using rank $r = 8$. When
756 $\eta = 10^{-4}$, the training loss catapults from a magnitude of
757 7 to 4 whereas other learning rates cannot decrease the loss
758 with such a magnitude. Consequently, $\eta = 10^{-4}$ achieves
759 the best Pearson correlation coefficient. This suggests that
760 learning rate plays an important role when the optimization
761 is restricted to a small subspace as used in LoRA. We leave
762 this for future work a careful study of this observation, aiming
763 to accurately select the learning rate to maximize the ef-
764 ficiency of LoRA.

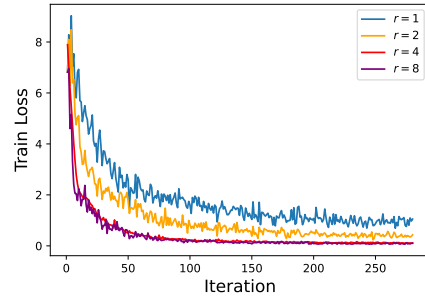


Figure 23: Catapults in the training loss for different ranks for LoRA.

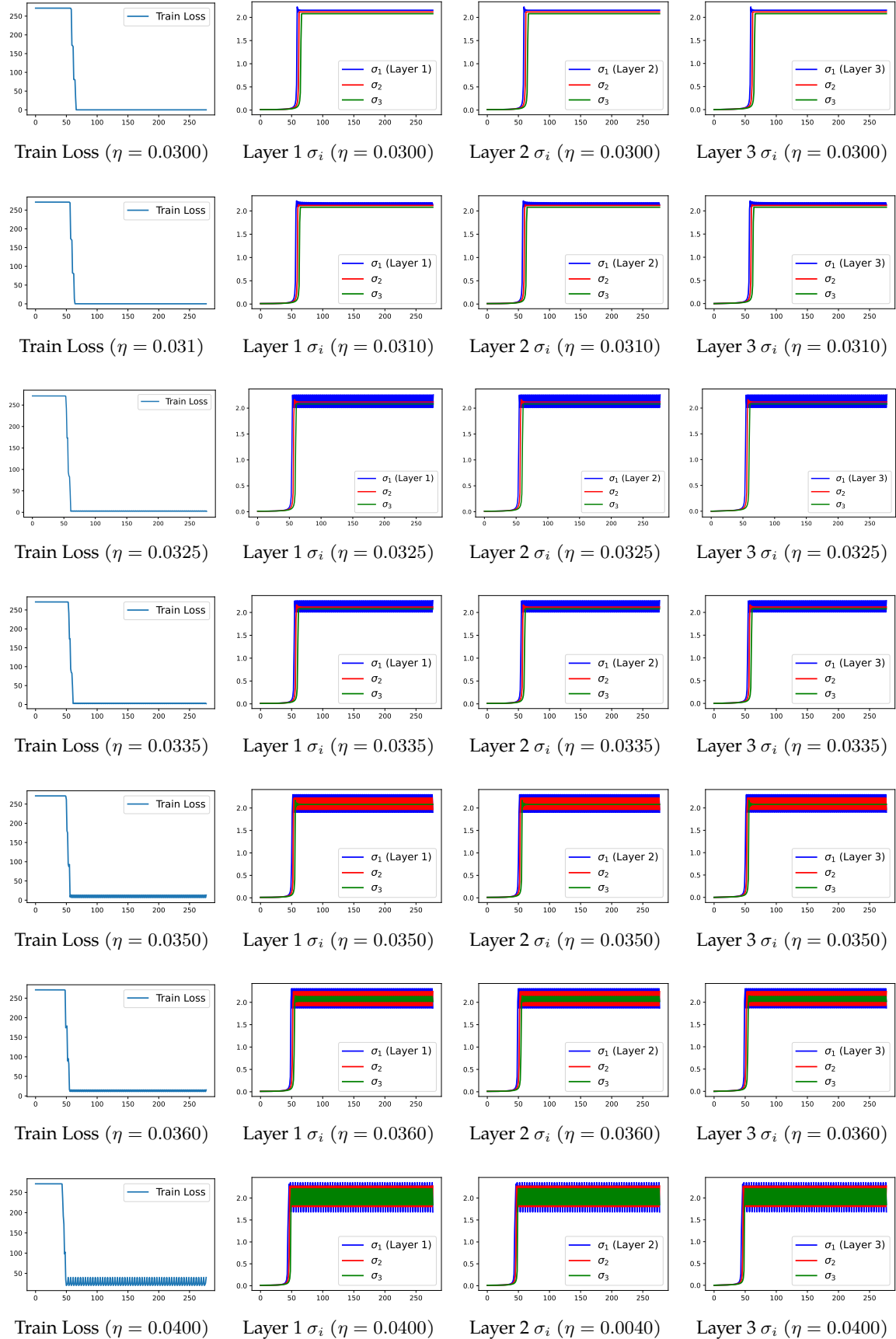
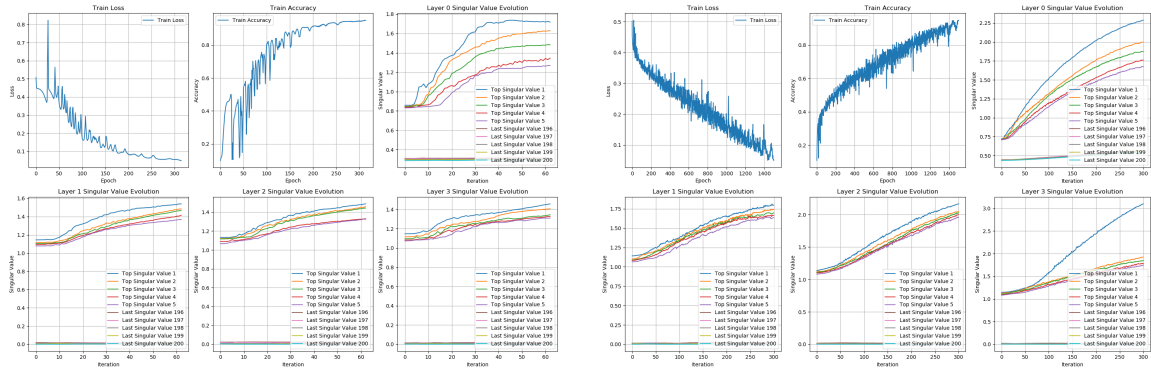


Figure 21: Depiction of the training loss and the singular values of each weight matrix for fitting a rank-3 matrix with singular values 10, 9.5, 9. The weights enter the EOS regime based on the learning rate $\eta > 2/K$, where $K = L\sigma_{*,i}^{2-2/L}$ and $L = 3$. For a sufficiently large learning rate (e.g., $\eta = 0.04$), the singular values start to enter a period-4 orbit.



MNIST Dataset with 4-Layer MLP

CIFAR-10 Dataset with 4-Layer MLP

Figure 22: Prevalence of oscillatory behaviors in top subspaces in 4-layer networks with ReLU activations on two different datasets.

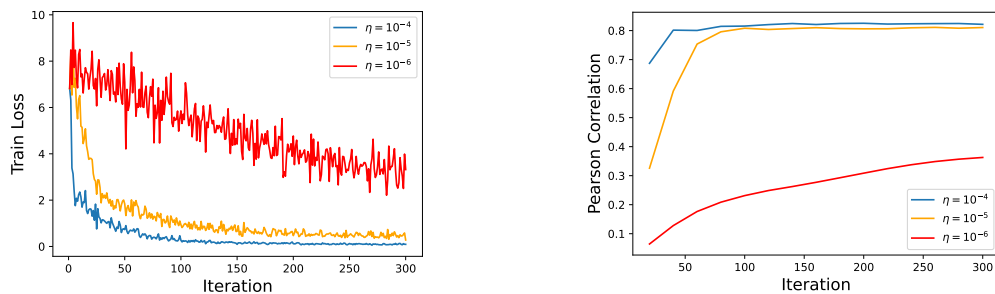


Figure 24: Illustration of different behaviors in the training loss for various learning rates with a fixed rank of $r = 8$ for fine-tuning BERT using LoRA. These plots indicate that larger learning rates lead to higher Pearson correlations. When $\eta = 10^{-4}$, the training loss catapults from a magnitude of 7 to 4 whereas other learning rates do not decrease the loss with such large magnitude.

765 C. Deferred Proofs

766 C.1. Deferred Proofs for Oscillations

767 **Proposition 1** (Singular Vector Stationary Set). *Consider the deep matrix factorization loss in Equa-*
 768 *tion (1). Let $\mathbf{M}_\star = \mathbf{U}_\star \boldsymbol{\Sigma}_\star \mathbf{V}_\star^\top$ and $\mathbf{W}_\ell(t) = \mathbf{U}_\ell(t) \boldsymbol{\Sigma}_\ell(t) \mathbf{V}_\ell^\top(t)$ denote the compact SVD for the target*
 769 *matrix and the ℓ -th layer weight matrix at time t , respectively. For any time $t \geq 0$, if $\dot{\mathbf{U}}_\ell(t) = \dot{\mathbf{V}}_\ell(t) = \mathbf{0}$ for*
 770 *all $\ell \in [L]$, then the singular vector stationary points for each weight matrix are given by*

$$\text{SVS}(f(\Theta)) = \begin{cases} (\mathbf{U}_L, \mathbf{V}_L) & = (\mathbf{U}_\star, \mathbf{Q}_L), \\ (\mathbf{U}_\ell, \mathbf{V}_\ell) & = (\mathbf{Q}_{\ell+1}, \mathbf{Q}_\ell), \quad \forall \ell \in [2, L-1], \\ (\mathbf{U}_1, \mathbf{V}_1) & = (\mathbf{Q}_2, \mathbf{V}_\star), \end{cases}$$

771 where $\{\mathbf{Q}_\ell\}_{\ell=2}^L$ can be any orthogonal matrices.

772 *Proof.* Let us consider the dynamics of $\mathbf{W}_\ell(t)$ in terms of its SVD with respect to time:

$$\dot{\mathbf{W}}_\ell(t) = \dot{\mathbf{U}}_\ell(t) \boldsymbol{\Sigma}_\ell(t) \mathbf{V}_\ell^\top(t) + \mathbf{U}_\ell(t) \dot{\boldsymbol{\Sigma}}_\ell(t) \mathbf{V}_\ell^\top(t) + \mathbf{U}_\ell(t) \boldsymbol{\Sigma}_\ell(t) \dot{\mathbf{V}}_\ell^\top(t). \quad (12)$$

773 By left multiplying by $\mathbf{U}_\ell^\top(t)$ and right multiplying by $\mathbf{V}_\ell(t)$, we have

$$\mathbf{U}_\ell^\top(t) \dot{\mathbf{W}}_\ell(t) \mathbf{V}_\ell(t) = \mathbf{U}_\ell^\top(t) \dot{\mathbf{U}}_\ell(t) \boldsymbol{\Sigma}_\ell(t) + \dot{\boldsymbol{\Sigma}}_\ell(t) + \boldsymbol{\Sigma}_\ell(t) \dot{\mathbf{V}}_\ell^\top(t) \mathbf{V}_\ell(t), \quad (13)$$

774 where we used the fact that $\mathbf{U}_\ell(t)$ and $\mathbf{V}_\ell(t)$ have orthonormal columns. Now, note that we also
 775 have

$$\mathbf{U}_\ell^\top(t) \mathbf{U}_\ell(t) = \mathbf{I}_r \implies \dot{\mathbf{U}}_\ell^\top(t) \mathbf{U}_\ell(t) + \mathbf{U}_\ell^\top(t) \dot{\mathbf{U}}_\ell(t) = \mathbf{0},$$

776 which also holds for $\mathbf{V}_\ell(t)$. This implies that $\dot{\mathbf{U}}_\ell^\top(t) \mathbf{U}_\ell(t)$ is a skew-symmetric matrix, and hence
 777 have zero diagonals. Since $\boldsymbol{\Sigma}_\ell(t)$ is diagonal, $\mathbf{U}_\ell^\top(t) \dot{\mathbf{U}}_\ell(t) \boldsymbol{\Sigma}_\ell(t)$ and $\boldsymbol{\Sigma}_\ell(t) \dot{\mathbf{V}}_\ell^\top(t) \mathbf{V}_\ell(t)$ have zero di-
 778 agonals as well. On the other hand, since $\dot{\boldsymbol{\Sigma}}_\ell(t)$ is a diagonal matrix, we can write

$$\hat{\mathbf{I}}_r \odot \left(\mathbf{U}_\ell^\top(t) \dot{\mathbf{W}}_\ell(t) \mathbf{V}_\ell(t) \right) = \mathbf{U}_\ell^\top(t) \dot{\mathbf{U}}_\ell(t) \boldsymbol{\Sigma}_\ell(t) + \boldsymbol{\Sigma}_\ell(t) \dot{\mathbf{V}}_\ell^\top(t) \mathbf{V}_\ell(t), \quad (14)$$

779 where \odot stands for the Hadamard product and $\hat{\mathbf{I}}_r$ is a square matrix holding zeros on its diago-
 780 nal and ones elsewhere. Taking transpose of Equation (14), while recalling that $\mathbf{U}_\ell^\top(t) \dot{\mathbf{U}}_\ell(t)$ and
 781 $\mathbf{V}_\ell^\top(t) \dot{\mathbf{V}}_\ell(t)$ are skew-symmetric, we have

$$\hat{\mathbf{I}}_r \odot \left(\mathbf{V}_\ell^\top(t) \dot{\mathbf{W}}_\ell^\top(t) \mathbf{U}_\ell(t) \right) = -\boldsymbol{\Sigma}_\ell(t) \mathbf{U}_\ell^\top(t) \dot{\mathbf{U}}_\ell(t) - \dot{\mathbf{V}}_\ell^\top(t) \mathbf{V}_\ell(t) \boldsymbol{\Sigma}_\ell(t). \quad (15)$$

782 Then, by right multiplying Equation (14) by $\boldsymbol{\Sigma}_\ell(t)$, left-multiply Equation (15) by $\boldsymbol{\Sigma}_\ell(t)$, and by
 783 adding the two terms, we get

$$\begin{aligned} \hat{\mathbf{I}}_r \odot \left(\mathbf{U}_\ell^\top(t) \dot{\mathbf{W}}_\ell(t) \mathbf{V}_\ell(t) \boldsymbol{\Sigma}_\ell(t) + \boldsymbol{\Sigma}_\ell(t) \mathbf{V}_\ell^\top(t) \dot{\mathbf{W}}_\ell^\top(t) \mathbf{U}_\ell(t) \right) \\ = \mathbf{U}_\ell^\top(t) \dot{\mathbf{U}}_\ell(t) \boldsymbol{\Sigma}_\ell^2(t) - \boldsymbol{\Sigma}_\ell^2(t) \dot{\mathbf{V}}_\ell^\top(t) \mathbf{V}_\ell(t). \end{aligned}$$

784 Since we assume that the singular values of \mathbf{M}_\star are distinct, the top- r diagonal elements of $\boldsymbol{\Sigma}_\ell^2(t)$
 785 are also distinct (i.e., $\Sigma_{r'}^2(t) \neq \Sigma_r^2(t)$ for $r \neq r'$). This implies that

$$\mathbf{U}_\ell^\top(t) \dot{\mathbf{U}}_\ell(t) = \mathbf{H}(t) \odot \left[\mathbf{U}_\ell^\top(t) \dot{\mathbf{W}}_\ell(t) \mathbf{V}_\ell(t) \boldsymbol{\Sigma}_\ell(t) + \boldsymbol{\Sigma}_\ell(t) \mathbf{V}_\ell^\top(t) \dot{\mathbf{W}}_\ell^\top(t) \mathbf{U}_\ell(t) \right],$$

786 where the matrix $\mathbf{H}(t) \in \mathbb{R}^{d \times d}$ is defined by:

$$H_{r,r'}(t) := \begin{cases} (\Sigma_{r'}^2(t) - \Sigma_r^2(t))^{-1}, & r \neq r', \\ 0, & r = r'. \end{cases} \quad (16)$$

787 Then, multiplying from the left by $\mathbf{U}_\ell(t)$ yields

$$\mathbf{P}_{\mathbf{U}_\ell(t)} \dot{\mathbf{U}}_\ell(t) = \mathbf{U}_\ell(t) \left(\mathbf{H}(t) \odot \left[\mathbf{U}_\ell^\top(t) \dot{\mathbf{W}}_\ell(t) \mathbf{V}_\ell(t) \boldsymbol{\Sigma}_\ell(t) + \boldsymbol{\Sigma}_\ell(t) \mathbf{V}_\ell^\top(t) \dot{\mathbf{W}}_\ell^\top(t) \mathbf{U}_\ell(t) \right] \right), \quad (17)$$

788 with $\mathbf{P}_{\mathbf{U}_\ell(t)} := \mathbf{U}_\ell(t) \mathbf{U}_\ell^\top(t)$ being the projection onto the subspace spanned by the (orthonormal) columns of $\mathbf{U}_\ell(t)$. Denote by $\mathbf{P}_{\mathbf{U}_{\ell\perp}(t)}$ the projection onto the orthogonal complement (i.e.,
789 $\mathbf{P}_{\mathbf{U}_{\ell\perp}(t)} := \mathbf{I}_r - \mathbf{U}_\ell(t) \mathbf{U}_\ell^\top(t)$). Apply $\mathbf{P}_{\mathbf{U}_{\ell\perp}(t)}$ to both sides of Equation (12):

$$\mathbf{P}_{\mathbf{U}_{\ell\perp}(t)} \dot{\mathbf{U}}_\ell(t) = \mathbf{P}_{\mathbf{U}_{\ell\perp}(t)} \dot{\mathbf{U}}_\ell(t) \boldsymbol{\Sigma}_\ell(t) \mathbf{V}_\ell^\top(t) + \mathbf{P}_{\mathbf{U}_{\ell\perp}(t)} \mathbf{U}_\ell(t) \dot{\boldsymbol{\Sigma}}_\ell(t) \mathbf{V}_\ell^\top(t) \quad (18)$$

$$+ \mathbf{P}_{\mathbf{U}_{\ell\perp}(t)} \mathbf{U}_\ell(t) \boldsymbol{\Sigma}_\ell(t) \dot{\mathbf{V}}_\ell^\top(t). \quad (19)$$

791 Note that $\mathbf{P}_{\mathbf{U}_{\ell\perp}(t)} \mathbf{U}_\ell(t) = 0$, and multiply from the right by $\mathbf{V}_\ell(t) \boldsymbol{\Sigma}_\ell^{-1}(t)$ (the latter is well-defined
792 since we have the compact SVD and the top- r elements are non-zero):

$$\mathbf{P}_{\mathbf{U}_{\ell\perp}(t)} \dot{\mathbf{U}}_\ell(t) = \mathbf{P}_{\mathbf{U}_{\ell\perp}(t)} \dot{\mathbf{W}}_\ell(t) \mathbf{V}_\ell(t) \boldsymbol{\Sigma}_\ell^{-1}(t) = (\mathbf{I}_r - \mathbf{U}_\ell(t) \mathbf{U}_\ell^\top(t)) \dot{\mathbf{W}}_\ell(t) \mathbf{V}_\ell(t) \boldsymbol{\Sigma}_\ell^{-1}(t). \quad (20)$$

793 Then by adding the two equations above, we obtain an expression for $\dot{\mathbf{U}}_\ell(t)$:

$$\begin{aligned} \dot{\mathbf{U}}_\ell(t) &= \mathbf{P}_{\mathbf{U}_\ell(t)} \dot{\mathbf{U}}_\ell(t) + \mathbf{P}_{\mathbf{U}_{\ell\perp}(t)} \dot{\mathbf{U}}_\ell(t) \\ &= \mathbf{U}_\ell(t) \left(\mathbf{H}(t) \odot \left[\mathbf{U}_\ell^\top(t) \dot{\mathbf{W}}_\ell(t) \mathbf{V}_\ell(t) \boldsymbol{\Sigma}_\ell(t) + \boldsymbol{\Sigma}_\ell(t) \mathbf{V}_\ell^\top(t) \dot{\mathbf{W}}_\ell^\top(t) \mathbf{U}_\ell(t) \right] \right) \\ &\quad + (\mathbf{I}_r - \mathbf{U}_\ell(t) \mathbf{U}_\ell^\top(t)) \dot{\mathbf{W}}_\ell(t) \mathbf{V}_\ell(t) \boldsymbol{\Sigma}_\ell^{-1}(t). \end{aligned} \quad (21)$$

794 We can similarly derive the dynamics for $\dot{\mathbf{V}}_\ell(t)$ and $\dot{\boldsymbol{\Sigma}}_\ell(t)$:

$$\dot{\mathbf{V}}_\ell(t) = \mathbf{V}_\ell(t) \left(\mathbf{H}(t) \odot \left[\boldsymbol{\Sigma}_\ell(t) \mathbf{U}_\ell^\top(t) \dot{\mathbf{W}}_\ell(t) \mathbf{V}_\ell(t) + \mathbf{V}_\ell^\top(t) \dot{\mathbf{W}}_\ell^\top(t) \mathbf{U}_\ell(t) \boldsymbol{\Sigma}_\ell(t) \right] \right) \quad (22)$$

$$+ (\mathbf{I}_r - \mathbf{V}_\ell(t) \mathbf{V}_\ell^\top(t)) \dot{\mathbf{W}}_\ell^\top(t) \mathbf{U}_\ell(t) \boldsymbol{\Sigma}_\ell^{-1}(t), \quad (23)$$

795

$$\dot{\boldsymbol{\Sigma}}_\ell(t) = \mathbf{I}_r \odot \left[\mathbf{U}_\ell^\top(t) \dot{\mathbf{W}}_\ell(t) \mathbf{V}_\ell(t) \right].$$

796 Now, we will left multiply $\dot{\mathbf{U}}_\ell(t)$ and $\dot{\mathbf{V}}_\ell(t)$ with $\mathbf{U}_\ell^\top(t)$ and $\mathbf{V}_\ell^\top(t)$, respectively, to obtain

$$\begin{aligned} \mathbf{U}_\ell^\top(t) \dot{\mathbf{U}}_\ell(t) &= -\mathbf{H}(t) \odot \left[\mathbf{U}_\ell^\top(t) \nabla_{\mathbf{W}_\ell} f(\boldsymbol{\Theta}) \mathbf{V}_\ell(t) \boldsymbol{\Sigma}_\ell(t) + \boldsymbol{\Sigma}_\ell(t) \mathbf{V}_\ell^\top(t) \nabla_{\mathbf{W}_\ell} f(\boldsymbol{\Theta}) \mathbf{U}_\ell(t) \right], \\ \mathbf{V}_\ell^\top(t) \dot{\mathbf{V}}_\ell(t) &= -\mathbf{H}(t) \odot \left[\boldsymbol{\Sigma}_\ell(t) \mathbf{U}_\ell^\top(t) \nabla_{\mathbf{W}_\ell} f(\boldsymbol{\Theta}) \mathbf{V}_\ell(t) + \mathbf{V}_\ell^\top(t) \nabla_{\mathbf{W}_\ell} f(\boldsymbol{\Theta}) \mathbf{U}_\ell(t) \boldsymbol{\Sigma}_\ell(t) \right], \end{aligned}$$

797 where we replaced $\dot{\mathbf{W}}_\ell(t) := -\nabla_{\mathbf{W}_\ell} f(\boldsymbol{\Theta})$, as $\dot{\mathbf{W}}_\ell(t)$ is the gradient of $f(\boldsymbol{\Theta})$ with respect to \mathbf{W}_ℓ by
798 definition. By rearranging and multiplying by $\boldsymbol{\Sigma}_\ell(t)$, we have

$$\mathbf{U}_\ell^\top(t) \dot{\mathbf{U}}_\ell(t) \boldsymbol{\Sigma}_\ell(t) - \boldsymbol{\Sigma}_\ell(t) \mathbf{V}_\ell^\top(t) \dot{\mathbf{V}}_\ell(t) = -\hat{\mathbf{I}}_r \odot \left[\mathbf{U}_\ell^\top(t) \nabla_{\mathbf{W}_\ell} f(\boldsymbol{\Theta}) \mathbf{V}_\ell(t) \right]. \quad (24)$$

799 Hence, when $\dot{\mathbf{U}}_\ell(t) = 0$ and $\dot{\mathbf{V}}_\ell(t) = 0$, it must be that the left-hand side is zero and so
800 $\mathbf{U}_\ell^\top(t) \nabla_{\mathbf{W}_\ell} f(\boldsymbol{\Theta}) \mathbf{V}_\ell(t)$ is a diagonal matrix.

801 Now, notice that for the given loss function $f(\boldsymbol{\Theta})$, we have

$$-\dot{\mathbf{W}}_\ell(t) = \nabla_{\mathbf{W}_\ell} f(\boldsymbol{\Theta}(t)) = \mathbf{W}_{L:\ell+1}^\top(t) \cdot (\mathbf{W}_{L:1}(t) - \mathbf{M}_\star) \cdot \mathbf{W}_{\ell-1:1}^\top(t).$$

802 Then, from Equation (24), when the singular vectors are stationary, we have

$$\mathbf{U}_\ell^\top(t) \mathbf{W}_{L:\ell+1}^\top(t) \cdot (\mathbf{W}_{L:1}(t) - \mathbf{M}_\star) \cdot \mathbf{W}_{\ell-1:1}^\top(t) \mathbf{V}_\ell(t)$$

803 must be a diagonal matrix for all $\ell \in [L]$. The only solution to the above should be (since the
804 intermediate singular vectors need to cancel to satisfy the diagonal condition), is the set

$$\text{SVS}(f(\boldsymbol{\Theta})) = \begin{cases} (\mathbf{U}_L, \mathbf{V}_L) &= (\mathbf{U}_\star, \mathbf{Q}_L), \\ (\mathbf{U}_\ell, \mathbf{V}_\ell) &= (\mathbf{Q}_{\ell+1}, \mathbf{Q}_\ell), \quad \forall \ell \in [2, L-1], \\ (\mathbf{U}_1, \mathbf{V}_1) &= (\mathbf{Q}_2, \mathbf{V}_\star), \end{cases}$$

805 where $\{\mathbf{Q}_\ell\}_{\ell=2}^L$ are any set of orthogonal matrices. Then, notice that when the singular vectors are
 806 stationary, the dynamics become isolated on the singular values:

$$\dot{\Sigma}_\ell(t) = \mathbf{I}_r \odot \left[\mathbf{U}_\ell^\top(t) \dot{\mathbf{W}}_\ell(t) \mathbf{V}_\ell(t) \right],$$

807 since $\left[\mathbf{U}_\ell^\top(t) \dot{\mathbf{W}}_\ell(t) \mathbf{V}_\ell(t) \right]$ is diagonal. This completes the proof.

808 □

809 **Theorem 1** (Stable Subspace Oscillations). Let $\alpha' := \left(\ln \left(\frac{2\sqrt{2}}{\eta\lambda_1} \right) \cdot \frac{\sigma_{*,1}^{4/L}}{L^2 \cdot 2^{\frac{2L-3}{L}}} \right)^{1/4}$. Consider running
 810 GD on the loss in (1) with initialization scale $0 < \alpha < \alpha'$. If $\eta = \frac{2}{K}$ with $\lambda_i \leq K < \lambda_{i+1}$, then under strict
 811 balancing, 2-period orbit oscillation occurs in the direction of Δ_i , where λ_i and Δ_i denote the i -th largest
 812 eigenvalue and eigenvector of the Hessian at the balanced minimum, respectively.

813 *Proof.* Define f_{Δ_i} as the 1-D function at the cross section of the loss landscape and the line following
 814 the direction of Δ_i passing the (balanced) minima. To prove the result, we will invoke Lemma 12,
 815 which states that two-period orbit oscillation occurs in the direction of Δ_i if the minima of f_{Δ_i}
 816 satisfies $f_{\Delta_i}^{(3)} > 0$ and $3[f_{\Delta_i}^{(3)}]^2 - f_{\Delta_i}^{(2)} f_{\Delta_i}^{(4)} > 0$, for $\eta > \frac{2}{\lambda_i}$. Recall that the initialization condition is an
 817 artifact of Lemma 2, which allows us to consider the balanced minimum.

818 First, we will derive the eigenvectors of the Hessian of the training loss at convergence (i.e., $\mathbf{M}_* =$
 819 $\mathbf{W}_{L:1}$). To obtain the eigenvectors of the Hessian of parameters $(\mathbf{W}_L, \dots, \mathbf{W}_2, \mathbf{W}_1)$, consider a small
 820 perturbation of the parameters:

$$\Theta := (\Delta \mathbf{W}_\ell + \mathbf{W}_\ell)_{\ell=1}^L = (\mathbf{W}_L + \Delta \mathbf{W}_L, \dots, \mathbf{W}_2 + \Delta \mathbf{W}_2, \mathbf{W}_1 + \Delta \mathbf{W}_1).$$

821 Given that $\mathbf{W}_{L:1} = \mathbf{M}_*$, consider and evaluate the loss function at this minima:

$$\mathcal{L}(\Theta) = \frac{1}{2} \left\| \sum_{\ell} \mathbf{W}_{L:\ell+1} \Delta \mathbf{W}_\ell \mathbf{W}_{\ell-1:1} \right\|_{\mathbb{F}}^2 \quad (25)$$

$$+ \sum_{\ell < m} \mathbf{W}_{L:\ell+1} \Delta \mathbf{W}_\ell \mathbf{W}_{\ell-1:m+1} \Delta \mathbf{W}_m \mathbf{W}_{m-1:1} + \dots + \Delta \mathbf{W}_{L:1} \left\|_{\mathbb{F}}^2. \quad (26)$$

822 By expanding each of the terms and splitting by the orders of $\Delta \mathbf{W}_\ell$ (perturbation), we get that the
 823 second-order term is equivalent to

$$\begin{aligned} \Theta \left(\sum_{\ell=1}^L \|\Delta \mathbf{W}_\ell\|^2 \right) &: \frac{1}{2} \left\| \sum_{\ell} \mathbf{W}_{L:\ell+1} \Delta \mathbf{W}_\ell \mathbf{W}_{\ell-1:1} \right\|_{\mathbb{F}}^2 \\ \Theta \left(\sum_{\ell=1}^L \|\Delta \mathbf{W}_\ell\|^3 \right) &: \text{tr} \left[\left(\sum_{\ell} \mathbf{W}_{L:\ell+1} \Delta \mathbf{W}_\ell \mathbf{W}_{\ell-1:1} \right)^\top \left(\sum_{\ell < m} \mathbf{W}_{L:\ell+1} \Delta \mathbf{W}_\ell \mathbf{W}_{\ell-1:m+1} \Delta \mathbf{W}_m \mathbf{W}_{m-1:1} \right) \right] \\ \Theta \left(\sum_{\ell=1}^L \|\Delta \mathbf{W}_\ell\|^4 \right) &: \frac{1}{2} \left\| \sum_{\ell < m} \mathbf{W}_{L:\ell+1} \Delta \mathbf{W}_\ell \mathbf{W}_{\ell-1:m+1} \Delta \mathbf{W}_m \mathbf{W}_{m-1:1} \right\|_{\mathbb{F}}^2 \\ &+ \text{tr} \left[\sum_l \left(\mathbf{W}_{L:\ell+1} \Delta \mathbf{W}_\ell \mathbf{W}_{\ell-1:1} \right)^\top \left(\sum_{l < m < p} \mathbf{W}_{L:\ell+1} \Delta \mathbf{W}_\ell \mathbf{W}_{\ell-1:m+1} \Delta \mathbf{W}_m \mathbf{W}_{m-1:p+1} \Delta \mathbf{W}_p \mathbf{W}_{p-1:1} \right) \right] \end{aligned}$$

824 The direction of the steepest change in the loss at the minima correspond to the largest eigenvector
 825 direction of the Hessian. Since higher order terms such as $\Theta \left(\sum_{\ell=1}^L \|\Delta \mathbf{W}_\ell\|^3 \right)$ are insignificant
 826 compared to the second order terms $\Theta \left(\sum_{\ell=1}^L \|\Delta \mathbf{W}_\ell\|^2 \right)$, finding the direction that maximizes the

827 second order term leads to finding the eigenvector of the Hessian. Then, the eigenvector corre-
 828 sponding to the maximum eigenvalue of $\nabla^2 \mathcal{L}$ is the solution of

$$\Delta_1 := \text{vec}(\Delta \mathbf{W}_L, \dots, \Delta \mathbf{W}_1) = \underset{\|\Delta \mathbf{W}_L\|_F^2 + \dots + \|\Delta \mathbf{W}_1\|_F^2 = 1}{\text{argmax}} f(\Delta \mathbf{W}_L, \dots, \Delta \mathbf{W}_1), \quad (27)$$

829 where

$$f(\Delta \mathbf{W}_L, \dots, \Delta \mathbf{W}_1) := \frac{1}{2} \|\Delta \mathbf{W}_L \mathbf{W}_{L-1:1} + \dots + \mathbf{W}_{L:3} \Delta \mathbf{W}_2 \mathbf{W}_1 + \mathbf{W}_{L:2} \Delta \mathbf{W}_1\|_F^2. \quad (28)$$

830 While the solution of Equation (27) gives the maximum eigenvector direction of the Hessian, Δ_1 ,
 831 the other eigenvectors can be found by solving

$$\Delta_r := \underset{\substack{\|\Delta \mathbf{W}_L\|_F^2 + \dots + \|\Delta \mathbf{W}_1\|_F^2 = 1, \\ \Delta_r \perp \Delta_{r-1}, \dots, \Delta_r \perp \Delta_1}}{\text{argmax}} f(\Delta \mathbf{W}_L, \dots, \Delta \mathbf{W}_1). \quad (29)$$

832 By expanding $f(\cdot)$, we have that

$$\begin{aligned} f(\Delta \mathbf{W}_L, \dots, \Delta \mathbf{W}_1) &= \|\Delta \mathbf{W}_L \mathbf{W}_{L-1:1}\|_F^2 + \dots + \|\mathbf{W}_{L:3} \Delta \mathbf{W}_2 \mathbf{W}_1\|_F^2 + \|\mathbf{W}_{L:2} \Delta \mathbf{W}_1\|_F^2 \\ &\quad + \text{tr} \left[(\Delta \mathbf{W}_L \mathbf{W}_{L-1:1})^\top (\mathbf{W}_{L:3} \Delta \mathbf{W}_2 \mathbf{W}_1 + \dots + \mathbf{W}_{L:2} \Delta \mathbf{W}_1) \right] + \dots + \\ &\quad \text{tr} \left[(\mathbf{W}_{L:2} \Delta \mathbf{W}_1)^\top (\mathbf{W}_{L:3} \Delta \mathbf{W}_2 \mathbf{W}_1 + \dots + \mathbf{W}_{L:3} \Delta \mathbf{W}_2 \mathbf{W}_1) \right]. \end{aligned} \quad (30)$$

833 We can solve Equation (27) by maximizing each of the terms, which can be done in two steps:

- 834 (i) Each Frobenius term in the expansion is maximized when the left singular vector of $\Delta \mathbf{W}_\ell$ aligns
 835 with $\mathbf{W}_{L:\ell+1}$ and the right singular vector aligns with $\mathbf{W}_{\ell-1:1}$. This is a result of Von Neumann's
 836 trace inequality [60]. Similarly, each term in the trace is maximized when the singular vector of
 837 the perturbations align with the products.
- 838 (ii) Due to the alignment, Equation (27) can be written in just the singular values. Let $\Delta s_{\ell,i}$ denote
 839 the i -th singular value of the perturbation matrix $\Delta \mathbf{W}_\ell$. Recall that all of the singular values of
 840 \mathbf{M}_\star are distinct (i.e., $\sigma_{\star,1} > \dots > \sigma_{\star,r}$). Hence, it is easy to see that Equation (27) is maximized
 841 when $\Delta s_{\ell,i} = 0$ (i.e, all the weight goes to $\Delta s_{\ell,1}$). Thus, each perturbation matrix must be rank-1.

842 Now since each perturbation is rank-1, we can write each perturbation as

$$\Delta \mathbf{W}_\ell = \Delta s_\ell \Delta \mathbf{u}_\ell \Delta \mathbf{v}_\ell^\top, \quad \forall \ell \in [L], \quad (31)$$

843 for $\Delta s_\ell > 0$ and orthonormal vectors $\Delta \mathbf{u}_\ell \in \mathbb{R}^d$ and $\Delta \mathbf{v}_\ell \in \mathbb{R}^d$ with $\sum_{\ell=1}^L \Delta s_\ell^2 = 1$. Plugging this in
 844 each term, we obtain:

$$\|\mathbf{W}_{L:\ell+1} \Delta_1 \mathbf{W}_\ell \mathbf{W}_{\ell-1:1}\|_2^2 = \Delta_1 s_\ell^2 \cdot \left\| \underbrace{\mathbf{V}_\star \sigma_{\star,1}^{\frac{L-\ell}{L}} \mathbf{V}_\star^\top}_{=: \mathbf{a}} \Delta \mathbf{u}_\ell \underbrace{\Delta \mathbf{v}_\ell^\top \mathbf{V}_\star \sigma_{\star,1}^{\frac{\ell-1}{L}} \mathbf{V}_\star^\top}_{=: \mathbf{b}^\top} \right\|_2^2.$$

845 Since alignment maximizes this expression as discussed in first point, we have:

846 $\mathbf{u}_\ell = \mathbf{v}_\ell = \mathbf{v}_{\star,1}$ for all $\ell \in [2, L-1]$, then

$$\mathbf{a} = \sigma_{\star,1}^{\frac{L-\ell}{L}} \mathbf{v}_{\star,1} \quad \text{and} \quad \mathbf{b}^\top = \sigma_{\star,1}^{\frac{\ell-1}{L}} \mathbf{v}_{\star,1}^\top \implies \mathbf{a} \mathbf{b}^\top = \sigma_{\star,1}^{1-\frac{1}{L}} \cdot \mathbf{v}_{\star,1} \mathbf{v}_{\star,1}^\top.$$

847 The very same argument can be made for the trace terms. Hence, in order to maximize $f(\cdot)$, we
 848 must have

$$\begin{aligned} \mathbf{v}_L &= \mathbf{v}_{\star,1}, \quad \text{and} \quad \mathbf{u}_1 = \mathbf{v}_{\star,1}, \\ \mathbf{u}_\ell &= \mathbf{v}_\ell = \mathbf{v}_{\star,1}, \quad \forall \ell \in [2, L-1]. \end{aligned}$$

849 To determine \mathbf{u}_L and \mathbf{v}_1 , we can look at one of the trace terms:

$$\text{tr} \left[(\Delta_1 \mathbf{W}_L \mathbf{W}_{L-1:1})^\top (\mathbf{W}_{L:3} \Delta_1 \mathbf{W}_2 \mathbf{W}_1 + \dots + \mathbf{W}_{L:2} \Delta_1 \mathbf{W}_1) \right] \leq \left(\frac{L-1}{L} \right) \cdot \sigma_{\star,1}^{2-\frac{2}{L}}.$$

850 To reach the upper bound, we require $\mathbf{u}_L = \mathbf{u}_{\star,1}$ and $\mathbf{v}_1 = \mathbf{v}_{\star,1}$. Finally, as for each index, the
 851 singular values are balanced, we will have $\Delta_{1\ell} = \frac{1}{\sqrt{L}}$ for all $\ell \in [L]$ to satisfy the constraint. Finally,
 852 we get that the leading eigenvector is

$$\Delta_1 := \text{vec} \left(\frac{1}{\sqrt{L}} \mathbf{u}_1 \mathbf{v}_1^\top, \frac{1}{\sqrt{L}} \mathbf{v}_1 \mathbf{v}_1^\top, \dots, \frac{1}{\sqrt{L}} \mathbf{v}_1 \mathbf{v}_1^\top \right).$$

853 Notice that we can also verify that $f(\Delta_1) = L\sigma_{\star,1}^{2-\frac{2}{L}}$, which is the leading eigenvalue (or sharpness)
 854 derived in Lemma 1.

855 To derive the remaining eigenvectors, we need to find all of the vectors in which $\Delta_i^\top \Delta_j = 0$ for $i \neq j$,
 856 where

$$\Delta_i = \text{vec}(\Delta_i \mathbf{W}_L, \dots, \Delta_i \mathbf{W}_1),$$

857 and $f(\Delta_i) = \lambda_i$, where λ_i is the i -th largest eigenvalue. By repeating the same process as above, we
 858 find that the eigenvector-eigenvalue pair as follows:

$$\begin{aligned} \Delta_1 &= \text{vec} \left(\frac{1}{\sqrt{L}} \mathbf{u}_1 \mathbf{v}_1^\top, \frac{1}{\sqrt{L}} \mathbf{v}_1 \mathbf{v}_1^\top, \dots, \frac{1}{\sqrt{L}} \mathbf{v}_1 \mathbf{v}_1^\top \right), & \lambda_1 &= L\sigma_{\star,1}^{2-\frac{2}{L}} \\ \Delta_2 &= \text{vec} \left(\frac{1}{\sqrt{L}} \mathbf{u}_1 \mathbf{v}_2^\top, \frac{1}{\sqrt{L}} \mathbf{v}_1 \mathbf{v}_2^\top, \dots, \frac{1}{\sqrt{L}} \mathbf{v}_1 \mathbf{v}_2^\top \right), & \lambda_2 &= \left(\sum_{i=0}^{L-1} \sigma_{\star,1}^{1-\frac{1}{L}-\frac{1}{L}i} \cdot \sigma_{\star,2}^{\frac{1}{L}i} \right) \\ \Delta_3 &= \text{vec} \left(\frac{1}{\sqrt{L}} \mathbf{u}_2 \mathbf{v}_1^\top, \frac{1}{\sqrt{L}} \mathbf{v}_2 \mathbf{v}_1^\top, \dots, \frac{1}{\sqrt{L}} \mathbf{v}_2 \mathbf{v}_1^\top \right), & \lambda_3 &= \left(\sum_{i=0}^{L-1} \sigma_{\star,1}^{1-\frac{1}{L}-\frac{1}{L}i} \cdot \sigma_{\star,2}^{\frac{1}{L}i} \right) \\ &\vdots & & \\ \Delta_d &= \text{vec} \left(\frac{1}{\sqrt{L}} \mathbf{u}_2 \mathbf{v}_2^\top, \frac{1}{\sqrt{L}} \mathbf{v}_2 \mathbf{v}_2^\top, \dots, \frac{1}{\sqrt{L}} \mathbf{v}_2 \mathbf{v}_2^\top \right), & \lambda_d &= L\sigma_{\star,2}^{2-\frac{2}{L}} \\ &\vdots & & \\ \Delta_{dr+r} &= \text{vec} \left(\frac{1}{\sqrt{L}} \mathbf{u}_d \mathbf{v}_r^\top, \frac{1}{\sqrt{L}} \mathbf{v}_d \mathbf{v}_r^\top, \dots, \frac{1}{\sqrt{L}} \mathbf{v}_d \mathbf{v}_r^\top \right), \end{aligned}$$

859 which gives a total of $dr + r$ eigenvectors.

860 Second, equipped with the eigenvectors, let us consider the 1-D function f_{Δ_i} generated by the cross-
 861 section of the loss landscape and each eigenvector Δ_i passing the minima:

$$\begin{aligned} f_{\Delta_i}(\mu) &= \mathcal{L}(\mathbf{W}_L + \mu \Delta \mathbf{W}_L, \dots, \mathbf{W}_2 + \mu \Delta \mathbf{W}_2, \mathbf{W}_1 + \mu \Delta \mathbf{W}_1), \\ &= \mu^2 \cdot \frac{1}{2} \|\Delta \mathbf{W}_L \mathbf{W}_{L-1:1} + \dots + \mathbf{W}_{L:3} \Delta \mathbf{W}_2 \mathbf{W}_1 + \mathbf{W}_{L:2} \Delta \mathbf{W}_1\|_{\mathbb{F}}^2 \\ &\quad + \mu^3 \cdot \sum_{\ell=1, \ell < m}^L \text{tr} \left[(\mathbf{W}_{L:\ell+1} \Delta \mathbf{W}_\ell \mathbf{W}_{\ell-1:1})^\top (\mathbf{W}_{L:\ell+1} \Delta \mathbf{W}_\ell \mathbf{W}_{\ell-1:m+1} \Delta \mathbf{W}_m \mathbf{W}_{m-1:1}) \right] \\ &\quad + \mu^4 \cdot \frac{1}{2} \left\| \left(\sum_{\ell < m} \mathbf{W}_{L:\ell+1} \Delta \mathbf{W}_\ell \mathbf{W}_{\ell-1:m+1} \Delta \mathbf{W}_m \mathbf{W}_{m-1:1} \right) \right\|_{\mathbb{F}}^2 \\ &\quad + \mu^4 \cdot \sum_{\ell < m < p}^L \text{tr} \left[(\mathbf{W}_{L:\ell+1} \Delta \mathbf{W}_\ell \mathbf{W}_{\ell-1:1})^\top (\mathbf{W}_{L:\ell+1} \Delta \mathbf{W}_\ell \mathbf{W}_{\ell-1:m+1} \Delta \mathbf{W}_m \mathbf{W}_{m-1:p+1} \Delta \mathbf{W}_p \mathbf{W}_{p-1:1}) \right]. \end{aligned}$$

862 Then, the several order derivatives of $f_{\Delta_i}(\mu)$ at $\mu = 0$ can be obtained from Taylor expansion as

$$\begin{aligned}
f_{\Delta_i}^{(2)}(0) &= \|\Delta_i \mathbf{W}_L \mathbf{W}_{L-1:1} + \dots + \mathbf{W}_{L:3} \Delta_i \mathbf{W}_2 \mathbf{W}_1 + \mathbf{W}_{L:2} \Delta_i \mathbf{W}_1\|_{\mathbb{F}}^2 = \lambda_i^2 \\
f_{\Delta_i}^{(3)}(0) &= 6 \sum_{\ell=1}^L \text{tr} \left[(\mathbf{W}_{L:\ell+1} \Delta_i \mathbf{W}_{\ell} \mathbf{W}_{\ell-1:1})^{\top} (\mathbf{W}_{L:\ell+2} \Delta_i \mathbf{W}_{\ell+1} \mathbf{W}_{\ell} \Delta_i \mathbf{W}_{\ell-1} \mathbf{W}_{\ell-2:1}) \right] \\
&= 6 \left\| \sum_{\ell} \mathbf{W}_{L:\ell+1} \Delta_i \mathbf{W}_{\ell} \mathbf{W}_{\ell-1:1} \right\|_{\mathbb{F}} \cdot \left\| \left(\sum_{\ell < m} \mathbf{W}_{L:\ell+1} \Delta \mathbf{W}_{\ell} \mathbf{W}_{\ell-1:m+1} \Delta \mathbf{W}_m \mathbf{W}_{m-1:1} \right) \right\|_{\mathbb{F}} \\
&:= 6\lambda_i \cdot \beta_i \\
f_{\Delta_i}^{(4)}(0) &= 12 \|\Delta_i \mathbf{W}_L \Delta_i \mathbf{W}_{L-1} \mathbf{W}_{L-2:1} + \dots + \mathbf{W}_{L:4} \Delta_i \mathbf{W}_3 \mathbf{W}_2 \Delta_i \mathbf{W}_1 + \mathbf{W}_{L:3} \Delta_i \mathbf{W}_2 \Delta_i \mathbf{W}_1\|_{\mathbb{F}}^2 \\
&+ 24 \sum_{\ell=1}^L \text{tr} \left[(\mathbf{W}_{L:\ell+1} \Delta_i \mathbf{W}_{\ell} \mathbf{W}_{\ell-1:1})^{\top} \left(\sum_{\ell < m < p} \mathbf{W}_{L:\ell+1} \Delta \mathbf{W}_{\ell} \mathbf{W}_{\ell-1:m+1} \Delta \mathbf{W}_m \mathbf{W}_{m-1:p+1} \Delta \mathbf{W}_p \mathbf{W}_{p-1:1} \right) \right] \\
&:= 12\beta_i^2 + 24\lambda_i \cdot \delta_i,
\end{aligned}$$

863 where we defined

$$\begin{aligned}
\lambda_i &= \left\| \sum_{\ell} \mathbf{W}_{L:\ell+1} \Delta_i \mathbf{W}_{\ell} \mathbf{W}_{\ell-1:1} \right\|_{\mathbb{F}} && \text{(Total } \binom{L}{1} \text{ terms)} \\
\beta_i &= \left\| \left(\sum_{\ell < m} \mathbf{W}_{L:\ell+1} \Delta \mathbf{W}_{\ell} \mathbf{W}_{\ell-1:m+1} \Delta \mathbf{W}_m \mathbf{W}_{m-1:1} \right) \right\|_{\mathbb{F}} && \text{(Total } \binom{L}{2} \text{ terms)} \\
\delta_i &= \left\| \left(\sum_{\ell < m < p} \mathbf{W}_{L:\ell+1} \Delta \mathbf{W}_{\ell} \mathbf{W}_{\ell-1:m+1} \Delta \mathbf{W}_m \mathbf{W}_{m-1:p+1} \Delta \mathbf{W}_p \mathbf{W}_{p-1:1} \right) \right\|_{\mathbb{F}}, && \text{(Total } \binom{L}{3} \text{ terms)}
\end{aligned}$$

864 and used the fact that $\text{tr}(\mathbf{A}^{\top} \mathbf{B}) = \|\mathbf{A}\|_{\mathbb{F}} \cdot \|\mathbf{B}\|_{\mathbb{F}}$ under singular vector alignment.

865 Then, since β_i has $\binom{L}{2}$ terms inside the sum, when the Frobenium term is expanded, it will have
866 $\frac{\binom{L}{2}(\binom{L}{2}+1)}{2}$ number of terms. Under alignment and balancedness, $\beta_i^2 = \Delta s_{\ell}^2 \sigma_i^{2-\frac{4}{L}} \times \frac{\binom{L}{2}(\binom{L}{2}+1)}{2}$ and
867 $\lambda_i \delta_i = \Delta s_{\ell}^2 \sigma_i^{2-\frac{4}{L}} \times \binom{L}{3} L$. Thus, we have the expression

$$\begin{aligned}
2\beta_i^2 - \lambda_i \delta_i &= \Delta s_{\ell}^2 \sigma_i^{2-\frac{4}{L}} \left(2 \frac{\binom{L}{2} \left(\binom{L}{2} + 1 \right)}{2} - \binom{L}{3} L \right) \\
&= \Delta s_{\ell}^2 \sigma_i^{2-\frac{4}{L}} \binom{L}{3} L \times \left(3 \frac{\left(\frac{L(L-1)}{2} + 1 \right)}{L(L-2)} - 1 \right) \\
&= \Delta s_{\ell}^2 \sigma_i^{2-\frac{4}{L}} \frac{2 \binom{L}{3} L}{L(L-2)} \times ((L-1)^2 + 5) > 0,
\end{aligned}$$

868 for any depth $L > 2$. Finally, the condition of stable oscillation of 1-D function is

$$3[f_{\Delta_i}^{(3)}]^2 - f_{\Delta_i}^{(2)} f_{\Delta_i}^{(4)} = 108\lambda_i^2 \beta_i^2 - (\lambda_i^2)(12\beta_i^2 + 24(2\lambda_i)(\delta_i)) = 48\lambda_i^2(2\beta_i^2 - \lambda_i \delta_i) > 0,$$

869 which we have proven to be positive for any depth $L > 2$, for all the eigenvector directions corre-
870 sponding to the non-zero eigenvalues. This completes the proof.

871 \square

872 **Theorem 2** (Rank- p Periodic Subspace Oscillations). *Let $\mathbf{M}_{\star} = \mathbf{U}_{\star} \mathbf{\Sigma}_{\star} \mathbf{V}_{\star}^{\top}$ denote the SVD of the target*
873 *matrix and define $S_p := L\sigma_{\star,p}^{2-\frac{2}{L}}$ and $K'_p := \max \left\{ S_{p+1}, \frac{S_p}{2\sqrt{2}} \right\}$. If we run GD on the deep matrix factoriza-*
874 *tion loss with initialization scale $\alpha < \alpha'$ from Theorem 1 and learning rate $\eta = \frac{2}{K}$, where $K'_p < K < S_p$,*

875 then under strict balancing, the top- p singular values of the end-to-end DLN oscillates in a 2-period orbit
 876 ($j \in \{1, 2\}$) around the balanced minimum and admits the following decomposition:

$$\mathbf{W}_{L:1} = \underbrace{\sum_{i=1}^p \rho_{i,j}^L \cdot \mathbf{u}_{*,i} \mathbf{v}_{*,i}^\top}_{\text{oscillation subspace}} + \underbrace{\sum_{k=p+1}^d \sigma_{*,k} \cdot \mathbf{u}_{*,k} \mathbf{v}_{*,k}^\top}_{\text{stationary subspace}}, \quad j \in \{1, 2\}, \quad \forall \ell \in [L-1], \quad (32)$$

877 where $\rho_{i,1} \in (0, \sigma_{*,i}^{1/L})$ and $\rho_{i,2} \in (\sigma_{*,i}^{1/L}, (2\sigma_{*,i})^{1/L})$ are the two real roots of the polynomial $g(\rho_i) = 0$ and

$$g(\rho_i) = \rho_i^L \cdot \frac{1 + (1 + \eta L(\sigma_{*,i} - \rho_i^L) \cdot \rho_i^{L-2})^{2L-1}}{1 + (1 + \eta L(\sigma_{*,i} - \rho_i^L) \cdot \rho_i^{L-2})^{L-1}} - \sigma_{*,i}.$$

878

879 *Proof.* To prove the result, we will consider the GD step on the i -th singular value and show that the
 880 2-period orbit condition holds given the learning rate $\eta = \frac{2}{R}$. For ease of exposition, let us denote
 881 the i -th singular value of each \mathbf{W}_ℓ as $\sigma_i := \sigma_{\ell,i}$. Under balancing, consider the two-step GD update
 882 on the first singular value:

$$\begin{aligned} \sigma_i(t+1) &= \sigma_i(t) + \eta L \cdot (\sigma_{*,i} - \sigma_i^L(t)) \cdot \sigma_i^{L-1}(t) \\ \sigma_i(t) &= \sigma_i(t+2) = \sigma_i(t+1) + \eta L \cdot (\sigma_{*,i} - \sigma_i^L(t+1)) \cdot \sigma_i^{L-1}(t+1). \end{aligned} \quad (\text{By 2-period orbit})$$

883 Define $z := (1 + \eta L \cdot (\sigma_{*,i} - \sigma_i^L(t)) \cdot \sigma_i^{L-2}(t))$ and by plugging in $\sigma_i(t+1)$ for $\sigma_i(t)$, we have

$$\begin{aligned} \sigma_i(t) &= \sigma_i(t)z + \eta L \cdot (\sigma_{*,i} - \sigma_i^L(t)z^L) \cdot \sigma_i^{L-1}(t)z^{L-1} \\ \implies 1 &= z + \eta L \cdot (\sigma_{*,i} - \sigma_i^L(t)z^L) \cdot \sigma_i^{L-2}(t)z^{L-1} \\ \implies 1 &= (1 + \eta L \cdot (\sigma_{*,i} - \sigma_i^L(t)) \cdot \sigma_i^{L-2}(t)) + \eta L \cdot (\sigma_{*,i} - \sigma_i^L(t)z^L) \cdot \sigma_i^{L-2}(t)z^{L-1} \\ \implies 0 &= (\sigma_{*,i} - \sigma_i^L(t)) + (\sigma_{*,i} - \sigma_i^L(t)z^L) \cdot z^{L-1} \end{aligned}$$

884 Simplifying this expression further, we have

$$\begin{aligned} 0 &= \sigma_{*,i} - \sigma_i^L(t) + \sigma_{*,i}z^{L-1} - \sigma_i^L(t)z^{2L-1} \\ \implies \sigma_i^L(t) + \sigma_i^L(t)z^{2L-1} &= \sigma_{*,i} + \sigma_{*,i}z^{L-1} \\ \implies \sigma_i^L(t) \cdot (1 + z^{2L-1}) &= \sigma_{*,i} \cdot (1 + z^{L-1}) \\ \implies \sigma_i^L(t) \frac{(1 + z^{2L-1})}{(1 + z^{L-1})} &= \sigma_{*,i}, \end{aligned}$$

885 and by defining $\rho_i := \sigma_i(t)$, we obtain the polynomial

$$\sigma_{*,i} = \rho_i^L \frac{1 + z^{2L-1}}{1 + z^{L-1}}, \quad \text{where } z := (1 + \eta L(\sigma_{*,i} - \rho_i^L) \cdot \rho_i^{L-2}).$$

886 Next, we show the existence of (real) roots within the ranges for $\rho_{i,1}$ and $\rho_{i,2}$. We note that these
 887 roots only exist within the EOS regime. First, consider $\rho_{i,1} \in (0, \sigma_{*,i}^{1/L})$. We will show that for two
 888 values within this range, there is a sign change for all $L \geq 2$. More specifically, we show that there
 889 exists $\rho_i \in (0, \sigma_{*,i}^{1/L})$ such that

$$\rho_i^L \frac{1 + z^{2L-1}}{1 + z^{L-1}} - \sigma_{*,i} > 0 \quad \text{and} \quad \rho_i^L \frac{1 + z^{2L-1}}{1 + z^{L-1}} - \sigma_{*,i} < 0.$$

890 For the positive case, consider $\rho_i = (\frac{1}{2}\sigma_{*,i})^{1/L}$. We need to show that

$$\frac{1 + z^{2L-1}}{1 + z^{L-1}} = \frac{1 + \left(1 + \eta L \cdot \left(\frac{\sigma_{*,i}}{2}\right)^{\frac{1-\frac{2}{L}}{2^{1-\frac{2}{L}}}}\right)^{2L-1}}{1 + \left(1 + \eta L \cdot \left(\frac{\sigma_{*,i}}{2}\right)^{\frac{1-\frac{2}{L}}{2^{1-\frac{2}{L}}}}\right)^{L-1}} > 2.$$

891 To do this, we will plug in the smallest possible value of $\eta = \frac{2}{L\sigma_{*,i}^{2-\frac{2}{L}}}$ to show that the fraction is still
 892 greater than 2, which gives us

$$u(L) := \frac{1 + \left(1 + \frac{1}{2^{1-\frac{2}{L}}}\right)^{2L-1}}{1 + \left(1 + \frac{1}{2^{1-\frac{2}{L}}}\right)^{L-1}}, \quad (33)$$

893 which is an increasing function of L for all $L \geq 2$. Since $u(2) > 2$, Equation (33) must always be
 894 greater than 2. For the negative case, we can simply consider $\rho_i = 0$. Hence, since the polynomial
 895 is continuous, by the Intermediate Value Theorem (IVT), there must exist a root within the range
 896 $\rho_i \in (0, \sigma_{*,i}^{1/L})$.

897 Next, consider the range $\rho_{i,2} \in (\sigma_{*,i}^{1/L}, (2\sigma_{*,i})^{1/L})$. Similarly, we will show sign changes for two
 898 values in $\rho_{i,2}$. For the positive case, consider $\rho_i = (\frac{3}{2}\sigma_{*,i})^{1/L}$. For η , we can plug in the smallest
 899 possible value within the range to show that this value of ρ_i provides a positive quantity. Specifically,
 900 we need to show that

$$\frac{1 + z^{2L-1}}{1 + z^{L-1}} > \frac{2}{3} \implies \frac{1 + \left(1 + \frac{2}{\sigma_{*,i}^{2-\frac{2}{L}}} \cdot (\sigma_{*,i} - \frac{3}{2}\sigma_{*,i}) \cdot (\frac{3}{2}\sigma_{*,i})^{1-\frac{2}{L}}\right)^{2L-1}}{1 + \left(1 + \frac{2}{\sigma_{*,i}^{2-\frac{2}{L}}} \cdot (\sigma_{*,i} - \frac{3}{2}\sigma_{*,i}) \cdot (\frac{3}{2}\sigma_{*,i})^{1-\frac{2}{L}}\right)^{L-1}} > \frac{2}{3}.$$

901 We can simplify the fraction as follows:

$$\frac{1 + \left(1 + \frac{2}{\sigma_{*,1}^{2-\frac{2}{L}}} \cdot (\sigma_{*,1} - \frac{3}{2}\sigma_{*,1}) \cdot (\frac{3}{2}\sigma_{*,1})^{1-\frac{2}{L}}\right)^{2L-1}}{1 + \left(1 + \frac{2}{\sigma_{*,1}^{2-\frac{2}{L}}} \cdot (\sigma_{*,1} - \frac{3}{2}\sigma_{*,1}) \cdot (\frac{3}{2}\sigma_{*,1})^{1-\frac{2}{L}}\right)^{L-1}} = \frac{1 + \left(1 - (\frac{3}{2})^{1-\frac{2}{L}}\right)^{2L-1}}{1 + \left(1 - (\frac{3}{2})^{1-\frac{2}{L}}\right)^{L-1}}.$$

902 Then, since we are subtracting by $(\frac{3}{2})^{1-\frac{2}{L}}$, we can plug in its largest value for $L \geq 2$, which is $3/2$.
 903 This gives us

$$\frac{1 + (-0.5)^{2L-1}}{1 + (-0.5)^{L-1}} > \frac{2}{3},$$

904 as for odd values of L , the function increases to 1 starting from $L = 2$, and decreases to 1 for even
 905 L . To check negativity, let us define

$$h(\rho) := \frac{f(\rho)}{g(\rho)} := \frac{\rho^L (1 + z^{2L-1})}{1 + z^{L-1}}.$$

906 We will show that $h'(\sigma_{*,i}^{1/L}) < 0$:

$$\begin{aligned} h'(\sigma_{*,i}^{1/L}) &= \frac{f'(\sigma_{*,i}^{1/L})g(\sigma_{*,i}^{1/L}) - f(\sigma_{*,i}^{1/L})g'(\sigma_{*,i}^{1/L})}{g^2(\sigma_{*,i}^{1/L})} \\ &= \frac{f'(\sigma_{*,i}^{1/L}) - \sigma_{*,i} \cdot g'(\sigma_{*,i}^{1/L})}{2} \\ &= \frac{L\sigma_{*,i}^{1-\frac{1}{L}} - \sigma_{*,i}(2L-1)(\eta L^2 \sigma_{*,i}^{2-\frac{3}{L}}) - \sigma_{*,i}(L-1)(\eta L^2 \sigma_{*,i}^{2-\frac{3}{L}})}{2} \\ &= \frac{L\sigma_{*,i}^{1-\frac{1}{L}} - (3L-2)(\eta L^2 \sigma_{*,i}^{3-\frac{3}{L}})}{2} < 0, \end{aligned}$$

907 as otherwise we need $\eta \leq \frac{\sigma_{*,i}^{2/L-2}}{3L^2-2L}$, which is out of the range of interest. Since $h'(\rho) < 0$, it follows
 908 that there exists a $\delta > 0$ such that $h(\rho) > h(x)$ for all x such that $\rho < x < \rho + \delta$. Lastly, since
 909 $h(\rho) - \sigma_{*,i} = 0$ for $\rho = \sigma_{*,i}^{1/L}$, it follows that $h(\rho) - \sigma_{*,i}$ must be negative at $\rho + \delta$. Similarly, by IVT,
 910 there must exist a root within the range $\rho_{i,2} \in \left(\sigma_{*,i}^{1/L}, (2\sigma_{*,i})^{1/L}\right)$. This proves that the i -th singular
 911 value undergoes a two-period orbit with the roots $\rho_{i,1}$ and $\rho_{i,2}$. Then, notice that if the learning rate
 912 is large enough to induce oscillations in the i -th singular value, then it is also large enough to have
 913 oscillations in all singular values from 1 to the $(i-1)$ -th singular value (assuming that it is not large
 914 enough for divergence). Finally, at the (balanced) minimum, we can express the dynamics as

$$\mathbf{W}_{L:1} = \underbrace{\sum_{i=1}^p \rho_{i,j}^L \cdot \mathbf{u}_{*,i} \mathbf{v}_{*,i}^\top}_{\text{oscillation subspace}} + \underbrace{\sum_{k=p+1}^d \sigma_{*,k} \cdot \mathbf{u}_{*,k} \mathbf{v}_{*,k}^\top}_{\text{stationary subspace}}, \quad j \in \{1, 2\}, \quad \forall \ell \in [L-1]. \quad (34)$$

915 This completes the proof.

916 □

917 **Lemma 1** (Hessian Eigenvalues at Convergence). *Consider running GD on the deep matrix factorization*
 918 *loss $f(\Theta)$ defined in Equation (1). The set of all non-zero eigenvalues of the training loss Hessian at the*
 919 *balanced minimum is given by*

$$\lambda_{\Theta} = \underbrace{\left\{ L\sigma_{*,i}^{2-\frac{2}{L}}, \sigma_{*,i}^{2-\frac{2}{L}} \right\}_{i=1}^r}_{\text{self-interaction}} \cup \underbrace{\left\{ \sum_{\ell=0}^{L-1} \left(\sigma_{*,i}^{1-\frac{1}{L}-\frac{1}{L}\ell} \cdot \sigma_{*,j}^{\frac{1}{L}\ell} \right)^2 \right\}_{i \neq j}}_{\text{interaction with other singular values}} \cup \underbrace{\left\{ \sum_{\ell=0}^{L-1} \left(\sigma_{*,k}^{1-\frac{1}{L}-\frac{1}{L}\ell} \cdot \alpha^\ell \right)^2 \right\}_{k=1}}_{\text{interaction with initialization}}$$

920 where $\sigma_{*,i}$ is the i -th singular value of the target matrix $\mathbf{M}_* \in \mathbb{R}^{d \times d}$, $\alpha \in \mathbb{R}$ is the initialization scale, L is
 921 the depth of the network, and the second element of the set under “self-interaction” has a multiplicity of $d-r$.

922 *Proof.* By Proposition 2, notice that we can re-write the loss in Equation (1) as

$$\frac{1}{2} \|\mathbf{W}_{L:1} - \mathbf{M}_*\|_{\mathbb{F}}^2 = \frac{1}{2} \|\Sigma_{L:1} - \Sigma_*\|_{\mathbb{F}}^2,$$

923 where $\Sigma_{L:1}$ are the singular values of $\mathbf{W}_{L:1}$. We will first show that the eigenvalues of the Hessian
 924 with respect to the weight matrices \mathbf{W}_ℓ are equivalent to those of the Hessian taken with respect to
 925 its singular values Σ_ℓ . To this end, consider the vectorized form of the loss:

$$f(\Theta) := \frac{1}{2} \|\mathbf{W}_{L:1} - \mathbf{M}_*\|_{\mathbb{F}}^2 = \frac{1}{2} \|\text{vec}(\mathbf{W}_{L:1}) - \text{vec}(\mathbf{M}_*)\|_2^2.$$

926 Then, each block of the Hessian $\nabla_{\Theta}^2 f(\Theta) \in \mathbb{R}^{d^2 L \times d^2 L}$ with respect to the vectorized parameters is
 927 given as

$$[\nabla_{\Theta}^2 f(\Theta)]_{m,\ell} = \nabla_{\text{vec}(\mathbf{W}_m)} \nabla_{\text{vec}(\mathbf{W}_\ell)}^\top f(\Theta) \in \mathbb{R}^{d^2 \times d^2}.$$

928 By the vectorization trick, each vectorized layer matrix has an SVD of the form $\text{vec}(\mathbf{W}_\ell) =$
 929 $\text{vec}(\mathbf{U}_\ell \Sigma_\ell \mathbf{V}_\ell^\top) = (\mathbf{V}_\ell \otimes \mathbf{U}_\ell) \cdot \text{vec}(\Sigma_\ell)$. Then, notice that we have

$$\nabla_{\text{vec}(\mathbf{W}_\ell)} f(\Theta(t)) = (\mathbf{V}_\ell \otimes \mathbf{U}_\ell) \cdot \nabla_{\text{vec}(\Sigma_\ell)} f(\Theta(t)),$$

930 which gives us that each block of the Hessian is given by

$$\begin{aligned} [\nabla_{\Theta}^2 f(\Theta)]_{m,\ell} &= \nabla_{\text{vec}(\mathbf{W}_m)} \nabla_{\text{vec}(\mathbf{W}_\ell)}^\top f(\Theta) \\ &= (\mathbf{V}_m \otimes \mathbf{U}_m) \cdot \underbrace{\nabla_{\text{vec}(\Sigma_m)} \nabla_{\text{vec}(\Sigma_\ell)}^\top f(\Theta)}_{=:\mathbf{H}_{m,\ell}} \cdot (\mathbf{V}_\ell \otimes \mathbf{U}_\ell)^\top. \end{aligned}$$

931 Then, since the Kronecker product of two orthogonal matrices is also an orthogonal matrix by
 932 Lemma 10, we can write the overall Hessian matrix as

$$\tilde{\mathbf{H}} = \begin{bmatrix} \mathbf{R}_1 \mathbf{H}_{1,1} \mathbf{R}_1 & \mathbf{R}_1 \mathbf{H}_{1,2} \mathbf{R}_2 & \cdots & \mathbf{R}_1 \mathbf{H}_{1,L} \mathbf{R}_L \\ \mathbf{R}_2 \mathbf{H}_{2,1} \mathbf{R}_1 & \mathbf{R}_2 \mathbf{H}_{2,2} \mathbf{R}_2 & \cdots & \mathbf{R}_2 \mathbf{H}_{2,L} \mathbf{R}_L \\ \vdots & \vdots & \ddots & \vdots \\ \mathbf{R}_L \mathbf{H}_{L,1} \mathbf{R}_1 & \mathbf{R}_L \mathbf{H}_{L,2} \mathbf{R}_2 & \cdots & \mathbf{R}_L \mathbf{H}_{L,L} \mathbf{R}_L \end{bmatrix},$$

933 for orthogonal matrices $\{\mathbf{R}_\ell\}_{\ell=1}^L$. Then, by Lemma 9, the eigenvalues of $\tilde{\mathbf{H}}$ are the same as those of
 934 \mathbf{H} , where $\mathbf{H} \in \mathbb{R}^{d^2 L \times d^2 L}$ is the Hessian matrix with respect to the vectorized Σ_ℓ :

$$\mathbf{H} = \begin{bmatrix} \mathbf{H}_{1,1} & \mathbf{H}_{1,2} & \cdots & \mathbf{H}_{L,1} \\ \mathbf{H}_{2,1} & \mathbf{H}_{2,2} & \cdots & \mathbf{H}_{L,2} \\ \vdots & \vdots & \ddots & \vdots \\ \mathbf{H}_{1,L} & \mathbf{H}_{2,L} & \cdots & \mathbf{H}_{L,L} \end{bmatrix}.$$

935 Now, we can consider the following vectorized loss:

$$\begin{aligned} f(\Theta) &= \frac{1}{2} \|\Sigma_{L:1} - \Sigma_\star\|_F^2 = \frac{1}{2} \|\text{vec}(\Sigma_{L:1} - \Sigma_\star)\|_2^2 \\ &= \frac{1}{2} \|\underbrace{(\Sigma_{\ell-1:1}^\top \otimes \Sigma_{L:\ell+1})}_{=: \mathbf{A}_\ell} \cdot \text{vec}(\Sigma_\ell) - \text{vec}(\Sigma_\star)\|_2^2. \end{aligned}$$

936 Then, the gradient with respect to $\text{vec}(\Sigma_\ell)$ is given by

$$\nabla_{\text{vec}(\Sigma_\ell)} f(\Theta) = \mathbf{A}_\ell^\top (\mathbf{A}_\ell \cdot \text{vec}(\Sigma_\ell) - \text{vec}(\Sigma_\star)).$$

937 Then, for $m = \ell$, we have

$$\mathbf{H}_{\ell,\ell} = \nabla_{\text{vec}(\Sigma_\ell)}^2 f(\Theta) = \mathbf{A}_\ell^\top \mathbf{A}_\ell.$$

938 For $m \neq \ell$, we have

$$\begin{aligned} \mathbf{H}_{m,\ell} &= \nabla_{\text{vec}(\Sigma_m)} \nabla_{\text{vec}(\Sigma_\ell)} f(\Theta) = \nabla_{\text{vec}(\Sigma_m)} [\mathbf{A}_\ell^\top (\mathbf{A}_\ell \text{vec}(\Sigma_\ell) - \text{vec}(\mathbf{M}^\star))] \\ &= \nabla_{\text{vec}(\Sigma_m)} \mathbf{A}_\ell^\top \cdot \underbrace{(\mathbf{A}_\ell \text{vec}(\Sigma_\ell) - \text{vec}(\mathbf{M}^\star))}_{=0 \text{ at convergence}} + \mathbf{A}_\ell^\top \cdot \nabla_{\text{vec}(\Sigma_m)} (\mathbf{A}_\ell \text{vec}(\Sigma_\ell) - \text{vec}(\mathbf{M}^\star)) \\ &= \mathbf{A}_\ell^\top \mathbf{A}_m, \end{aligned}$$

939 where we have used the product rule along with the fact that $\mathbf{A}_\ell \text{vec}(\Sigma_\ell) = \mathbf{A}_m \text{vec}(\Sigma_m)$.

940 Overall, the Hessian at convergence for GD is given by

$$\mathbf{H} = \begin{bmatrix} \mathbf{A}_1^\top \mathbf{A}_1 & \mathbf{A}_1^\top \mathbf{A}_2 & \cdots & \mathbf{A}_1^\top \mathbf{A}_L \\ \mathbf{A}_2^\top \mathbf{A}_1 & \mathbf{A}_2^\top \mathbf{A}_2 & \cdots & \mathbf{A}_2^\top \mathbf{A}_L \\ \vdots & \vdots & \ddots & \vdots \\ \mathbf{A}_L^\top \mathbf{A}_1 & \mathbf{A}_L^\top \mathbf{A}_2 & \cdots & \mathbf{A}_L^\top \mathbf{A}_L \end{bmatrix}$$

941 Now, we can derive an explicit expression for each $\mathbf{A}_{m,\ell}$ by considering the implicit balancing effect
 942 of GD in Lemma 2. Under balancing and Proposition 2, we have that at convergence,

$$\Sigma_{L:1} = \Sigma_\star \implies \Sigma_\ell = \begin{bmatrix} \Sigma_\star^{1/L} & \mathbf{0} \\ \mathbf{0} & \alpha \cdot \mathbf{I}_{d-r} \end{bmatrix}, \quad \forall \ell \in [L-1], \quad \text{and } \Sigma_L = \Sigma_\star^{1/L}.$$

943 Thus, we have

$$\mathbf{H}_{m,\ell} = \begin{cases} \Sigma_\ell^{2(\ell-1)} \otimes \Sigma_\star^{\frac{2(L-\ell)}{L}} & \text{for } m = \ell, \\ \Sigma_\ell^{m+\ell-2} \otimes \Sigma_\star^{2L-m-\ell} & \text{for } m \neq \ell. \end{cases}$$

944 Now, we are left with computing the eigenvalues of $\mathbf{H} \in \mathbb{R}^{d^2 L \times d^2 L}$. To do this, let us block diagonalize \mathbf{H} into $\mathbf{H} = \mathbf{P}\mathbf{C}\mathbf{P}^\top$, where \mathbf{P} is a permutation matrix and

$$\mathbf{C} = \begin{bmatrix} \mathbf{C}_1 & & \\ & \ddots & \\ & & \mathbf{C}_{d^2} \end{bmatrix} \in \mathbb{R}^{d^2 L \times d^2 L},$$

946 where each (i, j) -th entry of $\mathbf{C}_k \in \mathbb{R}^{L \times L}$ is the k -th diagonal element of $\mathbf{H}_{i,j}$. Since \mathbf{C} and \mathbf{H} are similar matrices, they have the same eigenvalues. Then, since \mathbf{C} is a block diagonal matrix, its eigenvalues (and hence the eigenvalues of \mathbf{H}) are the union of each of the eigenvalues of its blocks.

949 By observing the structure of $\mathbf{H}_{m,\ell}$, notice that each \mathbf{C}_k is a rank-1 matrix. Hence, when considering the top- r diagonal elements of $\mathbf{H}_{m,\ell}$ corresponding to each Kronecker product to construct \mathbf{C}_k , each \mathbf{C}_k can be written as an outer product $\mathbf{u}\mathbf{u}^\top$, where $\mathbf{u} \in \mathbb{R}^L$ is

$$\mathbf{u}^\top = \left[\sigma_{*,i}^{1-\frac{1}{L}} \sigma_{*,j}^0 \quad \sigma_{*,i}^{1-\frac{2}{L}} \sigma_{*,j}^{\frac{1}{L}} \quad \sigma_{*,i}^{1-\frac{3}{L}} \sigma_{*,j}^{\frac{2}{L}} \quad \dots \quad \sigma_{*,i}^0 \sigma_{*,j}^{1-\frac{1}{L}} \right]^\top. \quad (35)$$

952 Then, the non-zero eigenvalue of this rank-1 matrix is simply $\|\mathbf{u}\|_2^2$, which simplifies to

$$\|\mathbf{u}\|_2^2 = \sum_{\ell=0}^{L-1} \left(\sigma_{*,i}^{1-\frac{1}{L}-\frac{1}{L}\ell} \cdot \sigma_{*,j}^{\frac{1}{L}\ell} \right)^2.$$

953 Next, we can consider the remaining $d - r$ components of each Kronecker product of $\mathbf{H}_{m,\ell}$. Notice that for $m = \ell = L$, we have

$$\mathbf{H}_{L,L} = \begin{bmatrix} \sigma_{*,1}^{\frac{2(L-1)}{L}} \cdot \mathbf{I}_d & & & \\ & \ddots & & \\ & & \sigma_{*,r}^{\frac{2(L-1)}{L}} \cdot \mathbf{I}_d & \\ & & & \alpha^{2(L-1)} \mathbf{I}_{d-r} \otimes \mathbf{I}_d \end{bmatrix}.$$

955 This amounts to a matrix \mathbf{C}_k with a single element $\sigma_{*,i}^{\frac{2(L-1)}{L}}$ and 0 elsewhere. This gives an eigenvalue $\sigma_{*,i}^{\frac{2(L-1)}{L}}$ for all $i \in [r]$, with multiplicity $d - r$.

957 Lastly, we can consider the diagonal components of $\mathbf{H}_{m,\ell}$ that is a function of the initialization scale α . For this case, each \mathbf{C}_k can be written as an outer product $\mathbf{v}\mathbf{v}^\top$, where

$$\mathbf{v}^\top = \left[\sigma_{*,i}^{1-\frac{1}{L}} \alpha^0 \quad \sigma_{*,i}^{1-\frac{2}{L}} \alpha \quad \sigma_{*,i}^{1-\frac{3}{L}} \alpha^2 \quad \dots \quad \sigma_{*,i}^0 \alpha^{L-1} \right]^\top. \quad (36)$$

959 Similarly, the non-zero eigenvalue is simply $\|\mathbf{v}\|_2^2$, which corresponds to

$$\|\mathbf{v}\|_2^2 = \sum_{\ell=0}^{L-1} \left(\sigma_{*,i}^{1-\frac{1}{L}-\frac{1}{L}\ell} \cdot \alpha^\ell \right)^2.$$

960 This completes the proof. \square

961 **Lemma 2** (Balancing). Let $\sigma_{*,i}$ and $\sigma_{\ell,i}(t)$ denote the i -th singular value of $\mathbf{M}_* \in \mathbb{R}^{d \times d}$ and $\mathbf{W}_\ell(t)$, respectively and define $S_i := L\sigma_{*,i}^{2-\frac{2}{L}}$. Consider GD on the i -th index of the simplified loss in (4) with the unbalanced initialization and learning rate $\frac{2}{S_i} < \eta < \frac{2\sqrt{2}}{S_i}$. If the initialization scale α satisfies $0 < \alpha <$

964 $\left(\ln \left(\frac{2\sqrt{2}}{\eta S_i} \right) \cdot \frac{\sigma_{*,i}^{4/L}}{L^{2.2} \frac{2L-3}{L}} \right)^{1/4}$, then there exists a constant $c \in (0, 1]$ such that for all $\ell \in [L - 1]$, we have

965 $\left| \sigma_{L,i}^2(t+1) - \sigma_{\ell,i}^2(t+1) \right| < c \left| \sigma_{L,i}^2(t) - \sigma_{\ell,i}^2(t) \right|.$

966 *Proof.* To prove the result, we will use a quantity defined as the gradient flow solution (GFS) sharpness following Kreisler et al. [13]:

968 **Definition 3** (GFS Sharpness). *The GFS sharpness denoted by $\psi(x)$ is the sharpness achieved by the global*
 969 *minima which lies in the same GF trajectory of x (i.e., $\|\nabla^2 L(z)\|$ such that $L(z) = 0$ and $z = GF(x)$, where*
 970 *$GF(\cdot)$ denotes the gradient flow solution).*

971 Then, let us consider the i -th index of the simplified loss in (4):

$$\frac{1}{2} \left(\prod_{\ell=1}^L \sigma_{\ell,i} - \sigma_{*,i} \right)^2 =: \frac{1}{2} \left(\prod_{\ell=1}^L \sigma_{\ell} - \sigma_{*} \right)^2,$$

972 and omit the dependency on i for ease of exposition. Our goal is to show that the L -th singular
 973 value σ_L initialized to zero become increasingly balanced to σ_{ℓ} which are initialized to α . To that
 974 end, let us define the balancing dynamics between σ_i and σ_j as $b_{i,j}^{(t+1)} := \left(\sigma_i^{(t+1)} \right)^2 - \left(\sigma_j^{(t+1)} \right)^2$ and
 975 $\pi^{(t)} := \prod_{\ell=1}^L \sigma_{\ell}(t)$ for the product of singular values at iteration t . We can simplify the balancing
 976 dynamics as follows:

$$\begin{aligned} b_{i,j}^{(t+1)} &= \left(\sigma_i^{(t+1)} \right)^2 - \left(\sigma_j^{(t+1)} \right)^2 \\ &= \left(\sigma_i^{(t)} - \eta \left(\pi^{(t)} - \sigma_{*} \right) \frac{\pi^{(t)}}{\sigma_i^{(t)}} \right)^2 - \left(\sigma_j^{(t)} - \eta \left(\pi^{(t)} - \sigma_{*} \right) \frac{\pi^{(t)}}{\sigma_j^{(t)}} \right)^2 \\ &= \left(\sigma_i^{(t)} \right)^2 - \left(\sigma_j^{(t)} \right)^2 + \eta^2 \left(\pi^{(t)} - \sigma_{*} \right)^2 \left(\frac{\left(\pi^{(t)} \right)^2}{\left(\sigma_i^{(t)} \right)^2} - \frac{\left(\pi^{(t)} \right)^2}{\left(\sigma_j^{(t)} \right)^2} \right) \\ &= \left(\left(\sigma_i^{(t)} \right)^2 - \left(\sigma_j^{(t)} \right)^2 \right) \left(1 - \eta^2 \left(\pi^{(t)} - \sigma_{*} \right)^2 \frac{\left(\pi^{(t)} \right)^2}{\left(\sigma_i^{(t)} \right)^2 \left(\sigma_j^{(t)} \right)^2} \right) \\ &= b_{i,j}^{(t)} \left(1 - \eta^2 \left(\pi^{(t)} - \sigma_{*} \right)^2 \frac{\left(\pi^{(t)} \right)^2}{\left(\sigma_i^{(t)} \right)^2 \left(\sigma_j^{(t)} \right)^2} \right). \end{aligned}$$

977 Then, in order to show that $|b_{i,j}^{(t+1)}| < c |b_{i,j}^{(t)}|$ for some $0 < c \leq 1$, we need to prove that

$$\left| 1 - \eta^2 \left(\pi^{(t)} - \sigma_{*} \right)^2 \frac{\left(\pi^{(t)} \right)^2}{\left(\sigma_i^{(t)} \right)^2 \left(\sigma_j^{(t)} \right)^2} \right| < c,$$

978 for all iterations t . We complete this using the following two steps:

979 (i) We show that for all scalars σ in the trajectory, if $\psi(\sigma) < \frac{2\sqrt{1+c}}{\eta}$ and $\sigma > 0$, then it holds that
 980 $\sum_{i=1}^{\min\{2, L-1\}} \frac{\eta^2 (\pi(\sigma) - \sigma_{*})^2 \pi^2(\sigma)}{\sigma_{L-i}^2 \sigma_L^2} \leq 1 + c$, where $\pi(\sigma)$ denotes the product given the trajectory of all
 981 σ_i . This case is analyzed when $\pi(\sigma) \in [0, \sigma_{*}]$ where $0 < c < 1$ and when $\pi(\sigma) > \sigma_{*}$ where $c = 1$.

982 (ii) If $\sum_{i=1}^{\min\{2, L-1\}} \frac{\eta^2 (\pi(\sigma) - \sigma_{*})^2 \pi^2(\sigma)}{\sigma_{L-i}^2 \sigma_L^2} \leq 1 + c$, then iterates become more balanced, i.e., $|b_{i,j}^{(t+1)}| < c |b_{i,j}^{(t)}|$.

983 We prove (i) in Lemma 3 and (ii) in Lemma 4. Both of the proofs are originally from [13], which
 984 we adapted using our notation for ease of the reader. Then, in Lemma 5, we show that for each σ_{*} ,
 985 as long as the initialization scale satisfies

$$\alpha < \left(\ln \left(\frac{2\sqrt{2}}{\eta L \sigma_{*}^{2-\frac{2}{L}}} \right) \cdot \frac{\sigma_{*}^{\frac{4}{L}}}{L^2 \cdot 2^{\frac{2L-3}{L}}} \right)^{\frac{1}{4}},$$

986 then it holds that the GFS sharpness satisfies $\psi(\sigma) < \frac{2\sqrt{2}}{\eta}$, which is the necessary condition for
 987 balancing. Then, to satisfy this condition for all singular values $\sigma_{*,i}$ for all $i \in [r]$, we need

$$\alpha < \left(\ln \left(\frac{2\sqrt{2}}{\eta L \sigma_{*,1}^{2-\frac{2}{L}}} \right) \cdot \frac{\sigma_{*,1}^{\frac{4}{L}}}{L^2 \cdot 2^{\frac{2L-3}{L}}} \right)^{\frac{1}{4}} \implies \eta < \frac{2\sqrt{2}}{L \sigma_{*,1}^{2-\frac{2}{L}}}, \quad (37)$$

988 for the validity of the initialization scale. Thus, as long as the conditions in Equation (37) hold, we
 989 will have balancing. This completes the proof. \square

990 **Lemma 3.** *If the GFS sharpness $\psi(\sigma) \leq \frac{2\sqrt{1+c}}{\eta}$ and $\sigma > 0$, then $\sum_{i=1}^{\min\{2,L-1\}} \frac{\eta^2(\pi(\sigma) - \sigma_*)^2 \pi^2(\sigma)}{\sigma_{[L-i]}^2 \sigma_L^2} \leq (1+c)$
 991 for some $0 < c \leq 1$.*

992 *Proof.* We will consider two cases: (i) $\pi(\sigma) \in [0, \sigma_*)$ and (ii) $\pi(\sigma) > \sigma_*$ ¹.
 993

994 **Case 1:** Let $\sigma \in \mathbb{R}^D$ and consider the case where $\pi(\sigma) \in [0, \sigma_*)$. Then, we have

$$\sum_{i=1}^{\min\{2,L-1\}} \frac{\eta^2(\pi(\sigma) - \sigma_*)^2 \pi^2(\sigma)}{\sigma_{L-i}^2 \sigma_L^2} \leq \frac{\eta^2 \pi^2(\sigma)}{\sigma_{L-i}^2 \sigma_L^2}.$$

995 Our goal is to show that if $\psi(\sigma) \leq \frac{2\sqrt{1+c}}{\eta}$ for some $0 < c < 1$ then,

$$\sum_{i=1}^{\min\{2,L-1\}} \frac{\eta^2(\pi(\sigma) - 1)^2 \pi^2(\sigma)}{\sigma_{L-i}^2 \sigma_L^2} \leq \frac{\eta^2 \pi^2(\sigma)}{\sigma_{L-i}^2 \sigma_L^2} \leq 1 + c.$$

996 Since the GFS sharpness is constant for all the weights on the gradient flow (GF) trajectory by
 997 definition, we can focus on the singular values (or weights) at the global minima. Consider
 998 $z = \text{GF}(\sigma)$, the GF solution of σ . In Lemma 6, we proved that GF preserves unbalancedness, such
 999 that $\sigma_l^2 - \sigma_m^2 = z_l^2 - z_m^2$ for all layers. Hence, it is sufficient to show that $\sum_{i=1}^{\min\{2,L-1\}} \frac{\eta^2 \pi(z)^2}{z_{L-i}^2 z_L^2} \leq 1+c$ in
 1000 order to ensure $\sum_{i=1}^{\min\{2,L-1\}} \frac{\eta^2 \pi^2(\sigma)}{\sigma_{L-i}^2 \sigma_L^2} \leq 1+c$. Note that $\pi(z) = \sigma_*$, since it lies on the global minima.

1001 Then,

$$\sum_{i=1}^{\min\{2,L-1\}} \frac{\eta^2 \pi^2(z)}{z_{L-i}^2 z_L^2} = \sum_{i=1}^{\min\{2,L-1\}} \frac{\eta^2 \sigma_*^2}{z_{L-i}^2 z_L^2}. \quad (38)$$

1002 From Lemma 7, we know that the sharpness at the global minima is given as

$$\psi(\sigma) = \|\nabla^2 L(z)\| = \sum_{i=1}^L \frac{\sigma_*^2}{z_i^2}. \quad (39)$$

1003 This immediately implies that $\frac{\sigma_*^2}{z_L^2} \leq \psi(\sigma)$ and equivalently, $\exists \alpha \in [0, 1]$ such that $\frac{\sigma_*^2}{z_L^2} = \alpha \psi(\sigma)$.
 1004 Therefore, we have

$$\sum_{i=1}^{\min\{2,L-1\}} \frac{\sigma_*^2}{z_{L-i}^2} \leq (1-\alpha) \psi(\sigma). \quad (40)$$

1005 Substituting Equations (39) and (40) into the expression we aim to bound, we obtain

$$\sum_{i=1}^{\min\{2,L-1\}} \frac{\eta^2(\pi(\sigma) - \sigma_*^2)^2 \pi^2(\sigma)}{\sigma_{L-i}^2 \sigma_L^2} = \sum_{i=1}^{\min\{2,L-1\}} \frac{\eta^2 \sigma_*^2}{z_{L-i}^2 z_L^2} \leq \eta^2 \alpha (1-\alpha) \psi^2(\sigma) \leq \frac{\eta^2}{4} \psi^2(\sigma) \leq 1+c,$$

¹We ignore the case $\pi^{(t)} = \sigma_*$ when we get $b_{i,j}^{(t+1)} = b_{i,j}^{(t)}$. Since the occurrence $\pi^{(t)} = \sigma_*$ holds with a probability of zero where EOS ceases to exist.

1006 where we used the fact that the maximum of $\alpha(1 - \alpha)$ is $\frac{1}{4}$ when $\alpha = \frac{1}{2}$ and $\psi(\sigma) \leq \frac{2\sqrt{1+c}}{\eta}$. Thus, if
 1007 $\psi(\sigma) \leq \frac{2\sqrt{1+c}}{\eta}$, then for every weight σ lying on its GF trajectory, we have

$$\sum_{i=1}^{\min\{2, L-1\}} \frac{\eta^2(\pi(\sigma) - \sigma_*)^2 \pi^2(\sigma)}{\sigma_{L-i}^2 \sigma_L^2} \leq 1 + c.$$

1008 **Case 2:** Consider the case in which $\pi(\sigma) > \sigma_*$. We already have that $\sigma > 0$ throughout the trajectory
 1009 (refer to Lemma 3.11 in [13]) and so $\pi(\sigma) > 0$. So, the GD update from σ_i will also stay positive

$$\sigma_i - \eta(\pi(\sigma) - \sigma_*)\pi(\sigma) \frac{1}{\sigma_i} > 0.$$

1010 From this, we get

$$2 > \frac{\eta(\pi(\sigma) - \sigma_*)\pi(\sigma)}{\sigma_i^2} > 0,$$

1011 This implies $\sum_{i=1}^{\min\{2, L-1\}} \frac{\eta^2(\pi(\sigma) - \sigma_*)^2 \pi^2(\sigma)}{\sigma_{L-i}^2 \sigma_L^2} \leq (1 + c)$ with $c = 1$. This completes the proof. \square

1012 **Lemma 4.** If $\sum_{i=1}^{\min\{2, L-1\}} \frac{\eta^2(\pi(\sigma) - \sigma_*)^2 \pi^2(\sigma)}{\sigma_{L-i}^2 \sigma_L^2} \leq 1 + c$ for $i, j \in [L]$ for some $0 < c \leq 1$, then $|b_{i,j}^{(t+1)}| <$
 1013 $c |b_{i,j}^{(t)}|$.

1014 *Proof.* Recall that the condition for balancing was given by

$$b_{i,j}^{(t+1)} = b_{i,j}^{(t)} \left(1 - \eta^2(\pi^{(t)} - \sigma_*)^2 \frac{\pi^{(t)2}}{(\sigma_i^{(t)})^2 (\sigma_j^{(t)})^2} \right). \quad (41)$$

WLOG, suppose that the σ are sorted such that $\sigma_1 \geq \sigma_2 \geq \dots \geq \sigma_L$. We know that

$$\sum_{i=1}^{\min\{2, L-1\}} \frac{\eta^2(\pi(\sigma) - \sigma_*)^2 \pi^2(\sigma)}{\sigma_{L-i}^2 \sigma_L^2} \leq 1 + c,$$

1015 which implies

$$\frac{\eta^2(\pi(\sigma) - \sigma_*)^2 \pi^2(\sigma)}{\sigma_{L-1}^2 \sigma_L^2} < 1 + c \quad \text{and} \quad \frac{\eta^2(\pi(\sigma) - \sigma_*)^2 \pi^2(\sigma)}{\sigma_i^2 \sigma_j^2} < \frac{1 + c}{2}, \quad (42)$$

1016 for all $i \in [L], j \in [L-2]$ and $i < j$. Notice that the latter inequality comes from the fact that

$$\frac{\eta^2(\pi(\sigma) - \sigma_*)^2 \pi^2(\sigma)}{\sigma_{L-2}^2 \sigma_L^2} + \frac{\eta^2(\pi(\sigma) - \sigma_*)^2 \pi^2(\sigma)}{\sigma_{L-2}^2 \sigma_L^2} < \frac{\eta^2(\pi(\sigma) - \sigma_*)^2 \pi^2(\sigma)}{\sigma_{L-1}^2 \sigma_L^2} + \frac{\eta^2(\pi(\sigma) - \sigma_*)^2 \pi^2(\sigma)}{\sigma_{L-2}^2 \sigma_L^2} < 1 + c,$$

1017 which implies that

$$2 \frac{\eta^2(\pi(\sigma) - \sigma_*)^2 \pi^2(\sigma)}{\sigma_{L-2}^2 \sigma_L^2} < 1 + c \implies \frac{\eta^2(\pi(\sigma) - \sigma_*)^2 \pi^2(\sigma)}{\sigma_{L-2}^2 \sigma_L^2} < \frac{1 + c}{2},$$

1018 and since σ are sorted, it holds for all other σ . Therefore from Equation (41), we have for all $i \in$
 1019 $[L-2]$,

$$b_{i,i+1}^{(t+1)} < c b_{i,i+1}^{(t)} \quad \text{and} \quad b_{L-2,L}^{(t+1)} < c b_{L-2,L}^{(t)} \quad \text{and} \quad -c b_{L-1,L}^{(t)} < b_{L-1,L}^{(t+1)} < c b_{L-1,L}^{(t)}. \quad (43)$$

1020 Then, notice that since we initialized all of the singular values σ_ℓ for $\ell \in [L-1]$ to be the same, they
 1021 follow the same dynamics. Since we already showed that $|b_{L-1,L}^{(t+1)}| < c |b_{L-1,L}^{(t)}|$, it must follow that

$$|b_{i,j}^{(t+1)}| < c |b_{i,j}^{(t)}| \quad \text{for } i, j \in [L].$$

1022 This completes the proof.

1023 \square

1024 **Lemma 5.** Consider running GD with learning rate η in Equation (2) on the scalar loss

$$\mathcal{L}(\{\sigma_i\}_{i=1}^d) = \frac{1}{2} \left(\prod_{i=1}^L \sigma_i - \sigma_\star \right)^2,$$

1025 with initialization $\sigma_L(0) = 0$ and $\sigma_\ell(0) = \alpha$ for all $\ell \in [L-1]$. If $\alpha < \left(\ln \left(\frac{2\sqrt{2}}{\eta L \sigma_\star^{\frac{2-L}{L}}} \right) \cdot \frac{\sigma_\star^{\frac{L}{L-1}}}{L^2 \cdot 2^{\frac{L-3}{L}}} \right)^{\frac{1}{4}}$, then
 1026 the GFS sharpness $\psi(\sigma) \leq \frac{2\sqrt{1+c}}{\eta}$ for some $0 < c < 1$.

1027 *Proof.* Since the singular values σ_ℓ for all $\ell \in [L-1]$ are initialized to α , note that they all follow the
 1028 same dynamics. Then, let us define

$$y := \sigma_1 = \dots = \sigma_{L-1} \quad \text{and} \quad x := \sigma_L.$$

1029 The gradient flow (GF) solution is the intersection between

$$xy^{L-1} = \sigma_\star \quad \text{and} \quad x^2 - y^2 = -\alpha^2,$$

1030 where the first condition comes from convergence and the second comes from the conservation flow
 1031 law of GF which we prove in Lemma 6. Then, if we can find a solution at the intersection such that

$$(\hat{x}(\alpha), \hat{y}(\alpha)) = \begin{cases} xy^{L-1} = \sigma_\star \\ x^2 - y^2 = -\alpha^2, \end{cases} \quad (44)$$

1032 solely in terms of α , then we can plug in $(\hat{x}(\alpha), \hat{y}(\alpha))$ into the GFS² from Lemma 7

$$\psi(\hat{x}(\alpha), \hat{y}(\alpha)) = \psi(\sigma) = \sum_{i=1}^L \frac{\sigma_\star^2}{\sigma_i^2} = \sigma_\star^2 \left(\frac{1}{\hat{x}(\alpha)^2} + \frac{L-1}{\hat{y}(\alpha)^2} \right) < \frac{2\sqrt{2}}{\eta}$$

1033 and solve to find an upper bound on α . The strict inequality ensures that we can find a c in $c \in [0, 1)$
 1034 such that $\psi(\alpha) < \frac{2\sqrt{1+c}}{\eta}$. However, the intersection $(\hat{x}(\alpha), \hat{y}(\alpha))$ is a $2L$ -th order polynomial in $\hat{y}(\alpha)$
 1035 which does not have a straightforward closed-form solution solely in terms of α . Hence, we aim to
 1036 find the upper bound on α by using a calculus of variations. By plugging in x , the solution $\hat{y}(\alpha)$
 1037 satisfies

$$y^{2L} - \alpha^2 y^{2L-2} = \sigma_\star^2.$$

1038 Then, by differentiating the relation with respect to α , we obtain the following variational relation:

$$\begin{aligned} 2Ly^{2L-1}dy - \alpha^2 2(L-1)y^{2L-3}dy - 2\alpha y^{2L-2}d\alpha &= 0 \\ \implies y^{2L-3}(y^2L - \alpha^2(L-1))dy &= \alpha y^{2(L-1)}d\alpha \\ \implies dy &= \frac{y\alpha}{(y^2L - \alpha^2(L-1))}d\alpha, \end{aligned} \quad (45)$$

1039 where we used the fact that $y^{2L-2} > 0$ from Lemma 3 in the last line. Then, in order to have $\frac{dy}{d\alpha} > 0$,
 1040 we need $y > \sqrt{\frac{L-1}{L}}\alpha$, which is always true since $y > \alpha$ from initialization. Then, since $\alpha \rightarrow 0$,
 1041 $\lim_{\alpha \rightarrow 0} \hat{y}(\alpha) = \sigma_\star^{\frac{1}{L}}$ and $\lim_{\alpha \rightarrow 0} \hat{x}(\alpha) = \sigma_\star^{\frac{1}{L}}$, as it corresponds to exact balancing. Hence, $\frac{dy}{d\alpha} > 0$
 1042 implies as α increases from 0, $\hat{y}(\alpha)$ would increase from $\sigma_\star^{\frac{1}{L}}$ and $\hat{y}(\alpha)$ is an increasing function of α .
 1043 Similarly, the intersection at the global minima would satisfy the following relation for $\hat{x}(\alpha)$:

$$\begin{aligned} x^{(2+\frac{2}{L-1})} + x^{\frac{2}{(L-1)}}\alpha^2 &= \sigma_\star^{\frac{2}{L-1}} \\ \implies \left(2 + \frac{2}{L-1} \right) x^{1+\frac{2}{L-1}} dx + \left(\frac{2}{L-1} \right) \alpha^2 x^{\frac{2}{L-1}-1} dx + x^{\frac{2}{L-1}} (2\alpha d\alpha) &= 0 \\ \implies dx &= \frac{-\alpha}{\left(\frac{L}{L-1}x + \frac{\alpha^2}{L-1} \frac{1}{x} \right)} d\alpha. \end{aligned} \quad (46)$$

²Note that throughout the proof $(\hat{x}(\alpha), \hat{y}(\alpha))$ denotes the gradient flow solution as function of α . It does not refer to the GF trajectory.

1044 Note that since $x > 0$, we will always have $\frac{dx}{d\alpha} < 0$. Then, since $\lim_{\alpha \rightarrow 0} \hat{x}(\alpha) = \sigma_*^{\frac{1}{L}}$, $\frac{dx}{d\alpha} < 0$ implies
 1045 that as α increases, $\hat{x}(\alpha)$ would decrease from $\sigma_*^{\frac{1}{L}}$. Now, with the variational relations $\frac{d\hat{x}}{d\alpha}$ and $\frac{d\hat{y}}{d\alpha}$ in
 1046 place, we aim to find $\frac{d\psi}{d\alpha}$:

$$\begin{aligned} \Psi(\alpha) &:= \psi(\hat{x}(\alpha), \hat{y}(\alpha)) = \sigma_*^2 \left(\frac{1}{\hat{x}(\alpha)^2} + \frac{L-1}{\hat{y}(\alpha)^2} \right) \\ \implies d\Psi &= \sigma_*^2 \left(-\frac{2}{\hat{x}^3} d\hat{x} - \frac{2(L-1)}{\hat{y}^3} d\hat{y} \right) \\ \implies d\Psi &= \frac{1}{\hat{x}^3} \left[\frac{2\alpha\sigma_*^2}{\left(\frac{L}{L-1}\right)\hat{x} + \left(\frac{\alpha^2}{L-1}\right)\frac{1}{\hat{x}}} \right] d\alpha - \left[\frac{(L-1)}{\hat{y}^3} \frac{2\alpha\hat{y}\sigma_*^2}{(\hat{y}^2L - \alpha^2(L-1))} \right] d\alpha \\ \implies d\Psi &= \left[\frac{1}{\hat{x}^4 + \frac{\alpha^2}{L}\hat{x}^2} - \frac{1}{(\hat{y}^4 - \alpha^2\hat{y}^2\frac{(L-1)}{L})} \right] 2\frac{(L-1)\sigma_*^2}{L}\alpha d\alpha \\ \implies d\Psi &= G(\alpha)d\alpha, \end{aligned}$$

1047 where we defined $G(\alpha) := \left[\frac{1}{\hat{x}^4 + \frac{\alpha^2}{L}\hat{x}^2} - \frac{1}{(\hat{y}^4 - \alpha^2\hat{y}^2\frac{(L-1)}{L})} \right] 2\frac{(L-1)\sigma_*^2}{L}\alpha$ and used the notation $\hat{x} = \hat{x}(\alpha)$
 1048 and $\hat{y} = \hat{y}(\alpha)$ for simplicity.

1049

1050 Next, we will show the three following steps:

- 1051 (i) Prove that $G(\alpha) > 0$ for all $\alpha > 0$ to show that the sharpness $\Psi(\alpha)$ is an increasing function of α .
- 1052 (ii) Solve the differential $d\Psi$ to find the relationship between $d\Psi$ and $\Psi(\alpha)$.
- 1053 (iii) Find an upper bound on a part of $\frac{d\Psi}{\Psi(\alpha)}$ found in Step 2.

1054 These series of steps comes from the fact that the intersection does not have a closed-form solution.
 1055 The goal is to find a function in which we can upper bound $\frac{d\Psi}{\Psi(\alpha)}$ with a function with a closed-form
 1056 solution to find a bound on α such that the sharpness $\psi(\alpha) < \frac{2\sqrt{2}}{\eta}$.

1057

1058 **Step 1:** Prove $G(\alpha) > 0$ to show sharpness $\Psi(\alpha)$ is an increasing function of α .

1059

1060 There have been several lines of work such as those by [13] and [61] which showed that GD would
 1061 decrease the sharpness of the solution. The more balanced the solution (which corresponds to
 1062 smaller α), the smaller the sharpness. We prove this again here:

$$\begin{aligned} G(\alpha) > 0 &\implies \hat{y}^4 - \alpha^2\hat{y}^2\frac{(L-1)}{L} > \hat{x}^4 + \frac{\alpha^2}{L}\hat{x}^2 \\ &\implies (\hat{y}^4 - \hat{x}^4) > \alpha^2 \left(\frac{1}{L}\hat{x}^2 + \hat{y}^2\frac{(L-1)}{L} \right) \\ &\implies \underbrace{(\hat{y}^2 - \hat{x}^2)}_{=\alpha^2}(\hat{y}^2 + \hat{x}^2) > \alpha^2 \left(\frac{1}{L}\hat{x}^2 + \hat{y}^2\frac{(L-1)}{L} \right) \\ &\implies \hat{x}^2\left(1 - \frac{1}{L}\right) + \hat{y}^2\frac{1}{L} > 0, \end{aligned}$$

1063 where the last inequality always holds since we have $L > 2$. This proves that Ψ is an increasing
 1064 function of α since for $d\Psi = G(\alpha)d\alpha$, as it always holds that $G(\alpha) > 0$ for any $L > 2$ and $\alpha > 0$.

1065

1066 **Step 2:** Solve the differential to establish the relation between $\Psi(\alpha)$ and α .

1067

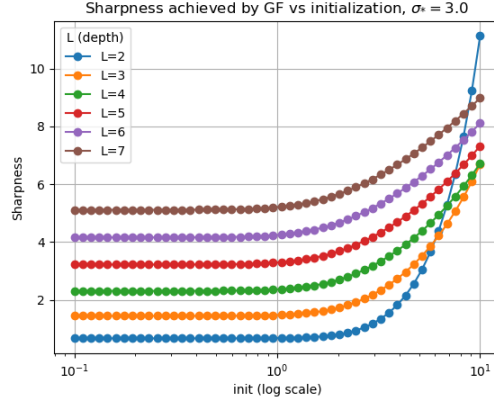


Figure 25: Sharpness $\Psi(\alpha)$ as a function of initialization α . The theoretical approximation bound $\Psi = \Psi_0 \exp\left(\frac{L^2 \cdot 2^{\frac{2(L-1)}{L}}}{2\sigma_*^{\frac{4}{L}}}\alpha^4\right)$ serves as proxy upper bound to this increasing function.

1068 Rewriting the expression for sharpness and establishing an equation we have

$$\Psi(\alpha) = \sigma_*^2 \left(\frac{1}{\hat{x}(\alpha)^2} + \frac{L-1}{\hat{y}(\alpha)^2} \right) \implies \Psi(\alpha) = \sigma_*^2 \left(\frac{\hat{y}^2 + (L-1)\hat{x}^2}{\hat{x}^2\hat{y}^2} \right) \quad (47)$$

$$\implies \frac{\hat{y}^2}{L} + \left(1 - \frac{1}{L}\right)\hat{x}^2 = \frac{\Psi(\alpha)\hat{x}^2\hat{y}^2}{L\sigma_*^2}. \quad (48)$$

1069 Now, we revisit the original differential between $\Psi(\alpha)$ and α :

$$\begin{aligned} d\Psi &= \left[\frac{1}{(\hat{x}^4 + \frac{\alpha^2}{L}\hat{x}^2)} - \frac{1}{(\hat{y}^4 - \alpha^2\hat{y}^2\frac{(L-1)}{L})} \right] 2\frac{(L-1)\sigma_*^2}{L}\alpha d\alpha \\ \implies d\Psi &= \frac{\hat{y}^4 - \hat{x}^4 - \alpha^2\left(\frac{\hat{x}^2}{L} + \left(1 - \frac{1}{L}\right)\hat{y}^2\right)}{(\hat{x}^4 + \frac{\alpha^2}{L}\hat{x}^2)(\hat{y}^4 - \alpha^2\hat{y}^2\frac{(L-1)}{L})} 2\left(1 - \frac{1}{L}\right)\sigma_*^2\alpha d\alpha \\ \implies d\Psi &= \frac{\alpha^2\left(\frac{\hat{y}^2}{L} + \left(1 - \frac{1}{L}\right)\hat{x}^2\right)}{(\hat{x}^4 + \frac{\alpha^2}{L}\hat{x}^2)(\hat{y}^4 - \alpha^2\hat{y}^2\frac{(L-1)}{L})} 2\left(1 - \frac{1}{L}\right)\sigma_*^2\alpha d\alpha \end{aligned} \quad (49)$$

1070 Using the expression for $\frac{\hat{y}^2}{L} + \left(1 - \frac{1}{L}\right)\hat{x}^2$ derived in Equation (48) and plugging it into Equation (49),
1071 we obtain

$$\begin{aligned} d\Psi &= \frac{\alpha^2\left(\frac{\Psi(\alpha)\hat{x}^2\hat{y}^2}{L\sigma_*^2}\right)}{(\hat{x}^4 + \frac{\alpha^2}{L}\hat{x}^2)(\hat{y}^4 - \alpha^2\hat{y}^2\frac{(L-1)}{L})} 2\left(1 - \frac{1}{L}\right)\sigma_*^2\alpha d\alpha \\ \implies \frac{d\Psi}{\Psi(\alpha)} &= \frac{2}{(\hat{x}^2 + \frac{\alpha^2}{L})(\hat{y}^2 - \alpha^2\frac{(L-1)}{L})} \left(\frac{1}{L} - \frac{1}{L^2}\right)\alpha^3 d\alpha \\ \implies \frac{d\Psi}{\Psi(\alpha)} &= \frac{2}{(\hat{x}^2 + \frac{\alpha^2}{L})^2} \left(\frac{1}{L} - \frac{1}{L^2}\right)\alpha^3 d\alpha \end{aligned} \quad (50)$$

$$\implies \frac{d\Psi}{\Psi(\alpha)} = P(\alpha)\alpha^3 d\alpha, \quad (51)$$

$$(52)$$

1072 where we have defined $P(\alpha) := \frac{2}{(\hat{x}^2 + \frac{\alpha^2}{L})^2} \left(\frac{1}{L} - \frac{1}{L^2}\right)$.

1073 Solving the differential $\frac{d\Psi}{\Psi(\alpha)} = P(\alpha)\alpha^3 d\alpha$ in exact closed-form is difficult since \hat{x} is also an function
1074 of α . However, in Step 1, we proved that $\Psi(\alpha)$ is an increasing function of α , and so instead of

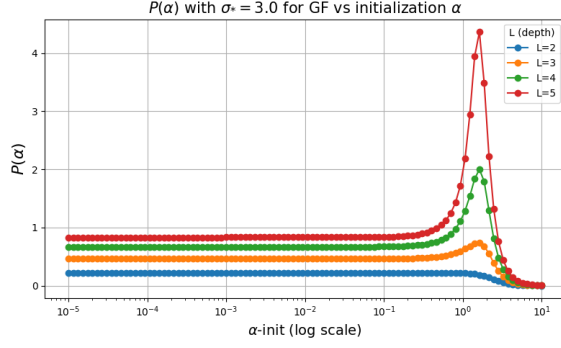


Figure 26: $P(\alpha)$ for GF has a unique maxima at $\alpha = \frac{\sigma_*^{\frac{1}{L}}}{\left(\frac{1}{\sqrt{L(L-2)}}(1 + \frac{1}{L(L-2)})^{\frac{L-1}{2}}\right)^{\frac{1}{L}}}$ for $L > 2$.

1075 solving exactly, we can find a differential equation $\frac{d\Psi}{\Psi(\alpha)} = F(\alpha)\alpha^3 d\alpha$ with $F(\alpha) > P(\alpha)$ such that
 1076 $F(\alpha)$ is more increasing, and use it to solve the PDE instead. Though, note that the initialization
 1077 limit on α that would be found after solving the surrogate PDE $\frac{d\Psi}{\Psi(\alpha)} = F(\alpha)\alpha^3 d\alpha$ would be smaller
 1078 than the α if it was found using the original PDE $\frac{d\Psi}{\Psi(\alpha)} = P(\alpha)\alpha^3 d\alpha$.
 1079

1080 **Step 3: Finding an upper bound function and solving for initialization.**

1081 Note that the original coefficient in $\frac{d\Psi}{\Psi(\alpha)} = P(\alpha)\alpha^3 d\alpha$ is of the form

$$P(\alpha) = \frac{2}{\left(\hat{x}^2 + \frac{\alpha^2}{L}\right)^2} \left(\frac{1}{L} - \frac{1}{L^2}\right) \quad (53)$$

1082 Let us consider the two corner cases for α . We showed before that $\lim_{\alpha \rightarrow 0} \hat{x}(\alpha) = \sigma_*^{\frac{1}{L}}$, so

$$\lim_{\alpha \rightarrow 0} P(\alpha) = \frac{2\left(\frac{1}{L} - \frac{1}{L^2}\right)}{\sigma_*^{\frac{4}{L}}}$$

1083 As $\alpha \rightarrow \infty$, we have $\lim_{\alpha \rightarrow \infty} P(\alpha) \rightarrow 0$ since $\lim_{\alpha \rightarrow \infty} \hat{x} = 0$. Furthermore, we have

$$\begin{aligned} P'(\alpha) &= \frac{-4}{\left(\hat{x}^2 + \frac{\alpha^2}{L}\right)^3} \left(\frac{1}{L} - \frac{1}{L^2}\right) \left(2\hat{x} \frac{d\hat{x}}{d\alpha} + \frac{2\alpha}{L}\right) \\ &= \frac{-4\left(\frac{1}{L} - \frac{1}{L^2}\right)}{\left(\hat{x}^2 + \frac{\alpha^2}{L}\right)^3} \left(2\hat{x} \left(\frac{-\alpha}{\left(\frac{L}{L-1}\hat{x} + \frac{\alpha^2}{L-1}\frac{1}{\hat{x}}\right)}\right) + \frac{2\alpha}{L}\right) \\ &= \frac{8\alpha\left(\frac{1}{L} - \frac{1}{L^2}\right)}{\left(\hat{x}^2 + \frac{\alpha^2}{L}\right)^3} \left(\frac{L-1}{L + \frac{\alpha^2}{\hat{x}^2}} - \frac{1}{L}\right) \end{aligned}$$

1084 For $L = 2$, we always have $P'(\alpha) < 0$. Hence, choosing $F(\alpha) = \lim_{\alpha \rightarrow 0} P(\alpha) = \frac{2\left(\frac{1}{L} - \frac{1}{L^2}\right)}{\sigma_*^{\frac{4}{L}}}$, will serve
 1085 as the correct upper bound.

1086 Then, let us consider $L > 2$. We can see that α at which $\hat{x}(\alpha) = \frac{\alpha}{\sqrt{L(L-2)}}$ is the critical point of $P(\alpha)$.
 1087 Further, we note that when $\hat{x}(\alpha) < \frac{\alpha}{\sqrt{L(L-2)}}$, $P'(\alpha) < 0$ meaning $P(\alpha)$ is decreasing. Since $\hat{x}(\alpha)$ is
 1088 itself decreasing in α , this states there for any $\alpha > \alpha_{crit}$, $P(\alpha)$ is decreasing. α_{crit} is the solution of
 1089 $\hat{x}(\alpha) = \frac{\alpha}{\sqrt{L(L-2)}}$.

1090 For any $\alpha < \alpha_{crit}$, $P'(\alpha) > 0$, so $P(\alpha)$ is increasing. So, $P(\alpha_{crit})$ corresponds to the maximum of
 1091 P in α . Choosing $F(\alpha) = P(\alpha_{crit})$, a constant allows us to find an upper bound function for the

1092 function in Equation (53). Furthermore, note that since $\frac{d\hat{x}}{d\alpha} < 0$ and $\hat{x} > 0$, $\alpha > 0$, there must be
 1093 only one critical point of $P(\alpha)$ which is at α_{crit} .

1094 Hence, we have $\hat{x}(\alpha_{crit}) = \frac{\alpha_{crit}}{\sqrt{L(L-2)}}$. From Equation (44), we also get $\hat{y} = \alpha_{crit} \sqrt{1 + \frac{1}{L(L-2)}}$ and

$$\begin{aligned} & \left(\frac{\alpha_{crit}}{\sqrt{L(L-2)}} \right) \left(\alpha_{crit} \sqrt{1 + \frac{1}{L(L-2)}} \right)^{L-1} = \sigma_* \\ \implies \alpha_{crit} &= \frac{\sigma_*^{\frac{1}{L}}}{\left(\frac{1}{\sqrt{L(L-2)}} \left(1 + \frac{1}{L(L-2)} \right)^{\frac{L-1}{2}} \right)^{\frac{1}{L}}} \end{aligned}$$

1095 Using α_{crit} , we obtain the maximum of $P(\alpha)$ to be

$$\begin{aligned} P(\alpha_{crit}) &= \frac{2}{(\hat{x}(\alpha_{crit})^2 + \frac{\alpha_{crit}^2}{L})^2} \left(\frac{1}{L} - \frac{1}{L^2} \right) \\ &= \frac{2}{\left(\alpha_{crit}^2 \left(\frac{1}{L(L-2)} + \frac{1}{L} \right) \right)^2} \left(\frac{1}{L} - \frac{1}{L^2} \right) \\ &= \frac{2}{\sigma_*^{\frac{4}{L}}} g(L) \end{aligned}$$

1096 where $g(L) = \frac{(\frac{1}{L} - \frac{1}{L^2}) [\frac{1}{\sqrt{L(L-2)}} (1 + \frac{1}{L(L-2)})]^{\frac{L-1}{2}}]^{\frac{4}{L}}}{(\frac{1}{L(L-2)} + \frac{1}{L})^2}$.

1097 Now, chosing $F(\alpha) = P(\alpha_{crit})$, we integrate the upper bound function as

$$\begin{aligned} \int \frac{d\Psi}{\Psi} &= \frac{2g(L)}{\sigma_*^{\frac{4}{L}}} \int \alpha^3 d\alpha \\ \implies \ln\left(\frac{\Psi}{\Psi_0}\right) &= \frac{g(L)}{2\sigma_*^{\frac{4}{L}}} (\alpha^4) \\ \implies \Psi &= \Psi_0 \exp\left(\frac{g(L)}{2\sigma_*^{\frac{4}{L}}} \alpha^4\right) \end{aligned}$$

1098 where $\Psi_0 = \lim_{\alpha \rightarrow 0} \Psi = L\sigma_*^{2-\frac{2}{L}}$. We verify this upper bound empirically from Figure 25, where we
 1099 see a near exponential growth in sharpness as function of α .

1100 Now, note that the function $\Psi = \Psi_0 \exp\left(\frac{g(L)}{2\sigma_*^{\frac{4}{L}}} \alpha^4\right)$ acts an upper bound to the original sharpness
 1101 function of α and both are increasing in α (Step 1). So, solving for an initialization α -upper limit
 1102 with $\Psi = \frac{2\sqrt{2}}{\eta}$ would mean that the original sharpness with this initialization would be less than
 1103 $\frac{2\sqrt{1+c}}{\eta}$ for some $0 < c < 1$. Hence, α is restricted to

$$\alpha < \left(\ln \left(\frac{\frac{2\sqrt{2}}{\eta}}{L\sigma_*^{2-\frac{2}{L}}} \right) \cdot \frac{2\sigma_*^{\frac{4}{L}}}{g(L)} \right)^{\frac{1}{4}}.$$

1104 We can simplify the bound further by finding an upper bound on $g(L)$ ³:

$$g(L) \leq \frac{\left(\left(1 + \frac{1}{L(L-2)} \right)^{\frac{L-1}{2}} \right)^{\frac{4}{L}}}{\left(\frac{1}{L(L-2)} + \frac{1}{L} \right)^2} \leq L^2 \cdot \left(\left(1 + \frac{1}{L(L-2)} \right)^{\frac{L-1}{2}} \right)^{\frac{4}{L}} \leq L^2 \cdot 2^{\frac{2(L-1)}{L}}.$$

1105 Then, we get obtain a lower bound on α :

$$\alpha < \left(\ln \left(\frac{2\sqrt{2}}{\eta L \sigma_\star^{2-\frac{2}{L}}} \right) \cdot \frac{2\sigma_\star^{\frac{4}{L}}}{L^2 \cdot 2^{\frac{2(L-1)}{L}}} \right)^{\frac{1}{4}} = \left(\ln \left(\frac{2\sqrt{2}}{\eta L \sigma_\star^{2-\frac{2}{L}}} \right) \cdot \frac{\sigma_\star^{\frac{4}{L}}}{L^2 \cdot 2^{\frac{2(L-1)}{L}}} \right)^{\frac{1}{4}}$$

1106 Hence, as long as α satisfies this upper bound, we will have balancing. This completes the proof.

1107 □

1108 **Lemma 6.** Consider the minimizing the loss

$$\mathcal{L}(\{\sigma_\ell\}_{\ell=1}^L) = \frac{1}{2} \left(\prod_{\ell=1}^L \sigma_\ell - \sigma_\star \right)^2,$$

1109 using gradient flow. Then, the balancedness between two singular values defined by $\sigma_\ell^2(t) - \sigma_m^2(t)$ for all
1110 $m, \ell \in [L]$ is constant for all t .

1111 *Proof.* Notice that the result holds specifically for gradient flow and not descent. The dynamics of
1112 each scalar factor for gradient flow can be written as

$$\dot{\sigma}_\ell(t) = - \left(\prod_{\ell=1}^L \sigma_\ell(t) - \sigma_\star \right) \cdot \prod_{i \neq \ell} \sigma_i(t)$$

1113 Then, the time derivative of balancing is given as

$$\begin{aligned} \frac{\partial}{\partial t} (\sigma_\ell^2(t) - \sigma_m^2(t)) &= \sigma_\ell(t) \dot{\sigma}_\ell(t) - \sigma_m(t) \dot{\sigma}_m(t) \\ &= -\sigma_\ell(t) \left(\prod_{\ell=1}^L \sigma_\ell(t) - \sigma_\star \right) \cdot \prod_{i \neq \ell} \sigma_i(t) + \sigma_m(t) \left(\prod_{m=1}^L \sigma_\ell(t) - \sigma_\star \right) \cdot \prod_{j \neq m} \sigma_j(t). \\ &= 0. \end{aligned}$$

1114 Hence, the quantity $\sigma_\ell^2(t) - \sigma_m^2(t)$ remains constant for all time t , hence preserving unbalancedness.

1115 □

1116 **Lemma 7.** Consider the scalar loss

$$\mathcal{L}(\{\sigma_i\}_{i=1}^L) = \frac{1}{2} \left(\prod_{i=1}^L \sigma_i - \sigma_\star \right)^2,$$

1117 The sharpness at the global minima is given as $\|\nabla^2 \mathcal{L}\|_2 = \sum_{i=1}^L \frac{\sigma_\star^2}{\sigma_i^2}$.

1118 *Proof.* The gradient is given by

$$\nabla_{\sigma_i} \mathcal{L} = \left(\prod_{\ell=1}^L \sigma_\ell(t) - \sigma_\star \right) \prod_{j \neq i} \sigma_j(t).$$

³This includes the case for $L = 2$ since $(\frac{1}{L} - \frac{1}{L^2}) < L^2 \cdot 2^{\frac{2(L-1)}{L}}$ for $L = 2$.

1119 Then,

$$\nabla_{\sigma_j} \nabla_{\sigma_i} \mathcal{L} = \prod_{\ell \neq i}^L \sigma_\ell(t) \prod_{\ell \neq j}^L \sigma_\ell(t) + \left(\prod_{\ell=1}^L \sigma_\ell(t) - \sigma_\star \right) \prod_{\ell \neq j, \ell \neq i}^L \sigma_\ell(t)$$

1120 Let $\pi(t) = \prod_{i=1}^L \sigma_i(t)$. Then, at the global minima, we have

$$\nabla_{\sigma_j} \nabla_{\sigma_i} \mathcal{L} = \frac{\pi^2}{\sigma_i \sigma_j} = \frac{\sigma_\star^2}{\sigma_i \sigma_j}$$

1121 Thus, the sharpness of the largest eigenvalue is given as $\|\nabla^2 \mathcal{L}\|_2 = \sum_{i=1}^L \frac{\sigma_\star^2}{\sigma_i^2}$. \square

1122 **Lemma 8.** Consider the loss

$$\mathcal{L}(\{\sigma_i\}_{i=1}^L) = \frac{1}{2} \left(\prod_{i=1}^L \sigma_i - \sigma_\star \right)^2$$

1123 The balanced minimum $\sigma_i = \sigma_\star^{1/L}$ has the smallest sharpness amongst all global minima with a value of
1124 $\|\nabla^2 \mathcal{L}\|_2 = L\sigma_\star^{2-2/L}$.

1125 *Proof.* By Lemma 7, recall that the sharpness at the global minima is given in the form

$$\|\nabla^2 \mathcal{L}\|_2 = \sum_{i=1}^L \frac{\sigma_\star^2}{\sigma_i^2}$$

1126 To show that the balanced minimum is the flattest (i.e., it has the smallest sharpness amongst all
1127 global minima), we will show that KKT stationarity condition of the constrained objective

$$\min_{\{\sigma_i\}_{i=1}^L} \sum_{i=1}^L \frac{\sigma_\star^2}{\sigma_i^2} \quad \text{s.t.} \quad \prod_{i=1}^L \sigma_i = \sigma_\star,$$

1128 are only met at the balanced minimum, which gives us the sharpness value $\|\nabla^2 \mathcal{L}\|_2 = L\sigma_\star^{2-2/L}$.

1129 The Lagrangian is given by

$$L(\sigma_1, \dots, \sigma_L, \mu) = \sum_{i=1}^L \frac{\sigma_\star^2}{\sigma_i^2} + \mu \left(\prod_{i=1}^L \sigma_i - \sigma_\star \right).$$

1130 Then, the stationary point conditions of the Lagrangian is given by

$$\frac{\partial L}{\partial \sigma_i} = -\frac{2\sigma_\star^2}{\sigma_i^3} + \mu \prod_{j \neq i} \sigma_j = 0, \quad (54)$$

$$\frac{\partial L}{\partial \mu} = \prod_{i=1}^L \sigma_i - \sigma_\star = 0. \quad (55)$$

1131 From Equation (54), the solution of the stationary point gives

$$\frac{2\sigma_\star^2}{\sigma_i^3} = \mu \prod_{j \neq i} \sigma_j \implies \mu = \frac{2\sigma_\star^2}{\sigma_i^3 \prod_{j \neq i} \sigma_j} = \frac{2\sigma_\star^2}{\sigma_i^2 \sigma_\star} = \frac{2\sigma_\star}{\sigma_i^2}.$$

1132 This also indicates that at the stationary point, $\sigma_i = \sqrt{\frac{2\sigma_\star}{\mu}}$ for all $i \in [L]$, which means that the
1133 condition is *only* satisfied at the balanced minimum, i.e, $\sigma_i = \sigma_\star^{1/L}$. Furthermore, notice that

$$\nabla^2 f(\sigma_i) = 6\sigma_\star^2 \cdot \text{Diag} \left(\frac{1}{\sigma_i^4} \right) \succ \mathbf{0},$$

1134 where $f(\sigma_i) = \sum_{i=1}^L \frac{\sigma_\star^2}{\sigma_i^2}$, indicating that f only has a minimum. Notice that Equation (55) holds
1135 immediately. Thus, the balanced minimum has the smallest sharpness (flattest), which plugging
1136 into f gives a sharpness of $\|\nabla^2 \mathcal{L}\|_2 = L\sigma_\star^{2-2/L}$.

1137 \square

1138 **Theorem 3** (Subspace Oscillation for Diagonal Linear Networks). Consider an L -layer diagonal linear
 1139 network on the loss

$$\mathcal{L}(\{\mathbf{s}_\ell\}_{\ell=1}^L) := \frac{1}{2} \|\mathbf{s}_1 \odot \dots \odot \mathbf{s}_L - \mathbf{s}_\star\|_2^2, \quad (56)$$

1140 where $\mathbf{s}_\star \in \mathbb{R}^d$ be an r -sparse vector with ordered coordinates such that $s_{\star,1} > \dots > s_{\star,d}$ and define $S_p :=$
 1141 $Ls_{\star,p}^{2-\frac{2}{L}}$ and $\alpha' := \left(\ln \left(\frac{2\sqrt{2}}{\eta L s_{\star,1}^{2-\frac{2}{L}}} \right) \cdot \frac{s_{\star,1}^{\frac{4}{L}}}{L^2 \cdot 2^{\frac{2L-3}{L}}} \right)^{\frac{1}{4}}$. For any $p < r - 1$ and $\alpha < \alpha'$, suppose we run GD
 1142 on Equation (5) with learning rate $\eta = \frac{2}{K}$, where $S_p \geq K > S_{p+1}$ with initialization $\mathbf{s}_\ell = \alpha \mathbf{1}_d$ for all
 1143 $\ell \in [L - 1]$ and $\mathbf{s}_L = \mathbf{0}_d$. Then, under strict balancing, the top- p coordinates of \mathbf{s}_ℓ oscillate within a 2-period
 1144 fixed orbit around the minima in the form

$$s_{\ell,i}(t) = \rho_{i,j}(t), \quad \forall i < p, \forall \ell \in [L],$$

1145 where $\rho_{i,j}(t) \in \{\rho_{i,1}, \rho_{i,2}\}$, $\rho_{i,1} \in (0, s_{\star,i}^{1/L})$ and $\rho_{i,2} \in (s_{\star,i}^{1/L}, (2s_{\star,i})^{1/L})$ are two real roots of the polyno-
 1146 mial $h(\rho) = 0$:

$$h(\rho) = \rho^L \cdot \frac{1 + (1 + \eta L(s_{\star,i} - \rho^L) \cdot \rho^{L-2})^{2L-1}}{1 + (1 + \eta L(s_{\star,i} - \rho^L) \cdot \rho^{L-2})^{L-1}} - s_{\star,i}.$$

1147

1148 *Proof.* This proof essentially mimics that of the DLN proof from Theorem 2, in that we will

- 1149 (i) Compute the eigenvalues and eigenvectors of the flattened training loss Hessian of the diagonal
 1150 linear network at convergence under the balancing assumption.
- 1151 (ii) Show that in 1D cross-section of the eigenvector, the stable condition oscillation $3[f_{\Delta_i}^{(3)}]^2 -$
 1152 $f_{\Delta_i}^{(2)} f_{\Delta_i}^{(4)} > 0$ is satisfied, where f_{Δ_i} denotes the 1D cross-section function at the i -th eigenvector
 1153 direction.

1154 With a slight abuse in notation, let $\mathbf{s} := \{\mathbf{s}_\ell\}_{\ell=1}^L$. Let us first derive the Hessian at convergence by
 1155 considering each block of the flattened Hessian matrix denoted by $\mathbf{H}_{m,\ell}$:

$$\mathbf{H}_{\ell,\ell} = \begin{bmatrix} \prod_{k \neq \ell} s_{k,1} & & \\ & \ddots & \\ & & \prod_{k \neq \ell} s_{k,d} \end{bmatrix} \quad \text{if } m = \ell \quad (57)$$

$$\mathbf{H}_{m,\ell} = \begin{bmatrix} \gamma_1 & & \\ & \ddots & \\ & & \gamma_d \end{bmatrix} \quad \text{if } m \neq \ell, \quad (58)$$

1156 where

$$\gamma_i := \left(\prod_{k \neq i} s_{k,i} \right) \left(\prod_{k \neq m} s_{k,i} \right) + \left(\prod_k s_{k,i} - s_{\star,i} \right) \left(\prod_{k \neq i, k \neq m} s_{k,i} \right).$$

1157 Then, under Lemma 2, at convergence (i.e. the gradient is zero), we have

$$\left(\prod_k s_{k,i} - s_{\star,i} \right) = 0 \implies s_{k,i} = s_{\star,i}^{\frac{1}{L}},$$

1158 which means that at convergence, the Hessian is given by

$$\mathbf{H} = \begin{bmatrix} \mathbf{A} & \dots & \mathbf{A} & \mathbf{A} \\ \vdots & \ddots & \vdots & \vdots \\ \mathbf{A} & \dots & \mathbf{A} & \mathbf{A} \\ \mathbf{A} & \dots & \mathbf{A} & \mathbf{B} \end{bmatrix} \in \mathbb{R}^{dL \times dL},$$

1174 two period orbit fixed point for $\eta > \frac{2}{\lambda_i}$, we show that the polynomial obtained by solving two step
 1175 fixed point has a real root. This is the same loss we analyzed in Theorem 1, where we showed that
 1176 the oscillations are real roots of the polynomial

$$\sigma_{*,1} = \rho^L \frac{1 + z^{2L-1}}{1 + z^{L-1}}, \quad \text{where } z := (1 + \eta L(\sigma_{*,1} - \rho^L) \cdot \rho^{L-2}).$$

1177 and $\rho_1 \in (0, \sigma_{*,1}^{1/L})$ and $\rho_2 \in (\sigma_{*,1}^{1/L}, (2\sigma_{*,1})^{1/L})$ are the two real roots of the polynomial which
 1178 exists and are unique. Hence, whenever the learning rate η lies between $[2/\lambda_p, 2/\lambda_{p+1}]$, we will
 1179 have oscillations in all of the p eigenvector directions. This completes the proof.

1180

□

1181 C.2. Deferred Proofs for Singular Vector Invariance

1182 **Proposition 2.** Let $\mathbf{M}_\star = \mathbf{U}_\star \boldsymbol{\Sigma}_\star \mathbf{V}_\star^\top$ denote the SVD of the target matrix. The initialization in Equa-
1183 tion (??) is a member of the singular vector stationary set in Proposition 1, where $\mathbf{Q}_L = \dots = \mathbf{Q}_2 = \mathbf{V}_\star$.

1184 *Proof.* Recall that the initialization is given by

$$\mathbf{W}_L(0) = \mathbf{0} \quad \text{and} \quad \mathbf{W}_\ell(0) = \alpha \mathbf{I}_d \quad \forall \ell \in [L-1].$$

1185 We will show that under this initialization, each weight matrix admits the following decomposition
1186 for all $t \geq 1$:

$$\mathbf{W}_L(t) = \mathbf{U}_\star \begin{bmatrix} \tilde{\boldsymbol{\Sigma}}_L(t) & \mathbf{0} \\ \mathbf{0} & \mathbf{0} \end{bmatrix} \mathbf{V}_\star^\top, \quad \mathbf{W}_\ell(t) = \mathbf{V}_\star \begin{bmatrix} \tilde{\boldsymbol{\Sigma}}(t) & \mathbf{0} \\ \mathbf{0} & \alpha \mathbf{I}_{d-r} \end{bmatrix} \mathbf{V}_\star^\top, \quad \forall \ell \in [L-1], \quad (65)$$

1187 where

$$\begin{aligned} \tilde{\boldsymbol{\Sigma}}_L(t) &= \tilde{\boldsymbol{\Sigma}}_L(t-1) - \eta \cdot \left(\tilde{\boldsymbol{\Sigma}}_L(t-1) \cdot \tilde{\boldsymbol{\Sigma}}^{L-1}(t-1) - \boldsymbol{\Sigma}_{\star,r} \right) \cdot \tilde{\boldsymbol{\Sigma}}^{L-1}(t-1) \\ \tilde{\boldsymbol{\Sigma}}(t) &= \tilde{\boldsymbol{\Sigma}}(t-1) \cdot \left(\mathbf{I}_r - \eta \cdot \tilde{\boldsymbol{\Sigma}}_L(t-1) \cdot \left(\tilde{\boldsymbol{\Sigma}}_L(t-1) \cdot \tilde{\boldsymbol{\Sigma}}^{L-1}(t-1) - \boldsymbol{\Sigma}_{\star,r} \right) \cdot \tilde{\boldsymbol{\Sigma}}^{L-3}(t-1) \right), \end{aligned}$$

1188 where $\tilde{\boldsymbol{\Sigma}}_L(t), \tilde{\boldsymbol{\Sigma}}(t) \in \mathbb{R}^{r \times r}$ is a diagonal matrix with $\tilde{\boldsymbol{\Sigma}}_L(1) = \eta \alpha^{L-1} \cdot \boldsymbol{\Sigma}_{\star,r}$ and $\tilde{\boldsymbol{\Sigma}}(1) = \alpha \mathbf{I}_r$.

1189 This will prove that the singular vectors are stationary with $\boldsymbol{\Sigma}_L = \dots = \boldsymbol{\Sigma}_2 = \mathbf{V}_\star$. We proceed with
1190 mathematical induction.

1191 **Base Case.** For the base case, we will show that the decomposition holds for each weight matrix at
1192 $t = 1$. The gradient of $f(\boldsymbol{\Theta})$ with respect to \mathbf{W}_ℓ is

$$\nabla_{\mathbf{W}_\ell} f(\boldsymbol{\Theta}) = \mathbf{W}_{L:\ell+1}^\top \cdot (\mathbf{W}_{L:1} - \mathbf{M}_\star) \cdot \mathbf{W}_{\ell-1:1}^\top.$$

1193 For $\mathbf{W}_L(1)$, we have

$$\begin{aligned} \mathbf{W}_L(1) &= \mathbf{W}_L(0) - \eta \cdot \nabla_{\mathbf{W}_L} f(\boldsymbol{\Theta}(0)) \\ &= \mathbf{W}_L(0) - \eta \cdot (\mathbf{W}_{L:1}(0) - \mathbf{M}_\star) \cdot \mathbf{W}_{L-1:1}^\top(0) \\ &= \eta \alpha^{L-1} \boldsymbol{\Sigma}_\star \\ &= \mathbf{U}_\star \cdot (\eta \alpha^{L-1} \cdot \boldsymbol{\Sigma}_\star) \cdot \mathbf{V}_\star^\top \\ &= \mathbf{U}_\star \begin{bmatrix} \tilde{\boldsymbol{\Sigma}}_L(1) & \mathbf{0} \\ \mathbf{0} & \mathbf{0} \end{bmatrix} \mathbf{V}_\star^\top. \end{aligned}$$

1194 Then, for each $\mathbf{W}_\ell(1)$ in $\ell \in [L-1]$, we have

$$\begin{aligned} \mathbf{W}_\ell(1) &= \mathbf{W}_\ell(0) - \eta \cdot \nabla_{\mathbf{W}_\ell} f(\boldsymbol{\Theta}(0)) \\ &= \alpha \mathbf{I}_d, \end{aligned}$$

1195 where the last equality follows from the fact that $\mathbf{W}_L(0) = \mathbf{0}$. Finally, we have

$$\mathbf{W}_\ell(1) = \alpha \mathbf{V}_\star \mathbf{V}_\star^\top = \mathbf{V}_\star \begin{bmatrix} \tilde{\boldsymbol{\Sigma}}(1) & \mathbf{0} \\ \mathbf{0} & \alpha \mathbf{I}_{d-r} \end{bmatrix} \mathbf{V}_\star^\top, \quad \forall \ell \in [L-1].$$

1196 **Inductive Step.** By the inductive hypothesis, suppose that the decomposition holds. Then, notice
1197 that we can simplify the end-to-end weight matrix to

$$\mathbf{W}_{L:1}(t) = \mathbf{U}_\star \begin{bmatrix} \tilde{\boldsymbol{\Sigma}}_L(t) \cdot \tilde{\boldsymbol{\Sigma}}^{L-1}(t) & \mathbf{0} \\ \mathbf{0} & \mathbf{0} \end{bmatrix} \mathbf{V}_\star^\top,$$

1198 for which we can simplify the gradients to

$$\begin{aligned} \nabla_{\mathbf{W}_L} f(\boldsymbol{\Theta}(t)) &= \left(\mathbf{U}_\star \begin{bmatrix} \tilde{\boldsymbol{\Sigma}}_L(t) \cdot \tilde{\boldsymbol{\Sigma}}^{L-1}(t) - \boldsymbol{\Sigma}_{\star,r} & \mathbf{0} \\ \mathbf{0} & \mathbf{0} \end{bmatrix} \mathbf{V}_\star^\top \right) \cdot \mathbf{V}_\star \begin{bmatrix} \tilde{\boldsymbol{\Sigma}}^{L-1}(t) & \mathbf{0} \\ \mathbf{0} & \mathbf{0} \end{bmatrix} \mathbf{V}_\star^\top \\ &= \mathbf{U}_\star \begin{bmatrix} \left(\tilde{\boldsymbol{\Sigma}}_L(t) \cdot \tilde{\boldsymbol{\Sigma}}^{L-1}(t) - \boldsymbol{\Sigma}_{\star,r} \right) \cdot \tilde{\boldsymbol{\Sigma}}^{L-1}(t) & \mathbf{0} \\ \mathbf{0} & \mathbf{0} \end{bmatrix} \mathbf{V}_\star^\top, \end{aligned}$$

1199 for the last layer matrix, and similarly,

$$\nabla_{\mathbf{W}_\ell} f(\Theta(t)) = \mathbf{V}_\star \begin{bmatrix} \tilde{\Sigma}_L(t) \cdot \left(\tilde{\Sigma}_L(t) \cdot \tilde{\Sigma}^{L-1}(t) - \Sigma_{\star,r} \right) \cdot \tilde{\Sigma}^{L-2}(t) & \mathbf{0} \\ \mathbf{0} & \mathbf{0} \end{bmatrix} \mathbf{V}_\star^\top, \quad \ell \in [L-1],$$

1200 for all other layer matrices. Thus, for the next GD iteration, we have

$$\begin{aligned} \mathbf{W}_L(t+1) &= \mathbf{W}_L(t) - \eta \cdot \nabla_{\mathbf{W}_L} f(\Theta(t)) \\ &= \mathbf{U}_\star \begin{bmatrix} \tilde{\Sigma}_L(t) - \eta \cdot \left(\tilde{\Sigma}_L(t) \cdot \tilde{\Sigma}^{L-1}(t) - \Sigma_{\star,r} \right) \cdot \tilde{\Sigma}^{L-1}(t) & \mathbf{0} \\ \mathbf{0} & \mathbf{0} \end{bmatrix} \mathbf{V}_\star^\top \\ &= \mathbf{U}_\star \begin{bmatrix} \tilde{\Sigma}_L(t+1) & \mathbf{0} \\ \mathbf{0} & \mathbf{0} \end{bmatrix} \mathbf{V}_\star^\top. \end{aligned}$$

1201 Similarly, we have

$$\begin{aligned} \mathbf{W}_\ell(t+1) &= \mathbf{W}_\ell(t) - \eta \cdot \nabla_{\mathbf{W}_\ell} f(\Theta(t)) \\ &= \mathbf{V}_\star \begin{bmatrix} \tilde{\Sigma}(t) - \eta \cdot \tilde{\Sigma}_L(t) \cdot \left(\tilde{\Sigma}_L(t) \cdot \tilde{\Sigma}^{L-1}(t) - \Sigma_{\star,r} \right) \cdot \tilde{\Sigma}^{L-2}(t) & \mathbf{0} \\ \mathbf{0} & \alpha \mathbf{I}_{d-r} \end{bmatrix} \mathbf{V}_\star^\top \\ &= \mathbf{V}_\star \begin{bmatrix} \tilde{\Sigma}(t) \cdot \left(\mathbf{I}_r - \eta \cdot \tilde{\Sigma}_L(t) \cdot \left(\tilde{\Sigma}_L(t) \cdot \tilde{\Sigma}^{L-1}(t) - \Sigma_{\star,r} \right) \cdot \tilde{\Sigma}^{L-3}(t) \right) & \mathbf{0} \\ \mathbf{0} & \alpha \mathbf{I}_{d-r} \end{bmatrix} \mathbf{V}_\star^\top \\ &= \mathbf{V}_\star \begin{bmatrix} \tilde{\Sigma}(t+1) & \mathbf{0} \\ \mathbf{0} & \alpha \mathbf{I}_{d-r} \end{bmatrix} \mathbf{V}_\star^\top, \end{aligned}$$

1202 for all $\ell \in [L-1]$. This completes the proof. \square

1203 **Proposition 3.** Let $\mathbf{M}_\star = \mathbf{V}_\star \Sigma_\star \mathbf{V}_\star^\top \in \mathbb{R}^{d \times d}$ denote the SVD of the target matrix. The balanced
1204 initialization in Equation (??) is a member of the singular vector stationary set in Proposition 1, where
1205 $\mathbf{U}_L = \mathbf{Q}_L = \dots = \mathbf{Q}_2 = \mathbf{V}_1 = \mathbf{V}_\star$.

1206 *Proof.* Using mathematical induction, we will show that with the balanced initialization in Equa-
1207 tion (??), each weight matrix admits a decomposition of the form

$$\mathbf{W}_\ell(t) = \mathbf{V}_\star \Sigma_\ell(t) \mathbf{V}_\star^\top, \quad (66)$$

1208 which implies that the singular vectors are stationary for all t such that $\mathbf{U}_L = \mathbf{Q}_L = \dots = \mathbf{Q}_2 =$
1209 $\mathbf{V}_1 = \mathbf{V}_\star$.

1210 **Base Case.** Consider the weights at iteration $t = 0$. By the initialization scheme, we can write each
1211 weight matrix as

$$\mathbf{W}_\ell(0) = \alpha \mathbf{I}_d \implies \mathbf{W}_\ell(0) = \alpha \mathbf{V}_\star \mathbf{V}_\star^\top,$$

1212 which implies that $\mathbf{W}_\ell(0) = \mathbf{V}_\star \Sigma_\ell(0) \mathbf{V}_\star^\top$ with $\Sigma_\ell(0) = \alpha \mathbf{I}_d$.

1213 **Inductive Step.** By the inductive hypothesis, assume that the decomposition holds for all $t \geq 0$.
1214 We will show that it holds for all iterations $t + 1$. Recall that the gradient of $f(\Theta)$ with respect to
1215 \mathbf{W}_ℓ is

$$\nabla_{\mathbf{W}_\ell} f(\Theta) = \mathbf{W}_{L:\ell+1}^\top \cdot (\mathbf{W}_{L:1} - \mathbf{M}_\star) \cdot \mathbf{W}_{\ell-1:1}^\top.$$

1216 Then, for $\mathbf{W}_\ell(t+1)$, we have

$$\begin{aligned} \mathbf{W}_\ell(t+1) &= \mathbf{W}_\ell(t) - \eta \cdot \nabla_{\mathbf{W}_\ell} f(\Theta(t)) \\ &= \mathbf{V}_\star \Sigma_\ell(t) \mathbf{V}_\star^\top - \eta \mathbf{W}_{L:\ell+1}^\top(t) \cdot (\mathbf{W}_{L:1}(t) - \mathbf{M}_\star) \cdot \mathbf{W}_{\ell-1:1}^\top(t) \\ &= \mathbf{V}_\star \Sigma_\ell(t) \mathbf{V}_\star^\top - \eta \mathbf{V}_\star \cdot \left(\Sigma_\ell^{L-\ell}(t) \cdot \left(\Sigma_\ell^L(t) - \Sigma_\star \right) \cdot \Sigma_\ell^{\ell-1}(t) \right) \cdot \mathbf{V}_\star^\top \\ &= \mathbf{V}_\star \cdot \left(\Sigma_\ell(t) - \eta \cdot \Sigma_\ell^{L-\ell}(t) \cdot \left(\Sigma_\ell^L(t) - \Sigma_\star \right) \cdot \Sigma_\ell^{\ell-1}(t) \right) \cdot \mathbf{V}_\star^\top \\ &= \mathbf{V}_\star \Sigma(t) \mathbf{V}_\star^\top, \end{aligned}$$

1217 where $\Sigma(t) = \Sigma_\ell(t) - \eta \cdot \Sigma_\ell^{L-\ell}(t) \cdot \left(\Sigma_\ell^L(t) - \Sigma_\star \right) \cdot \Sigma_\ell^{\ell-1}(t)$. This completes the proof. \square

1218 **C.3. Auxiliary Results**

1219 **Lemma 9.** Let $\{\mathbf{R}_\ell\}_{\ell=1}^L \in \mathbb{R}^{n \times n}$ be orthogonal matrices and $\mathbf{H}_{i,j} \in \mathbb{R}^{n^2 \times n^2}$ be diagonal matrices. Consider
 1220 the two following block matrices:

$$\mathbf{H} = \begin{bmatrix} \mathbf{H}_{1,1} & \mathbf{H}_{1,2} & \cdots & \mathbf{H}_{L,1} \\ \mathbf{H}_{2,1} & \mathbf{H}_{2,2} & \cdots & \mathbf{H}_{L,2} \\ \vdots & \vdots & \ddots & \vdots \\ \mathbf{H}_{1,L} & \mathbf{H}_{2,L} & \cdots & \mathbf{H}_{L,L} \end{bmatrix}$$

$$\tilde{\mathbf{H}} = \begin{bmatrix} \mathbf{R}_L \mathbf{H}_{1,1} \mathbf{R}_L^\top & \mathbf{R}_L \mathbf{H}_{1,2} \mathbf{R}_{L-1}^\top & \cdots & \mathbf{R}_L \mathbf{H}_{1,L} \mathbf{R}_1^\top \\ \mathbf{R}_{L-1} \mathbf{H}_{2,1} \mathbf{R}_L^\top & \mathbf{R}_{L-1} \mathbf{H}_{2,2} \mathbf{R}_{L-1}^\top & \cdots & \mathbf{R}_{L-1} \mathbf{H}_{2,L} \mathbf{R}_1^\top \\ \vdots & \vdots & \ddots & \vdots \\ \mathbf{R}_1 \mathbf{H}_{L,1} \mathbf{R}_L^\top & \mathbf{R}_1 \mathbf{H}_{L,2} \mathbf{R}_{L-1}^\top & \cdots & \mathbf{R}_1 \mathbf{H}_{L,L} \mathbf{R}_1^\top \end{bmatrix}.$$

1221 Then, the two matrices \mathbf{H} and $\tilde{\mathbf{H}}$ are similar, in the sense that they have the same eigenvalues.

1222 *Proof.* It suffices to show that \mathbf{H} and $\tilde{\mathbf{H}}$ have the same characteristic polynomials. Let us define

$$\tilde{\mathbf{H}} := \begin{bmatrix} \mathbf{A} & \mathbf{B} \\ \mathbf{C} & \mathbf{D} \end{bmatrix},$$

1223 where

$$\mathbf{A} := \mathbf{R}_L \mathbf{H}_{1,1} \mathbf{R}_L^\top \quad \mathbf{B} := [\mathbf{R}_L \mathbf{H}_{1,2} \mathbf{R}_{L-1}^\top \quad \cdots \quad \mathbf{R}_L \mathbf{H}_{1,L} \mathbf{R}_1^\top] \quad (67)$$

$$\mathbf{C} := \begin{bmatrix} \mathbf{R}_{L-1} \mathbf{H}_{2,1} \mathbf{R}_L^\top \\ \vdots \\ \mathbf{R}_1 \mathbf{H}_{L,1} \mathbf{R}_L^\top \end{bmatrix} \quad \mathbf{D} := \begin{bmatrix} \mathbf{R}_{L-1} \mathbf{H}_{2,2} \mathbf{R}_{L-1}^\top & \cdots & \mathbf{R}_{L-1} \mathbf{H}_{2,L} \mathbf{R}_1^\top \\ \vdots & \ddots & \vdots \\ \mathbf{R}_1 \mathbf{H}_{L,2} \mathbf{R}_{L-1}^\top & \cdots & \mathbf{R}_1 \mathbf{H}_{L,L} \mathbf{R}_1^\top \end{bmatrix}. \quad (68)$$

1224 Then, we have

$$\begin{aligned} \det(\tilde{\mathbf{H}} - \lambda \mathbf{I}) &= \det \left(\begin{bmatrix} \mathbf{A} - \lambda \mathbf{I} & \mathbf{B} \\ \mathbf{C} & \mathbf{D} - \lambda \mathbf{I} \end{bmatrix} \right) \\ &= \det(\mathbf{A} - \lambda \mathbf{I}) \cdot \det((\mathbf{D} - \lambda \mathbf{I}) - \mathbf{C}(\mathbf{A} - \lambda \mathbf{I})^{-1} \mathbf{B}), \end{aligned}$$

1225 where the second equality is by the Schur complement. Notice that

$$\begin{aligned} (\mathbf{A} - \lambda \mathbf{I})^{-1} &= (\mathbf{R}_L \mathbf{H}_{1,1} \mathbf{R}_L^\top - \lambda \mathbf{I})^{-1} = (\mathbf{R}_L \mathbf{H}_{1,1} \mathbf{R}_L^\top - \lambda \mathbf{R}_L \mathbf{R}_L^\top)^{-1} \\ &= \mathbf{R}_L \cdot (\mathbf{H}_{1,1} - \lambda \mathbf{I})^{-1} \cdot \mathbf{R}_L^\top. \end{aligned}$$

1226 Then, we also see that,

$$\mathbf{C}(\mathbf{A} - \lambda \mathbf{I})^{-1} \mathbf{B} = \underbrace{\begin{bmatrix} \mathbf{R}_{L-1} & & \\ & \ddots & \\ & & \mathbf{R}_1 \end{bmatrix}}_{=:\hat{\mathbf{V}}} \cdot \mathbf{E} \cdot \underbrace{\begin{bmatrix} \mathbf{R}_{L-1}^\top & & \\ & \ddots & \\ & & \mathbf{R}_1^\top \end{bmatrix}}_{=:\hat{\mathbf{V}}^\top}.$$

1227 where

$$\mathbf{E} := \begin{bmatrix} \mathbf{H}_{2,1} \cdot (\mathbf{H}_{1,1} - \lambda \mathbf{I})^{-1} \cdot \mathbf{H}_{1,2} & \cdots & \mathbf{H}_{2,1} \cdot (\mathbf{H}_{1,1} - \lambda \mathbf{I})^{-1} \cdot \mathbf{H}_{1,L} \\ \vdots & \ddots & \vdots \\ \mathbf{H}_{L,1} \cdot (\mathbf{H}_{1,1} - \lambda \mathbf{I})^{-1} \cdot \mathbf{H}_{1,2} & \cdots & \mathbf{H}_{L,1} \cdot (\mathbf{H}_{1,1} - \lambda \mathbf{I})^{-1} \cdot \mathbf{H}_{1,L} \end{bmatrix}.$$

1228 Similarly, we can write \mathbf{D} as

$$\mathbf{D} = \hat{\mathbf{V}} \underbrace{\begin{bmatrix} \mathbf{H}_{2,2} & \cdots & \mathbf{H}_{2,L} \\ \vdots & \ddots & \vdots \\ \mathbf{H}_{L,2} & \cdots & \mathbf{H}_{L,L} \end{bmatrix}}_{=:\mathbf{F}} \hat{\mathbf{V}}^\top.$$

1229 Then, we have

$$\begin{aligned}\det(\tilde{\mathbf{H}} - \lambda\mathbf{I}) &= \det(\mathbf{R}_L \cdot (\mathbf{H}_{1,1} - \lambda\mathbf{I}) \cdot \mathbf{R}_L^\top) \cdot \det(\hat{\mathbf{V}} \cdot (\mathbf{E} - \mathbf{F}) \cdot \hat{\mathbf{V}}^\top) \\ &= \det(\mathbf{H}_{1,1} - \lambda\mathbf{I}) \cdot \det(\mathbf{E} - \mathbf{F}),\end{aligned}$$

1230 which is not a function of $\mathbf{U}, \mathbf{V}, \{\mathbf{R}_\ell\}_{\ell=1}^L$. By doing the same for $\tilde{\mathbf{H}}$, we can show that both $\tilde{\mathbf{H}}$ and
1231 \mathbf{H} have the same characteristic polynomials, and hence the same eigenvalues. This completes the
1232 proof.

1233 □

1234 **Lemma 10.** Let $\mathbf{A}, \mathbf{B} \in \mathbb{R}^{d \times d}$ be two orthogonal matrices. Then, the Kronecker product of \mathbf{A} and \mathbf{B} is also
1235 an orthogonal matrix:

$$(\mathbf{A} \otimes \mathbf{B})^\top (\mathbf{A} \otimes \mathbf{B}) = (\mathbf{A} \otimes \mathbf{B})(\mathbf{A} \otimes \mathbf{B})^\top = \mathbf{I}_{d^2}.$$

1236 *Proof.* We prove this directly by using properties of Kronecker products:

$$\begin{aligned}(\mathbf{A} \otimes \mathbf{B})^\top (\mathbf{A} \otimes \mathbf{B}) &= \mathbf{A}^\top \mathbf{A} \otimes \mathbf{B}^\top \mathbf{B} \\ &= \mathbf{I}_d \otimes \mathbf{I}_d = \mathbf{I}_{d^2}.\end{aligned}$$

1237 Similarly, we have

$$\begin{aligned}(\mathbf{A} \otimes \mathbf{B})(\mathbf{A} \otimes \mathbf{B})^\top &= \mathbf{A}\mathbf{A}^\top \otimes \mathbf{B}\mathbf{B}^\top \\ &= \mathbf{I}_d \otimes \mathbf{I}_d = \mathbf{I}_{d^2}.\end{aligned}$$

1238 This completes the proof. □

1239 **Lemma 11.** Let $\{a(t)\}_{t=1}^N$ be a sequence such that $a(t) \geq 0$ for all t . If there exists a constant $c \in (0, 1)$ such
1240 that $a(t+1) < c \cdot a(t)$ for all t , then $\lim_{t \rightarrow \infty} a(t) = 0$.

1241 *Proof.* We prove this by direct reasoning. From the assumption $a(t+1) < c \cdot a(t)$ for some $c \in (0, 1)$,
1242 we can iteratively expand this inequality:

$$a(t+1) < c \cdot a(t), \quad a(t+2) < c \cdot a(t+1) < c^2 \cdot a(t),$$

1243 and, more generally, by induction:

$$a(t+k) < c^k \cdot a(t), \quad \text{for all } k \geq 0.$$

1244 Since $c \in (0, 1)$, the sequence $\{c^k\}_{k=0}^\infty$ converges to 0 as $k \rightarrow \infty$. Hence:

$$0 \leq \lim_{k \rightarrow \infty} a(t+k) \leq \lim_{k \rightarrow \infty} c^k \cdot a(t) = 0.$$

1245 Therefore, by the squeeze theorem, the sequence $\{a(t)\}$ converges to 0 as $t \rightarrow \infty$. □

1246 **Lemma 12** ([16]). Consider any 1-D differentiable function $f(x)$ around a local minima \bar{x} , satisfying (i)
1247 $f^{(3)}(\bar{x}) \neq 0$, and (ii) $3[f^{(3)}]^2 - f''f^{(4)} > 0$ at \bar{x} . Then, there exists ϵ with sufficiently small $|\epsilon|$ and $\epsilon \cdot f^{(3)} > 0$
1248 such that: for any point x_0 between \bar{x} and $\bar{x} - \epsilon$, there exists a learning rate η such that $F_\eta^2(x_0) = x_0$, and

$$\frac{2}{f''(\bar{x})} < \eta < \frac{2}{f''(\bar{x}) - \epsilon \cdot f^{(3)}(\bar{x})}.$$